



UNIVERSITY OF
BIRMINGHAM

Ageing and Crystallisation of Polycaprolactone

Kate Phillipson

A thesis submitted to the
University of Birmingham
for the degree of

Doctor of Philosophy

School of Metallurgy & Materials
College of Engineering & Physical Sciences
University of Birmingham

October 2014

UNIVERSITY OF
BIRMINGHAM

University of Birmingham Research Archive

e-theses repository

This unpublished thesis/dissertation is copyright of the author and/or third parties. The intellectual property rights of the author or third parties in respect of this work are as defined by The Copyright Designs and Patents Act 1988 or as modified by any successor legislation.

Any use made of information contained in this thesis/dissertation must be in accordance with that legislation and must be properly acknowledged. Further distribution or reproduction in any format is prohibited without the permission of the copyright holder.

Acknowledgements

Firstly, I would like to express my sincere thanks and gratitude to my supervisors, Professor Jim Hay and Dr. Mike Jenkins. Their support, encouragement and guidance has been invaluable and I would not have made it to the end of this thesis without them. Their knowledge and understanding of the subject area has been of great value and they have never been hesitant in answering my questions or providing explanations. I could not have asked for more caring and helpful supervisors.

I would also like to mention Mr. Frank Biddlestone, who has never failed to provide invaluable technical support. His broad knowledge and experience has provided constructive feedback and alternative approaches in the experimental work, which has been greatly appreciated.

The support of friends throughout the course of this PhD has proved to be vital in enabling me to reach completion. In particular, Shona Murphy and Catherine Kelly have been a great sounding board and have offered their opinions and expertise in particular areas, which have provided opportunity for reflection. Their understanding of this experience has helped me cope with situations I would have struggled through alone.

Finally, I could not have gone through the last 4 years without the help and support from my family. They have provided great confidence and belief and have pulled me through to completion. I could not have done this without them, or my partner Jason.

Synopsis

This thesis concerns the study of crystallisation kinetics and aging process of polycaprolactone (PCL) using thermal analysis techniques; differential scanning calorimetry (DSC), Fourier transform infra-red spectroscopy (FTIR) and 2D infra-red correlation spectroscopy (2D-FTIR).

DSC has been used to characterise the crystallisation kinetics of PCL under isothermal and non-isothermal conditions and analysed using the Avrami equation and Ozawa equation respectively. It has been found that isothermal crystallisation illustrates crystal growth via pre-determined spheres but the Ozawa equation was found to be unsuitable as a method of analysis of non-isothermal crystallisation, producing parameters of little meaning and suggesting crystallisation via an undetermined mechanism. It has also been suggested that at high cooling rates, non-isothermal conditions may exhibit isothermal growth mechanisms.

FTIR has been used to study the secondary crystallisation kinetics of PCL, as this technique has been found to be more effective for this purpose than DSC. It was found that changes in band position and intensity occur during crystallisation, most notably in the carbonyl peak, in which the amorphous band located at 1735 cm^{-1} reduces in intensity simultaneously with an increase in the crystalline band at 1725 cm^{-1} . This has been analysed using 2D-FTIR and has shown to exhibit an *angel* pattern, confirming the presence of overlapping bands attributed to amorphous and crystalline components. This recognition was used as an indication that the absorption could be used to measure fractional crystallinity and hence analyse crystallisation kinetics.

The study of crystallisation has identified two consecutive processes which have been attributed to primary and secondary crystallisation. Modified versions of the Avrami equation have been applied and n values of 3.0 ± 0.4 for primary and 1.0 ± 0.2 for secondary were deduced. These have been attributed to the growth and impingement of spherulites and the thickening of lamellae in a one-dimensional growth respectively. It has also been found that primary crystallisation was initiated by secondary nucleation in Regime I, as outlined by Hoffman & Lauritzen. Secondary crystallisation was found to be initiated in Regime II.

The most significant section of work has been the study of aging within PCL. Secondary crystallisation has been found to develop over time, with the effects of this exhibited in the melting endotherm. The stem length was also found to increase with the square root of time, and this has led to the suggestion that secondary crystallisation is a diffusion controlled process, with crystal growth becoming restricted as entanglements diffuse away from the growth face. It has also been suggested that this diffusion mechanism is that of reptation.

Contents

Chapter 1. – Introduction	1
1.1 Polycaprolactone (PCL)	1
1.2 Degree of Crystallinity	3
1.3 Mechanism of Crystallisation.....	4
1.3.1 Nucleation	5
1.3.2 Crystal Growth	7
1.3.3 The Temperature Dependence of Growth.....	8
1.4 Crystallisation Kinetics	11
1.5 Polymer Morphology	13
1.5.1 Single Crystals	13
1.5.2 Spherulites.....	14
1.6 The Melting of Polymers.....	16
1.7 Physical Ageing in Polymeric Materials	18
1.7.1 The Thermodynamics of Ageing	19
1.7.2 Ageing in Semi-Crystalline Polymers.....	21
1.8 Project Aims and Objectives	22
1.9 References	22
Chapter 2. – Materials, Apparatus and Experimental Procedures	28
2.1 Materials	28
2.1.1 Poly (ϵ -caprolactone).	28
2.1.2 Potassium Bromide	29
2.1.3 Dichloromethane	29
2.2 Apparatus and Experimental Procedures.....	30
2.2.1 Differential Scanning Calorimetry (DSC)	30
2.2.2 Fourier Transform Infra-Red Spectroscopy (FTIR).....	36
2.2.3 Hot Press	41
2.2.4 Instron Mechanical Tester.....	42
2.3 References	44

Chapter 3. – Thermal Analysis of PCL by DSC.....	46
3.1 Results and Discussion.....	46
3.1.1 Isothermal Crystallisation	46
3.1.2 Nonisothermal Crystallisation.....	52
3.1.3 High Cooling Rates	63
3.2 Conclusions	66
3.3 References	67
Chapter 4. – FTIR Spectroscopic Analysis of PCL on Crystallisation.....	72
4.1 Principles of 2D Infrared Spectroscopy	72
4.2 Analysing 2D spectral features.....	73
4.3 Results and Discussion	75
4.3.1 FTIR Spectrum of PCL	75
4.3.2 Analysis of FTIR Spectrum of PCL.....	79
4.4 Conclusions	86
4.5 References	86
Chapter 5. – Isothermal Crystallisation Kinetics as measured by FTIR Spectroscopy ..	88
.....	88
5.1 Results and Discussion	88
5.1.1 Changes in FTIR Spectrum of PCL during Crystallisation	88
5.1.2 Kinetic Analysis of Crystallisation from FTIR Spectroscopy	97
5.2 Conclusions.....	108
5.3 References.....	108
Chapter 6. – Ageing in PCL	113
6.1 Results	113
6.1.1 Mechanical Properties.....	113
6.1.2 Effect of Ageing on Melting	120
6.1.3 Effect of Ageing on Crystallinity.....	126
6.1.4 Effect of Ageing on Lamellae Stem Length.....	131
6.2 Conclusions.....	135
6.3 References	131

Chapter 7. Secondary Crystallisation of PCL.....	138
7.1 Reptation Theory and Segmental Diffusion	142
7.2 Conclusions	144
7.3 References	149
Chapter 8. Conclusions and Further Work.....	147
8.1 Conclusions.....	147
8.2 Future Work.....	149
8.3 References.....	151

List of Figures

Figure 1.1 – Chemical structure of polycaprolactone	1
Figure 1.2 – Schematic diagram of the change in free energy during nucleation.....	6
Figure 1.3 – Schematic representation of three nucleation regimes	11
Figure 1.4 - Formation of spherulites.....	15
Figure 1.5 – Illustration of the three measures of melting	16
Figure 1.6 – Graphical representation of Hoffman-Weeks plot for equilibrium melting temperature.....	18
Figure 1.7 - Change in length, volume and enthalpy with temperature and the effect of ageing	20
Figure 2.1 – Typical DSC trace.....	30
Figure 2.2 – DSC pan heaters (a) and schematic diagram of a DSC (b).....	32
Figure 2.3 – Three measures of melting.....	34
Figure 2.4 – Mettler Toledo DSC 1/500	35
Figure 2.5 – Typical FTIR spectrum.....	37
Figure 2.6 – ThermoScientific Spectrometer (a) and Linkham Hotstage (b) fitted in the FTIR spectrometer (c).....	38
Figure 2.7 – Example of peak resolution within Omnic	41
Figure 2.8 – Instron Mechanical Tester	42
Figure 2.9 – Illustration of a typical stress-strain curve, highlighting its main components	44
Figure 3.1 – Change in heat flow with time during crystallisation at 38-42 °C	47
Figure 3.2 – Growth of relative crystallinity with time during crystallisation at 38-42 °C	47
Figure 3.3 – Avrami double-log plot for isothermal crystallisation at 38-42 °C.....	49
Figure 3.4 – Variation in half-life with crystallisation temperature	51
Figure 3.5 – Variation in growth rate (Z) with crystallisation temperature	51
Figure 3.6 – Change in heat flow with temperature for cooling rates of 1-7 °C.....	53
Figure 3.7 – Development of relative crystallinity with temperature for cooling rates of 1-7 °C	54
Figure 3.8 - Ozawa plots at fixed temperatures from 33 to 37 °C	56
Figure 3.9 – Variation in K(T) with temperature	56
Figure 3.10 – Linear extrapolation of isothermal $t_{1/2}$ data	60
Figure 3.11 – $t_{1/2}$ values for nonisothermal fixed temperatures of 33-37 °C determined from extrapolated data.....	60
Figure 3.12 – Double-log plot produced from application of the Avrami equation to nonisothermal data	62
Figure 3.13 – Growth in relative crystallinity for samples tested at higher cooling rates	64
Figure 3.14 – Avrami double-log plot for samples tested at higher cooling rates	65
Figure 4.1 – The FTIR spectrum of PCL	75

Figure 4.2 – Changes to the FTIR spectrum on heating from 70 – 30 °C	77
Figure 4.3 – Changes to the FTIR spectrum of PCL on heating from 30 to 70°C in the region 2750-3000 cm ⁻¹	79
Figure 4.4 – Change to the carbonyl absorption band on cooling from 70 °C – 30 °C ..	80
Figure 4.5 – 3D (A) and 2D (B) synchronous correlation intensity contour map of the carbonyl band in region 1800-1650 cm ⁻¹	82
Figure 4.6 – 3D (A) and 2D (B) asynchronous correlation map of the carbonyl absorption band in region 1800-1650 cm ⁻¹	83
Figure 4.7 – Changes to the FTIR spectrum on heating from 30 to 70°C in the region 1350-1600 cm ⁻¹	84
Figure 4.8 – Change to the FTIR spectrum of heating from 30 to 70°C in the region 1000-1350 cm ⁻¹	85
Figure 5.1 - Change in peak position and intensity of amorphous and crystalline bands with time	89
Figure 5.2 - Illustration of the deconvolution of the carbonyl band into its component parts	90
Figure 5.3 - Result of resolving the carbonyl absorption band into its two component parts on crystallisation.....	90
Figure 5.4 - Increase in absorbance of the crystalline band at 1725 cm ⁻¹ with log(t).....	92
Figure 5.5 - Decrease in absorbance of the amorphous band at 1735 cm ⁻¹ with log(t) ..	92
Figure 5.6 - Dependence of the crystalline on amorphous absorption with crystalline temperature.....	94
Figure 5.7 - Development of the fractional crystallinity with log(t).....	94
Figure 5.8 - Decrease in fractional amorphous content with log(t)	95
Figure 5.9 - Consistency of the data with Equation 5.1 over the total crystallisation ...	96
Figure 5.10 - Comparison of fractional crystallinity determined from the absorption of the crystalline and amorphous bands	96
Figure 5.11 - Avrami double-log plot for the primary process of crystallisation between 43-47 °C	99
Figure 5.12 - The effect of induction time on the linearity of the log(-ln(X _{p,inf} - X _t /X _{p,inf})) plots.....	100
Figure 5.13 - Effect of induction time of A - degree of fit and B - n value	101
Figure 5.14 - Avrami fit to secondary crystallisation	104
Figure 5.15 – Dependence of half-life on the degree of super-cooling	106
Figure 6.1 - Engineering stress-strain curve at t ₀ and after 6 months at room temperature	113
Figure 6.2 - As in Figure 6.1 up to 50% strain.....	114
Figure 6.3 - Development of yield stress with ageing time	118
Figure 6.4 - Development of yield stress over the first 200 hours of ageing.....	118
Figure 6.5 - Variation of modulus with ageing time.....	119
Figure 6.6 - Variation of modulus over the first 200 hours of ageing	119

Figure 6.7 - Melt endotherms for samples stored at -18 °C at 0, 24, 68, 2520 and 3696 hours.....	121
Figure 6.8 - Melt endotherms for samples stored at 5 °C at 0, 24, 68, 2352 and 3696 hours.....	122
Figure 6.9 - Melt endotherms for samples stored at 20 °C at 0, 24, 68, 2352 and 3696 hours.....	124
Figure 6.10 - Melt endotherms for samples stored at 50°C at 0, 24, 168 2520 and 3696 hours.....	125
Figure 6.11 - Effect of time on the peak melting point.....	126
Figure 6.12 – Change in the percentage crystallinity on ageing up to 200 hours.....	127
Figure 6.13 – Change in the percentage crystallinity on ageing up to 4000 hours.....	127
Figure 6.14 - Increase in yield stress as a function of % crystallinity at 50, 20, 5 and -18°C	129
Figure 6.15 - Increase in modulus as a function of % crystallinity at 50, 20 , 5 and -18°C	129
Figure 6.16 - The increase in melting point as a function of % crystallinity at 50, 20 , 5 and -18°C	130
Figure 6.17 - Linear dependence of melting point on log(t).....	131
Figure 6.18 – Change in average stem length with time.....	133
Figure 6.19 - Dependence of the average stem length on the square root of time.....	134
Figure 6.20 - Arrhenius plot of the logarithm of stem growth rate against reciprocal temperature.....	134
Figure 7.1 - The increase in fractional crystallinity due to secondary crystallisation with the square root of the crystallisation time.....	138

List of Tables

Table 1.1 – Avrami exponent value for different crystallisation mechanisms	13
Table 2.1 – Properties of PCL.....	28
Table 2.2 – Properties of KBr, as given on manufacturer’s data sheet.....	29
Table 2.3 – Properties of DCM, as given on manufacturers data sheet.....	29
Table 3.1 - Avrami Rate Parameters	52
Table 3.2 – Ozawa exponent ‘m’ values.....	57
Table 3.3 – Avrami parameters for nonisothermal data considered as crystallising at constant temperature	62
Table 3.4 – Avrami parameters for higher cooling rates of 10-30 °C	65
Table 4.1 – Molecular assignment of the characteristic IR bands – change on crystallisation	78
Table 5.1 – Avrami parameters for primary crystallisation.	99
Table 5.2 –Avrami parameters for secondary crystallisation.....	104
Table 6.1 – The change in yield stress and modulus and the standard deviation (SD) with time at different storage temperatures.....	117
Table 7.1 – R ² values to show the strength of linear relationship between fractional crystallinity and the square root of time.....	139
Table 7.2 – Diffusion coefficient for secondary crystallisation.....	139

Chapter 1. – Introduction

1.1 Polycaprolactone (PCL)

Polycaprolactone is a biodegradable, thermoplastic, semi-crystalline polyester with a glass transition temperature (T_g) about -60°C and a melting temperature (T_m) of 60°C [1]. The chemical structure is shown in Figure 1.1. Although polycaprolactone is a fully biodegradable material it is not produced from renewable raw materials, but is derived from the distillation products of crude oil, in particular cyclohexene.

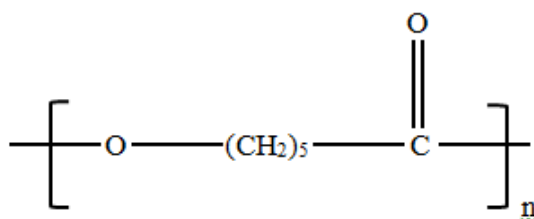


Figure 1.1 – Chemical structure of polycaprolactone

There are two main ways of producing polycaprolactone, as described in the literature; the polycondensation of a hydroxycarboxylic acid, namely 6-hydroxyhexanoic acid, and by the ring-opening polymerisation (ROP) of the lactone; ϵ -caprolactone (ϵ -CL). Polycondensation is a form of step-growth polymerisation whereby a polymer is formed by the addition of two monomer units and the elimination of a small molecule. The condensation process releases water as a by-product and this eliminates the need for a catalyst. The reaction is rarely described in detail but this preparation of PCL has been carried out by Braud et al [2] from 6-hydroxyhexanoic acid producing the polymer under vacuum to shift the equilibrium towards the production of the polymer.

ROP is the preferred route for synthesis of the polymer since it produces higher molecular weight and lower polydispersity. ROP is an example of chain-growth polymerisation whereby the terminal end of the polymer acts as an active centre, and further cyclic monomers add to form a longer chain through ionic propagation. There are four main mechanisms for the ROP of lactones, which depend on the catalyst used; anionic, cationic, monomer-activated and coordination insertion ROP. However, the process can cause loss of control of the polymerisation, as well as a broadening of polydispersity, due to chain transfer steps by both inter- and intra- molecular transesterification occurring. These reactions generally occur at the later stages of the polymerisation and particularly at higher temperatures [3].

Due to its biodegradability and biocompatibility polycaprolactone is a popular material for use in bio-applications. It has been used as a biodegradable packaging material and since it is biodegraded by microorganisms it can be composted or added to landfill. It can also be degraded by hydrolysis in physiological conditions, and so has been approved for use in the human body as part of a long-term drug delivery system (particularly contraceptive delivery), sutures and tissue scaffolds [4]. Polycaprolactone is especially useful for applications involving the controlled release of bioactive molecules such as growth factors, hormones and extended residence supports for cell growth and tissue development.

It is a partially crystalline polymer and since its glass transition temperature is well below ambient it is always crystalline. Its properties depend on the degree of crystallinity and are sensitive to thermal history and processing conditions.

1.2 Degree of Crystallinity

The degree of crystallinity of a polymer is an important factor in determining how a polymer is used, as it influences morphology and mechanical properties.

Crystallinity can be influenced by several factors. The symmetry of a polymer affects its ability to form crystallites, with linear symmetrical chains enabling greater close-packing of the chains and therefore increasing crystallinity. Large irregular units such as phenyl groups and cis-double bonds encourage bending in the chains making close-packing more difficult. Intermolecular bonding is another factor affecting the degree of crystallinity. Chains that are closely packed allow Van der Waals forces to act between the chains and provide additional stability within the polymer. Chains containing polar groups can be held rigid and aligned by dipole-dipole interactions and polymers containing hydrogen bonds also show greatly enhanced levels of crystallinity.

Levels of crystallinity can also be improved by increased tacticity, as this enables flexible chains to form regular helices and encourage close-packing of the chains. Large pendant groups are more rigid and prevent this close-packing, so reducing the crystallinity.

Finally, crystallinity can be increased when chains exhibit limited levels of branching. Higher levels of chain branching reduces the packing efficiency and so reduces crystallinity.

1.3 Mechanism of Crystallisation

Crystallisation is the process by which an ordered structure is produced from a disordered phase, usually a liquid. The maximum rate of crystallisation occurs half way between the glass transition temperature (T_g) and the melting point (T_m) and cannot occur either side of this range due to the fact that the chains are not mobile enough to reorganise and fold (below the T_g), or the fact that the polymer is liquid above T_m , [5].

Usually, bulk crystallised polymers will achieve between 10-80% crystallinity; complete crystallinity within polymers is very rarely achieved, as the chains cannot completely untangle and align properly during a finite period of cooling [6]. The overall rate of crystallisation and degree of crystallinity can be determined by external factors such as cooling rate or crystallisation temperature, as well as factors described above in section 1.2. Higher levels of crystallinity lead to improvements in mechanical properties, e.g. tensile strength and rigidity but can lead to brittle failure.

Crystallisation involves two processes, nucleation and growth. Nuclei form within small regions of the randomly organised entangled molecules in the melt and alignment of clusters of these produce small crystallites. This is encouraged by intramolecular forces and secondary valence forces, aiding close-packing and an ordered three-dimensional structure [7]. These potential crystals can either grow or dissipate into the disordered melt. However once the particles are larger than a 'critical size' by the accumulation of further chain segments [8] they become stable and nucleate the crystallisation.

1.3.1 Nucleation

Nucleation can occur either by the homogeneous mechanism, or heterogeneously; homogeneous nucleation is a spontaneous process whereby small nuclei are developed randomly within the melt but heterogeneous nucleation is artificially induced by foreign bodies such as dust particles or other impurities and is the form of nucleation seen most often in polymer crystallisation. It is more thermodynamically favoured over homogeneous nucleation with heterogeneous nucleation occurring at lower degrees of super-cooling. The number of nuclei formed is temperature dependent, with low degrees of super-cooling producing fewer larger nuclei and higher degrees of super-cooling forming many smaller nuclei so a large number of spherulites may be achieved [8].

An important driving force in polymer crystallisation is the Gibbs free energy difference between the solid and the liquid, ΔG , which is temperature dependent,

$$\Delta G = \Delta H - T\Delta S \quad \text{Equation 1.1}$$

where ΔH is the enthalpy of crystallisation, T is the thermodynamic temperature and ΔS is the entropy difference between solid and liquid.

At the melting point, T_m , $\Delta G = 0$ and

$$T_m = \Delta H / \Delta S \quad \text{Equation 1.2}$$

Above T_m , $\Delta G > 0$ and crystallisation cannot occur while below T_m , $\Delta G < 0$ crystallisation will occur if there is a mechanism by which it can occur. As the temperature decreases further from T_m , ΔG becomes more negative and the driving force for crystallisation increases.

The initial production of nuclei from the melt is called primary nucleation and begins by the packing of a few molecules to form a small critical size crystal. During this process there is a change in free energy as the crystal surface forms, which has a positive surface energy, causing ΔG_f the free energy of formation of the nucleus to increase. When the nuclei is small the surface-to-volume ratio is high, and so the value of ΔG increases due to the relative importance of the surface free energy. As the nuclei grows, the surface-to-volume ratio decreases and so there is a critical size of nuclei at which the value of ΔG_f will start to decrease and decrease further as the nucleus grows. A schematic diagram of this and for the critical nucleus is given in Figure 1.2.

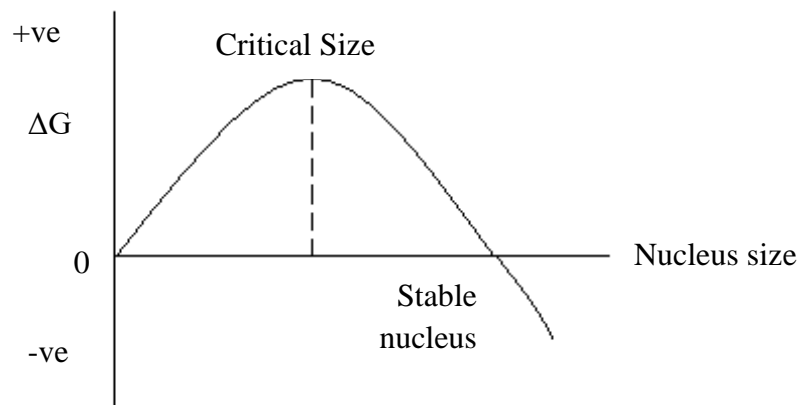


Figure 1.2 – Schematic diagram of the change in free energy during nucleation

The development of the nucleus can be separated into three stages; the first (primary nucleation), as already mentioned, describes the initial forming of a nuclei. Secondary nucleation defines the building up of a new layer of material on the growth face of the crystal and determines the rate at which the crystal grows. Secondary nucleation has a lower free energy than primary since it nucleates a pre-existing surface and the surface-to-volume ratio is correspondingly lower. There is less new surface area

added compared to the creation of the new nucleus and the free energy barrier of the process is lower. Tertiary nucleation occurs along an existing crystal edge and has the lowest free energy value due to the surface to volume ratio being even smaller.

1.3.2 Crystal Growth

The temperature dependence of nucleation is illustrated by the variation in the half-life ($t_{1/2}$) with increasing crystallisation temperature, which is attributed to the competition between nucleation and growth. A study by Zhang & Zeng in 1993 [9] found that the nucleation rate dropped as crystallisation temperature increased, enabling faster crystallisation at lower crystallisation temperatures, and a reduced half-life.

Growth occurs from secondary nucleation of the crystal growth faces and depending on the geometric shape of the crystals growth will develop in 1-, 2- or 3- dimensions, i.e. as rods, discs, spheres or more complex structures. Polymers usually crystallise from the melt as branching lamellae in which the polymer chain segments align perpendicular to the base. The initial nucleus starts as a single lamella which by continuous and frequent branching develops a spherical contour; the whole aggregate being called a spherulite. The spherulites grow radially and linearly with time until they impinge with neighbouring ones.

$$r = vt \qquad \text{Equation 1.3}$$

where r is the spherulite radius, v is the growth rate and t is time. The growth rate is strongly dependent on temperature and increases with decreasing temperature from the melting point, i.e the degree of super-cooling up to a maximum value, after which it decreases to zero as the glass temperature is approached.. The presence of a peak in growth rate occurs due to the combination of two competing factors; the

thermodynamic drive for crystallising increases as crystallisation temperature decreases and an increase in melt viscosity which makes transport of material to the growth face increasingly more difficult.

As a result of these effects, at high crystallisation temperatures close to the melting temperature, the growth rate reduces with increasing temperature and the half-life increases whereas close to the glass transition the rate decreases with decreasing temperature. This results in a maximum rate at a temperature about half way between the melting point and the glass transition temperature.

1.3.3 The Temperature Dependence of Growth

Due to the two effects of nucleation and viscosity the temperature dependence of this growth has been described by Turnbull & Fisher [10], as

$$g = g_0 \exp\left(-\frac{\Delta E_{act}}{RT}\right) \exp\left(\frac{\Delta fG^*}{RT}\right) \quad \text{Equation 1.4}$$

where g_0 is a constant, ΔE_{act} is the activation energy of viscous flow and ΔfG^* is the free energy of formation of the critical size nucleus. Near the glass transition temperature, $\left(-\frac{\Delta E_{act}}{RT}\right)$ is the dominant term, and growth occurs as polymer chains diffuse to the growth face. At temperatures near the melting point, $\left(\frac{\Delta fG^*}{RT}\right)$ is the dominant term, and the process is controlled by nucleation. The opposing temperature dependencies of the two exponential terms results in a peak in the plot of growth rate against temperature [11].

Equation 1.4 was modified by Hoffman & Lauritzen [12] to describe the temperature dependence of crystallisation of polymers over a wide range of temperatures to

$$g = g_0 \exp \left[\frac{-U^*}{R(T-T_\infty)} \right] \exp \left[\frac{-K_g}{T(\Delta T)} \right] \quad \text{Equation 1.5}$$

where U^* is the activation energy of viscous flow (taken as 6284 J mol^{-1}), T_∞ is the thermodynamic glass transition temperature, K_g the nucleation constant, T the crystallisation temperature, and ΔT the degree of super-cooling from the equilibrium melting temperature, T_m^0 .

The nucleation constant, K_g , takes a value dependent on the nucleation mechanism present and includes information on the geometry of the critical size nucleus. For lamellar crystals,

$$K_g = \frac{nb\sigma\sigma_e T_m^0}{\Delta H_v k} \quad \text{Equation 1.6}$$

where b is the layer thickness, taken to be the perpendicular separation of (010) planes. σ is the side surface free energy of the polymer crystal, σ_e the fold surface free energy, k is the Boltzmann constant, ΔH_v the enthalpy of fusion per unit volume and T_m^0 the equilibrium melting temperature.

The value of n depends on the nucleation regime defined by Hoffman & Lauritzen and the dependence of the nucleation rate on the degree of super-cooling. This analysis is based on several assumptions; the thickness of the lamellae remains constant, the lateral growth grows at the same rate as radial growth of the spherulite, there is no defect structures present and no lamellar thickening. The three regimes

differ in the relative rates of secondary nucleation on the growth surface, and rates of chain extension along the surface once nucleation has occurred.

Following the theory of nucleation of Hoffman and Lauritzen, Regime I is considered to occur at lower degrees of super-cooling, i.e. at higher crystallisation temperatures. Secondary nucleation of the surface is rate determining and dominates linear growth since the first act of nucleation is slow compared with coverage of the growth surface, with a crystalline mono-layer and there is a delay before the next layer is nucleated. Once a single nucleus has formed, chains are fully incorporated on to the crystal surface before any more nuclei are formed. For this model the growing surface is smooth and the value of n in Equation 1.6 is 4.

Regime II is normally observed at lower temperatures, where there is a higher degrees of super-cooling, and secondary nucleation is considered to be much quicker and occurs before the surface layer is covered. The rate of chain growth is roughly equal to the rate of secondary nucleation and each crystal is covered as the new nuclei formed have time to cover the surface. For this model, the surface is rough and there are numerous secondary nuclei on the growth face. The value of n for this nucleation regime is 2.

On further cooling and higher degree of super-cooling, the rate of nucleation is faster and greater than the rate of crystal growth. The crystal surface is almost entirely covered by the creation of new secondary nuclei and there is limited coverage of the growth surface by the mono-layer. This is Regime III, where crystallisation occurs near the glass transition temperature, and chains diffusion to the growth face is rate controlling [11]. Here the n value increases again to 4.

K_g illustrates the change in regime and the nucleation mechanism can be determined from the slope of the dependence of $\ln(g) + \frac{U^*}{R(T-T_\infty)}$ versus $\frac{1}{T\Delta T}$. Figure 1.3 represents a schematic diagram of the regime transitions between I, II and III.

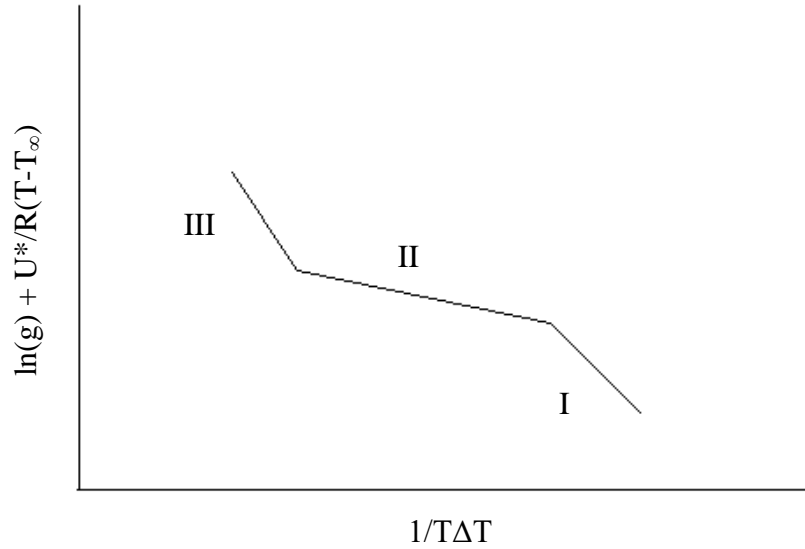


Figure 1.3 – Schematic representation of three nucleation regimes

1.4 Crystallisation Kinetics

The kinetics of the crystallisation process have generally been analysed using the Avrami equation [13-14], relating fractional crystallinity to time, i.e.

$$1 - X_t = \exp [-Zt^n] \quad \text{Equation 1.7}$$

where X_t is the fractional crystallinity, Z is a composite rate constant incorporating the characteristics of nucleation and growth, and n is the Avrami exponent, which takes different values depending on the crystallisation mechanism. Table 1.1 lists the crystallisation mechanisms and the corresponding values of n .

The Avrami equation is widely used as a means of analysing the time dependence of the crystallisation and has been applied to several polymers by many different authors. Some of these include polypropylene [15], poly(ϵ -caprolactone) [16], PET [17], PLLA [18] and PEEK [11]. Although this method of analysis has been widely used, it has been severely criticised since it invariably gives fractional constant n values which have little or no meaning in terms of the assumptions adopted by Avrami and the crystallisation mechanisms. It is likely many errors to occur from experimentation not being correctly implemented, to fast rates adopted, lack of isothermal conditions, the presence of induction periods before crystallisation occurs, and pre-crystallisation on cooling time [19]. There are also limitations to the Avrami equation itself, in assumptions made in its derivation, namely constant radial growth, where it is likely that the rate slows as the spheres start to impinge with each other. Other assumptions include constant crystallinity throughout the spherulites and constant nucleation rate or density throughout the polymer, and the presence of only one crystallisation mechanism [20]. There is evidence that two processes are present; primary and secondary crystallisations, each with different time dependences. Nevertheless in the absence of an alternative the Avrami equation is widely adopted and its limitations accepted. The Avrami equation exhibits the greater validity in following the primary process which appears to describe the growth of the spherulites up to the point where the primary process ends. Hay [21] reported that the Avrami equation provided a poor approximation at the latter stages of crystallisation, as the experimental data deviated from widely from the exponential dependence.

Table 1.1 – Avrami exponent value for different crystallisation mechanisms

Crystallisation Mechanism	Nucleation Type	n Value	Growth
Spheres	Sporadic	4.0	3 dimensions
	Pre-determined	3.0	3 dimensions
Discs	Sporadic	3.0	2 dimensions
	Pre-determined	2.0	2 dimensions
Rods	Sporadic	2.0	1 dimension
	Pre-determined	1.0	1 dimension

1.5 Polymer Morphology

The morphology developed within a polymeric melt during crystallisation is dependent on several factors including temperature, strain induced orientation, nucleating agents and cooling rate. If there is a high number of nuclei present, i.e. at low temperatures, then the spherulites are small and may not reach spherical contours whereas if there is a small number of nuclei, at higher crystallisation temperature the spherulites are large and well developed.

1.5.1 Single Crystals

Single crystals have been produced when polymers are crystallised from dilute solution, typically when the polymer content is less than 0.1% by weight. These crystals are very small and are made up of thin lamellae, often lozenge shaped and measuring about 10-20 nanometres (nm) thick depending on the crystallisation temperature. The polymer chains can be up to 1000 nm long when fully extended and

hence a single chain must be folded many times to enable it to be contained within the crystal. The top and bottom surfaces of the lozenge shaped crystal are made up of regular folds produced by adjacent re-entry of the chain.

There are two models used to describe the structure of the lamellae and their surface produced in polymer melt crystallisation. The 'regular folded array' model suggests regular or adjacent re-entry of the chains, with some loose folding occurring and some emergent chain ends present. The 'switch-board' model presents some folding of chains but with random re-entry and little adjacent re-entry. Most evidence suggests that this model is the morphology produced in the melt [22]. Random re-entry reduces the level of folding and so the solidification model proposed by Fischer [23] offers the theory that crystallisation takes place via straightening of sections of polymer coil followed by the alignment of these arrangements in regular arrays forming the lamellar structure.

1.5.2 Spherulites

Spherulites are regular birefringent structures with circular symmetry and exhibit a Maltese cross-optical extinction pattern. They grow radially via fibrillar growth in bundles into the amorphous phase from a nucleus and vary in size and number depending on the crystallisation temperature. This determines the critical size of the nucleating centre. Larger spherulites form near the melting point and more numerous smaller spherulites form at lower temperatures.

Spherulitic growth occurs in two stages. During primary crystallisation the spherulite grows from an initial fibril or lamella, which results from the primary nucleus. The thickness of the lamellae is constant determined by the critical size

nucleus and growth occurs by extension of the length and breadth so that it grows into a thin sheet of constant thickness. However, as crystallisation continues branching occurs until a branched lamellar assembly is created and these branches bend and twist upon growth to produce a spherical boundary which grows radially. Further radial growth produces larger spherulites until impingement between adjacent spherulites stops further growth. Once impingement takes place, further development occurs via in-filling between the lamellae. Additional secondary crystallisation by which the lamellae as originally laid down thicken with time at the expense of amorphous material between the lamellae. This process has a lower time dependency than that of primary crystallisation and is readily distinguished by a change in the analysis of the crystallisation kinetics. The rate and extent of secondary crystallisation depends on crystallisation temperature.

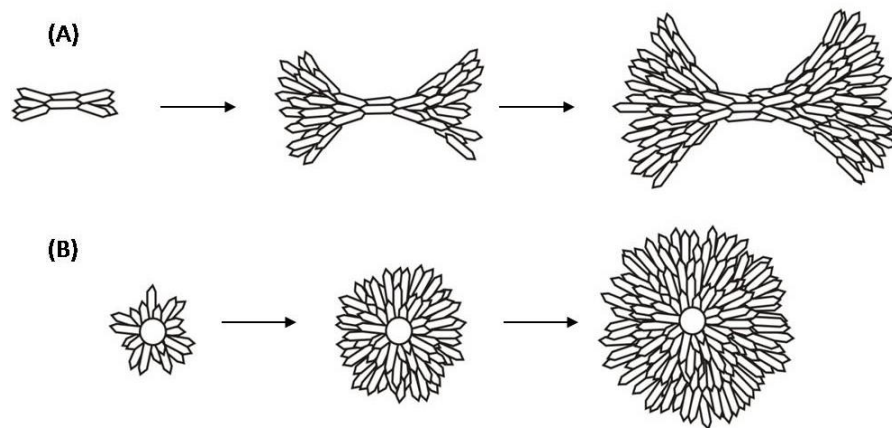


Figure 1.4 – Formation of spherulites [39]

1.6 The Melting of Polymers

The process of melting is the reverse transition of crystallisation and eradicates any crystal order present in the material by the production of a liquid structure. Melting characteristics of polymers differ substantially from those of low molecular weight materials as melting takes place over a range of temperatures. The melting point also depends on thermal history, particularly crystallisation temperature, and heating rate. Other factors affecting the melting point of a polymer include symmetry, flexibility and polarity where chains without large pendant groups or polar groups have a reduced melting point as less thermal energy is required to encourage chain motion and promote rotation around the chain.

Generally the melting point is taken to be the temperature of the last trace of crystallinity, as this represents melting of the thickest crystals, however peak temperature is also used since it is measured more accurately and represents some average value of the lamellae thickness. The three melting points which have been adopted, onset, peak and last trace, are illustrated in Figure 1.5.

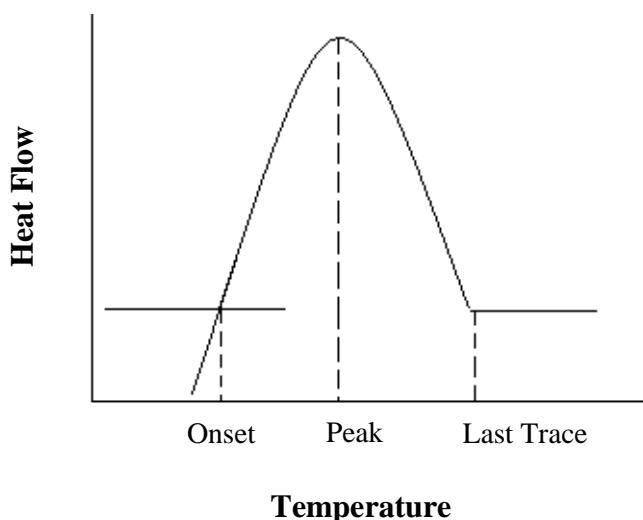


Figure 1.5 – Illustration of the three measures of melting

Due to the variability in the measurement of melting on heating rate, crystallisation temperature, and thermal history the equilibrium melting temperature, T_m^0 , alone has some thermodynamic significance and used in analysing the temperature dependence of crystallisation. This is defined as the temperature at which infinitely thick crystals melt, and the point at which melting temperature is not suppressed by surface energy terms. T_m^0 is measured via extrapolation of experimentally measured melting points at different crystallisation temperatures.

Hoffman & Weeks [24] have derived a relationship between the melting point and crystallisation temperature, which produces a value of T_m^0 from the observed melting temperature. This relationship is

$$T_m = T_m^0 (1 - 1/2\beta) + T_c/2\beta \quad \text{Equation 1.8}$$

where β is equal to $(\sigma_e l / \sigma l_e)$ and σ is the fold surface free energy, l is the lamellae thickness and the subscript e refers to equilibrium conditions. A plot of T_m against T_c is linear and the intersection of this line with the line $T_m = T_c$ gives the equilibrium melting point. A graphical representation of this is shown in Figure 1.6. If there is no annealing or recrystallization during melting, β is equal to 1.0 and the plot of T_m versus T_c is linear with a slope of $1/2\beta$. This line interpolates to the line of $T_m = T_c$ at T_m^0 when the slope is equal to 0.5. Assumptions made when deriving Equation 1.8 ignore the presence of any recrystallization or annealing.

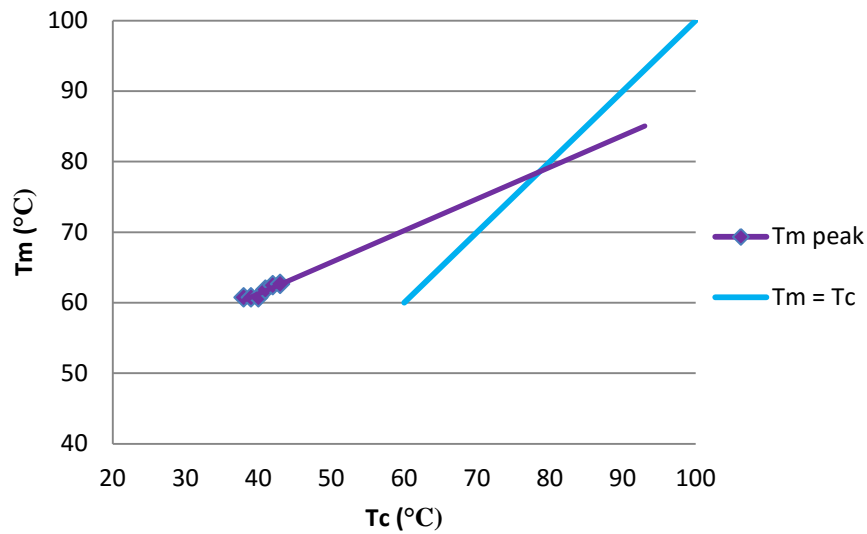


Figure 1.6 – Graphical representation of Hoffman-Weeks plot for equilibrium melting temperature

1.7 Physical Ageing in Polymeric Materials

Physical ageing is commonly observed in polymeric materials and is exhibited as a change in property as a function of storage time at constant temperature, when no other external condition is influencing the material properties. Ageing can be measured either via mechanical response, or change in specific volume or enthalpy [25]. The term *physical* ageing distinguishes this process from thermal or oxidative degradation, environmental or biological ageing as it exhibits reversible rather than irreversible changes in structure and chemical modification.

Physical ageing has most commonly been associated with amorphous polymers and is observed when samples are cooled from above to below the glass transition temperature, T_g . This is illustrated by a reduction in enthalpy and a shift in the creep response to longer time scales. These changes in properties occur due to the non-equilibrium state of amorphous polymers below the T_g as ageing is isolated from the

external environment, and there is a thermodynamic drive encouraging a move to equilibrium conditions, as observed above the T_g . [25-26].

1.7.1 The Thermodynamics of Ageing

On cooling through the T_g the molecular vibrations and rotations required for the material to accommodate the changes in properties with temperature slow down to such an extent that they require more time than is allowed by the cooling rate. This means that chains configurations are 'frozen in' and remain so for as long as the temperature is maintained below the T_g . This means that below the T_g the material has excess thermodynamic quantities (volume, entropy, enthalpy) and so there is a driving force towards equilibrium limited in extent by the difference between the observed quantity and the extrapolated equilibrium value, such that the maximum enthalpy change is

$$\Delta H_{\infty} = \Delta c_p \Delta T \quad \text{Equation 1.9}$$

where Δc_p is the difference in heat capacity between the liquid and the glass at T_g and ΔT the difference between T_g and the ageing temperature, and the temperature dependent rate of achieving this equilibrium.

At constant temperature below T_g , molecular motions gradually allow equilibrium to be achieved over time and the process of physical ageing will result in a reduction of volume and enthalpy towards the equilibrium value. This continues until equilibrium is attained; the time taken to reach equilibrium increases as ageing temperature is reduced. This is represented graphically in Figure 1.7, which shows the change in length, volume or enthalpy as a function of temperature.

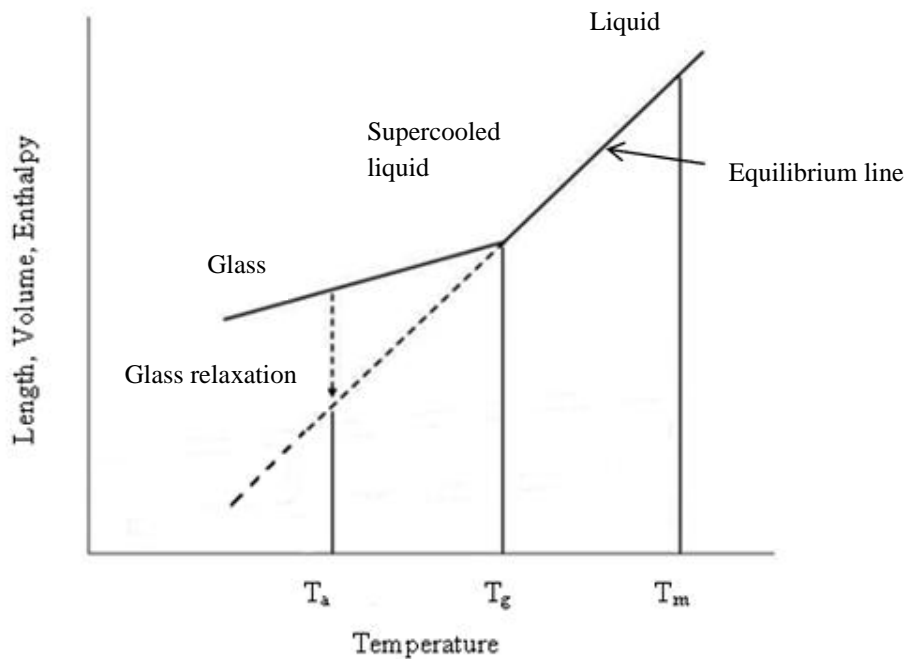


Figure 1.7 – Change in length, volume and enthalpy with temperature and the effect of ageing

On cooling, the thermodynamic properties deviate from the equilibrium line at the T_g , and this temperature depends on cooling rate. Ageing below T_g at a constant temperature will allow the enthalpy to decrease progressively with time from its original value depending on the rate of ageing and approach equilibrium for that temperature. On reheating after ageing the sample does not follow the same temperature dependent pathway as on cooling but lags behind it until it is above T_g when it rapidly returns with time to the equilibrium property versus temperature dependence. This results in an increase in enthalpy which is attributed to the extent of ageing.

Physical ageing is associated with glass formation in amorphous material. It is a reversible process and the properties are completely restored on heating above T_g and the sample subsequently re-ages on cooling below T_g .

1.7.2 Ageing in Semi-Crystalline Polymers

Ageing in semi-crystalline polymers is a much more complicated process and has caused considerable confusion in the literature as regards its nature. It appears to occur as a result of structural changes in the amorphous phase above T_g but physical ageing associated with the relaxation of amorphous regions below T_g has also been observed in the amorphous phase below a T_g raised by the sample being partially crystalline. In the study of ageing of semi-crystalline PCL we will rule out the latter since it is very unlikely to be a problem when the glass transition of the material is so low (-60°C) and as such is unlikely to be a technical problem in conventional uses of the polymer. Accordingly the study of ageing has been limited to that associated with structural changes in amorphous regions above T_g .

Semi-crystalline polymers consist of two amorphous regions; the mobile amorphous fraction or bulk, which makes up at least 50% of the material and is relatively distant from the crystalline regions, is able to move unrestricted as in amorphous polymers; the rigid amorphous fraction is close to the surface of the lamellae and so is more constrained with limited mobility. The distinction between the two areas of amorphous material within the semi-crystalline polymer results in an increase in the observed T_g with crystallinity extending above that of the bulk amorphous material. This is due to the presence of constrained material which requires a higher level of energy to encourage motion within the chains and has been used to explain why semi-crystalline material can age above its T_g [27-28].

Finally there is a crystalline phase made up of branching lamellae which may further crystallise and alter the material properties due to the increased crystallinity.

1.8 Project Aims and Objectives

Polycaprolactone (PCL) is a re-emerging material, with numerous studies investigating its performance when blended with other polymers [29-33]. Due to its biodegradability and ability to function within the human body, the material also has importance as an independent polymer, though little research seems to have been done in this area. As the material properties are largely dependent on crystallinity, this project focuses on the crystallisation kinetics and the impact of ageing on morphology, mechanical properties and melting behaviour of the polymer.

Several methods have been adopted within this thesis to study the crystallisation kinetics of polycaprolactone. Differential Scanning Calorimetry is used to study the primary crystallisation kinetics, as this method has been widely publicised as a suitable technique for this purpose [34-37]. Fourier Transform Infra-Red Spectroscopy (FTIR) is used to explore the thermal behaviour of PCL at a molecular level within individual functional groups during heating and cooling. This is combined with 2D-spectrometry correlation mapping to interpret the change in intensity of amorphous and crystalline bands, which could then be used to analyse secondary crystallisation, as the DSC is not sensitive enough to provide information about this process [38].

Once the crystallisation kinetics of the material are analysed, the effect of ageing and the development of crystallinity is assessed in relation to change in mechanical properties as well as the melt behaviour of the polymer. This provides a platform from which suggestions will be made regarding the mechanism of aging in crystalline polymers above T_g .

1.9 References

1. PCL data sheet (www.perstorp.com)
2. Braud, C., Devarieux, R., Atlan, A., Ducos, C. & Michel, V. (1998), Capillary zone electrophoresis in normal or reverse polarity separation modes for the analysis of hydroxy acid oligomers in neutral phosphate buffer, *Journal of Chromatography B: Biomedical Science Applications*, **706**, 73-82
3. Labert, M. & Thielemans, W. (2009), Synthesis of polycaprolactone: a review, *Chemical Society Reviews*, **38**, 3484-3504
4. Woodruff, M. A. & Hutmacher, D. W. (2010), The return of a forgotten polymer – polycaprolactone in the 21st century, *Progress in Polymer Science*, **35**, 1217-1256
5. Wunderlich, B. (1976), *Macromolecular Physics 2: Crystal Nucleation, Growth, Annealing*, Academic Press, New York: USA
6. Yang, J., McCoy, B. J. & Madras, G. (2005), Distribution kinetics of polymer crystallisation and the Avrami equation, *Journal of Chemical Physics*, **122**, 064901
7. Cowie, J. M. G. (1973), *Polymers: Chemistry and Physics of Modern Materials*, International Textbook Company Limited, Aylesbury: UK
8. Young, R. J. & Lovell, P. A. (1991), *Introduction to Polymers 2nd Edition*, Chapman & Hall, London: UK
9. Zhang, Z. & Zeng, H. (1993), Nucleation and crystal growth of PEEK on carbon fiber, *Journal of Applied Polymer Science*, **48**, 1987-1995
10. Turnbull, D. & Fisher, J. C. (1949), Rate of nucleation in condensed systems, *Journal of Chemical Physics*, **17**, 71-73

11. Jenkins, M. J., Hay, J. N. & Terrill, N. J. (2003), Structure evolution in melt crystallised PEEK, *Polymer*, **44**, 6781-6787
12. Lauritzen, J. I. & Hoffman, J. D. (1973), Extension of theory of growth of chain-folded polymer crystals to large under-coolings, *Journal of Applied Physics*, **44**, 4340-4352
13. Avrami, M. (1940), Kinetics of phase change II transformation – time relaxations for random distribution of nuclei, *Journal of Chemical Physics*, **8**, 212-224
14. Avrami, M. (1941), Kinetics of phase change and microstructure kinetics of phase change III, *Journal of Chemical Physics*, **9**, 177-184
15. Dudic, D., Djokovic, V. & Kostoski, D. (2004), The high temperature secondary crystallisation of aged isotactic polypropylene, *Polymer Testing*, **23**, 621-627
16. Xie, W. Y., Jinag, N. & Gan, Z. H. (2008), Effects of multi-arm structure on crystallisation and biodegradation of star-shaped poly(ϵ -caprolactone), *Macromolecular Biosciences*, **8**, 775-784
17. Li, G., Yang, S. L., Jiang, J. M., Jin, J. H. & Wu, C. X. (2008), The complicated influence of branching on crystallisation behaviour of poly(ethylene-terephthalate), *Journal of Applied Polymer Science*, **110**, 1649-1655
18. He, Y., Fan, Z. Y., Hu, Y. F., Wu, T., Wei, J. & Li, S. M. (2007), DSC analysis of isothermal melt crystallisation, glass transition and melting behaviour of poly(L-lactide) with different molecular weights, *European Polymer Journal*, **43**, 4431-4439
19. Lorenzo, A. T., Arnal, M. L., Albuerne, J. & Müller, A. J. (2007), DSC isothermal polymer crystallisation kinetics measurements and the use of the Avrami equation to fit the data: guidelines to avoid common problems, *Polymer Testing*, **26**, 222-231

20. Hay, J. N. & Przekop, Z. J. (1978), On a non-exponential transformation equation for spherulitic crystallisation, *Journal of Polymer Science: Polymer Physics Edition*, **16**, 81-89
21. Hay, J. N. (1971), Application of the modified Avrami equations to polymer crystallisation kinetics, *British Polymer Journal*, **3**, 74-82
22. Mandelkern, L. (1975), *Characterisation of Materials in Research: Ceramics and Polymers*, Syracuse Uni Press, New York: USA
23. Fischer, E. W. (1978), mStudies of structure and dynamics of solid polymers by elastic and inelastic neutron scattering, *Pure Applied Chemistry*, **50**, 1319-1341
24. Hoffman, J. D. & Weeks, J. J. (1962), Melting processes and equilibrium melting temperature of polychlorotrifluoroethylene, *Journal of Research of the National Bureau of Standards Section A: Physics and Chemistry*, **66A**, 13-28
25. Hutchinson, J. M. (1995), Physical aging of polymers, *Progress in Polymer Science*, **20**, 703-760
26. White, J. R. (2006), Polymer aging: physics, chemistry or engineering? Time to reflect, *Comptes Rendus Chimie*, **9**, 1396-1408
27. Zuza, E., Ugartemendia, J. M., Lopez, A. & Meaurio, E. (2008), Glass transition behaviour and dynamic fragility in polylactides containing mobile and rigid amorphous fractions, *Polymer*, **49**, 4427-4432
28. Righetti, M. C., Tombari, E. & Di Lorenzo, M. L. (2008), Crystalline, mobile amorphous and rigid amorphous fractions in isotactic polystyrene, *European Polymer Journal*, **44**, 2659-2667

29. Pérez, E., Pérez, C. J., Alvarez, V. A. & Bernal, C. (2013), Fracture behaviour of a commercial starch/polycaprolactone blend reinforced with different layered silicates, *Carbohydrate Polymers*, **97**, 269-276
30. Dong, J., Yuan, T., Yu, X. T., Jia, L. Y. & Mei, Z. (2012), Melting and crystallisation behaviours of electrostatic spinning polycaprolactone/polyethylene glycol blends, *High Performance Polymers*, **24**, 441-446
31. Xiong, R., Hameed, N. & Guo, Q. (2012), Cellulose/polycaprolactone blends regenerated from ionic liquid 1-butyl-3-methylimidazolium chloride, *Carbohydrate Polymers*, **90**, 575-582
32. Yasin, M. & Tighe, B. J. (1992), Polymers for biodegradable medical devices: VIII. Hydroxybutyrate-hydroxyvalerate copolymers: physical and degradative properties of blends with polycaprolactone, *Biomaterials*, **13**, 9-16
33. Defieux, G., Groenickx, G. & Reynaers, H. (1989), Miscibility, crystallisation and melting behaviour, and semicrystalline morphology of binary blends of polycaprolactone with poly(hydroxyl ether of bisphenol A), *Polymer*, **30**, 2164-2169
34. Hay, J. N. & Mills, P. J. (1982), The use of differential scanning calorimetry to study polymer crystallisation kinetics, *Polymer*, **23**, 1380-1384
35. Lui, M., Zhao, Q., Wang, Y., Zhang, C., Mo, Z. & Cao, S. (2003), Melting behaviours, isothermal and non-isothermal crystallisation kinetics of nylon 1212, *Polymer*, **44**, 2537-2545
36. Mucha, M. & Krolkowski, Z. (2003), Application of DSC to study crystallisation kinetics and polypropylene containing fillers, *Journal of Thermal Analysis and Calorimetry*, **74**, 549-557

37. Saadi, S., Ariffin, A. A., Ghazali, H. M., Miskandar, M. S., Boo, H. C. & Abdulkarim. S. M. (2012), Application of differential scanning calorimetry (DSC), HPLC and pNMR for interpretation of primary crystallisation caused by combined low and high melting TAGs, *Food Chemistry*, **132**, 603-612
38. Chen, Z., Hay, J. N. & Jenkins, M. J. (2013), The kinetics of crystallisation of poly(ethylene terephthalate) measured by FTIR spectroscopy, *European Polymer Journal*, **49**, 1722-1730
39. <http://gower.mse.ufl.edu/images/research/53-%20spherulites.jpg> <accessed 10/09/14>

Chapter 2. – Materials, Apparatus and Experimental Procedures

2.1 Materials

2.1.1 Poly (ϵ -caprolactone).

Polycaprolactone PCL, (CAPA 6800) was supplied in pellet form by Perstorp (Warrington, UK). The number and weight average molecular weights were 80 and 120 kg mol⁻¹ respectively, and polydispersity 1.50 (manufacturer's data). The polymer was prepared using various methods, depending on the experiment being carried out, and is described in the following sections.

Property	Value
Melting Point	58-60 °C [1]
Glass Transition Temperature	(-65)-(-60) °C [2-4]
Density	1.07-1.20 g/cm ³ [2-3]
Melt Flow Index	4.03-2.01 g/10 min [1]
Elongation to break	800% [1]
Young's Modulus	210-440 MPa [2-3]

Table 2.1 – Properties of PCL

2.1.2 Potassium Bromide

Potassium bromide (KBr) powder, of FTIR grade, was supplied by Sigma Aldrich (Dorset, UK), and pre-dried in an air-oven overnight at 120 °C, before being pressed into discs.

Property	Value
Vapour Pressure	< 0.01 mmHg (20 °C) 1 mmHg (795 °C)
Purity	≥ 99% (trace metals basis)
Melting Point	734 °C

Table 2.2 – Properties of KBr, as given on manufacturer’s data sheet

2.1.3 Dichloromethane

Dichloromethane (research grade) was used as a solvent for PCL. It was supplied by Sigma Aldrich (Dorset, UK) and used as received.

Property	Value
Molecular Weight	84.93
Density	1.325 g/ml (25°C)
Melting Point	-97°C
Boiling Point	40°C

Table 2.3 – Properties of DCM, as given on manufacturers data sheet

2.2 Apparatus and Experimental Procedures

2.2.1 Differential Scanning Calorimetry (DSC)

Differential Scanning Calorimetry (DSC) was used as a thermo-analytical technique to measure the temperature and heat produced at phase transitions of PCL, as a function of time and temperature. These measurements provided detailed information about any physical or chemical changes which are endothermic or exothermic. During phase transitions heat is evolved or taken in, required to maintain the sample at the same temperature as the reference and DSC measures this as a function of time and temperature.

During melting, which is an endothermic process, additional heat is required to maintain the sample at the programmed temperature of the DSC and this is supplied by increasing the electrical energy of the sample furnace. On crystallisation, which is an exothermic process, less power is required to maintain the sample at the temperature as heat is evolved. The DSC is a 'power compensation' calorimeter and measures the difference in heat flow between the sample and reference and produces an output of heat flow versus time or temperature. A typical DSC trace is depicted in Figure 2.1.

The DSC can be used to measure:

- Glass transitions [9]
- Melting points [8-9]
- Crystallisation time [5, 8-9]
- Crystallisation temperature [5-6]
- Heats of fusion [7, 10]

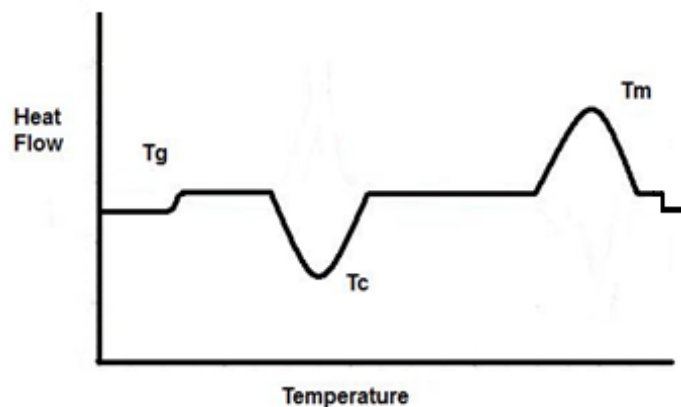


Figure 2.1 – Typical DSC trace

- % crystallinity [7, 10]

2.2.1.1 Experimental Procedure

A Perkin Elmer DSC 7 (Cambridge, UK), controlled by proprietary Pyris software, linked to a computer was used to measure the changes in relative heat flow with time and temperature on heating or cooling a sample at fixed rate. A schematic representation of the DSC used in this project can be seen in

Figure 2.2. This power-compensation DSC consisted of a sample and reference calorimeter whose temperature are controlled independently using separate heaters, and matched to keep them at the same temperature by varying the power input into each heater. A cooling system was attached to the DSC to enable controlled cooling, as well as maintain isothermal conditions at temperatures approaching room temperature. The temperature of the instrument was calibrated using a 2-point calibration using thermodynamic sub-standard calibrants by measuring the melting points of ultra-pure metals (99.999%): indium (m.pt. 156.6 °C) and tin (m.pt. 231.9 °C). These were recorded at a heating rate of 5 °C/min. The thermal response of the calorimeter was calibrated from the enthalpy of fusion of a known mass of indium; the heat of fusion was taken to be 28.45 J/g.

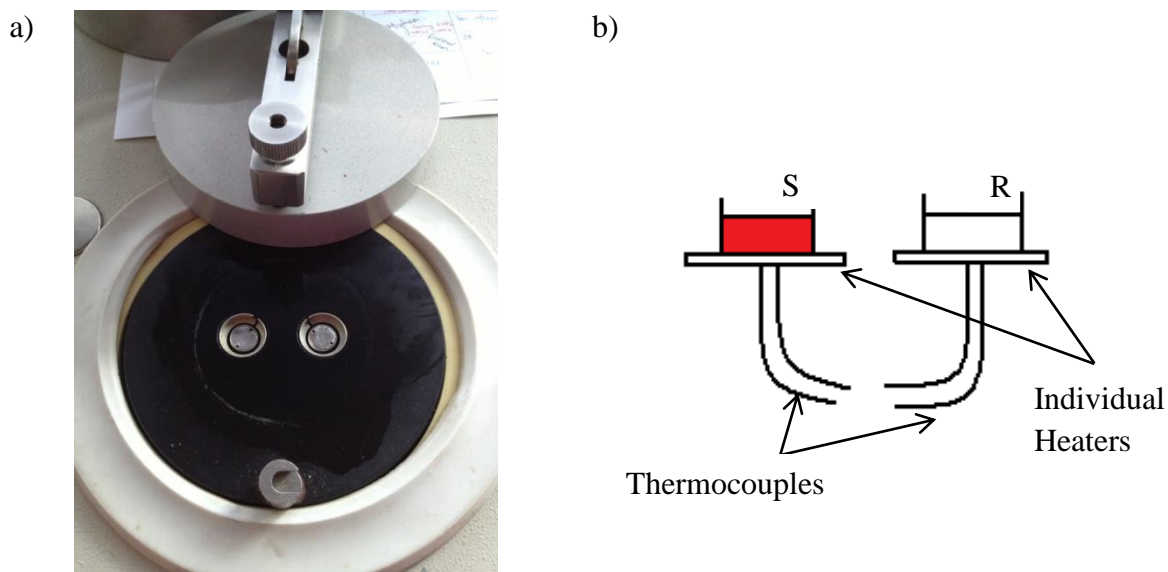


Figure 2.2 – DSC pan heaters (a) and schematic diagram of a DSC (b)

2.2.1.1.1 Isothermal Crystallisation

Isothermal crystallisation experiments were carried out on film samples of PCL 6800 prepared by dissolving 3.5 g of polymer pellets in 30 cm³ of dichloromethane. The solution was then transferred into a petri-dish from and the solvent allowed to evaporate in a fume cupboard to a thin film of approximately 500 μm. Two circular disc shaped samples, cut to the size of a DSC sample pan using a hole-punch, were placed on top of one another in the DSC pan, sealed with an aluminium lid. This gave a sample thickness of approximately 1 mm and a mass of 15 mg ± 1 mg. The size of sample provided a measurable change of heat on crystallisation and melting over a reasonable temperature range or rate of heating.

These samples were heated to 70°C and held in the melt for 2 min before being rapidly cooled, at 320°C/min, to specific isothermal temperatures and the heat evolved during crystallisation measured as a function of time. Heat flow was measured until the

response returned to the calorimeter baseline. Each experiment was followed for 40 to 120 min depending on the crystallization temperature to enable full crystallisation of the sample. All results are an average of three.

2.2.1.1.2 Nonisothermal Crystallisation

Non-isothermal crystallisation experiments were also carried out on samples of PCL 6800, prepared as outlined above. These samples were heated to 70 °C and held in the melt for 2 min before being cooled to room temperature at a range of cooling rates. All rate results are an average of three.

2.2.1.1.3 Melting

The melting behaviour of PCL was also investigated by re-melting each sample after crystallisation and on cooling to room temperature. The samples were heated from room temperature to 70 °C at a rate of 10 °C/min and the melting endotherms recorded. Three measurements of melting were recorded, as different authors have suggested different definitions for the ‘melting point’. It may be considered as either the onset of melting, the peak temperature corresponding to the temperature of maximum rate of melting, or as the last trace of crystallinity where all traces of crystallinity have disappeared. The latter is suggested by Hoffman & Weeks [11], as the temperature at which all lamellae have melted upon examination by optical microscope, and so is the melting point most often adopted in this thesis. The three suggested measures of melting are shown in Figure 2.3.

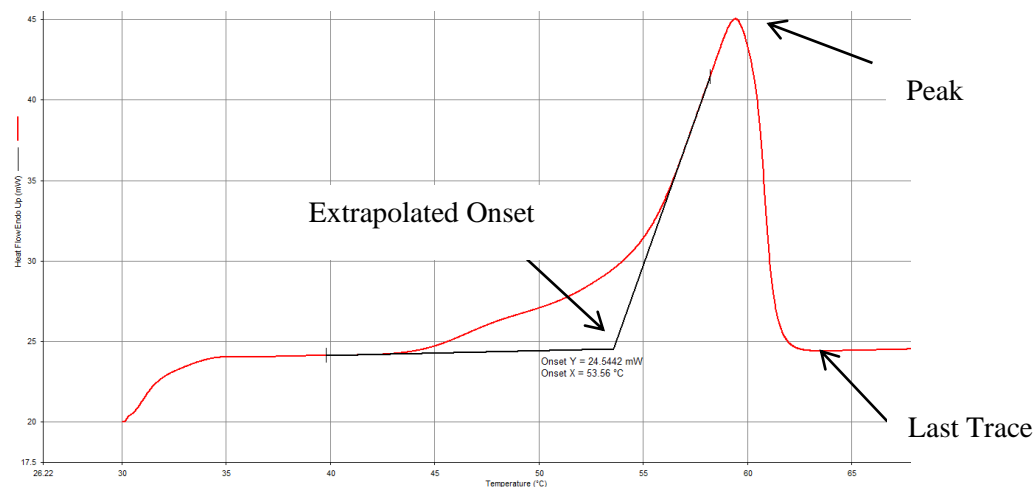


Figure 2.3 – Three measures of melting

2.2.1.1.4 Annealing Studies

Melting traces of samples of PCL 6800, cut from a hot-pressed plaque (see section 2.4) and cut to the size of a DSC sample pan using a hole-punch were measured after being stored in different environments over time. The storage conditions were chosen so to cover a range of temperatures across the operational temperature range for the polymer. These included conditioning in a freezer at -18 °C, in a fridge at 5 °C, at room temperature measured at 20 °C and in an oven set at 50 °C. The samples weighed 22.5 mg ± 1 mg and were heated to the melt at a rate of 10 °C/min with the melting endotherm measured as a function of time. The enthalpy was measured from under the endotherm integrated with respect to time and the weight fraction crystallinity of the sample calculated using the theoretical value for 100% crystalline PCL, which can be shown mathematically as;

$$X_c = \frac{\Delta H_f(T_m)}{\Delta H_f^0(T_m^0)} \quad \text{Equation 2.1}$$

The heat of fusion of 100% crystalline PCL was taken as 139.3 J/g [12]. Each result is an average of three.

2.2.1.1.5 High Cooling Rates

A Mettler Toledo DSC 1/500, controlled by STARE software, and linked to a computer was used to measure changes in heat flow with temperature. Circular disc samples of $15 \text{ mg} \pm 1 \text{ mg}$, stamped with a hole-punch from a solvent cast thin film, were sealed within aluminium pans. This equipment was preferred to the Perkin Elmer DSC7 for these experiments as the enhanced cooling system enabled lower temperatures to be achieved and controlled cooling at faster rates.



Figure 2.4 – Mettler Toledo DSC 1/500

High cooling rate experiments consisted of heating samples to the melt temperature of $70 \text{ }^\circ\text{C}$, where they were held for 2 min before being cooled at high cooling rates of 20 to $50 \text{ }^\circ\text{C}/\text{min}$, down to a temperature at which the calorimeter response had returned to baseline. Cooling curves were produced for each cooling rate,

using an empty sample pan, to eliminate slope of the baseline. Each result is an average of three.

2.2.2 Fourier Transform Infra-Red Spectroscopy (FTIR)

Fourier Transform Infrared Spectrometry (FTIR) was the preferred method of measuring infrared (IR) spectrum since it could produce a series rapidly with temperature or time as the sample was changing phase or chemical composition. The spectra could readily be used to analyse the structure, chain conformation and change in order. An IR spectrum acts as a fingerprint, since each organic compound produces a different pattern of absorption peaks at different frequency characteristics of the groups present and their environment. This enables qualitative analysis of every different material.

FTIR spectrometry involves the use of an interferometer, which has a beam-splitter to divide an incoming infrared beam into two separate beams. One of these beams is reflected by a stationary mirror, whilst the other is reflected off a moving mirror, causing the two beams to travel different distances. These are recombined at the beam-splitter, and the resulting signal is an interferogram since the two beams are out of phase. A frequency spectrum can be produced from the interferogram, which is the sum of waves containing information about wavenumber of a particular infrared peak and peak intensity at that wavenumber, has been decoded. This occurs via the mathematical technique of Fourier transformation, which calculates the spectra from summed sinusoidal waves in the interferogram.

It is possible to analyse conformational changes within the polymer sample by changing the experimental conditions, such as temperature and crystallinity, and by

monitoring changes in absorbance and peak position within the IR spectrum on heating and cooling. FTIR has been used to study conformational changes and the crystallisation behaviour of polymer samples in the form of thin films and can provide information about the molecular arrangement within the polymer whilst it is amorphous or crystalline.

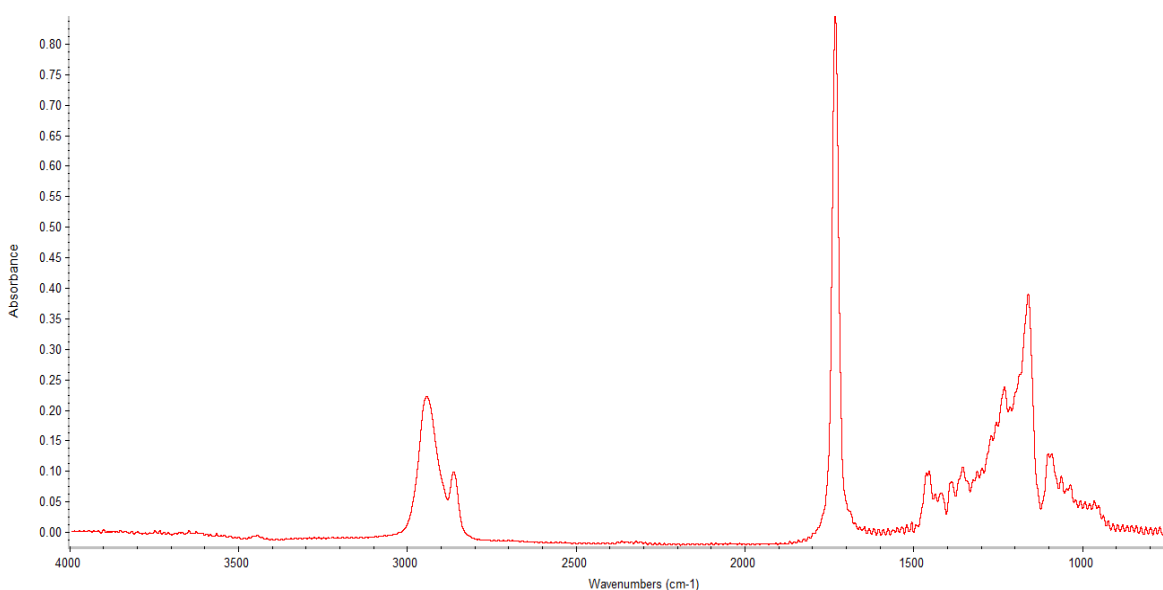


Figure 2.5 – Typical FTIR spectrum

IR spectra are produced by detecting changes in absorption intensity as a function of frequency. An absorbance peak is produced due to continuous vibrations of the individual atoms within molecular groups. When the frequency of a specific vibration is equal to that of the IR radiation directed on the molecule, then radiation will be absorbed [13]. Stretching, rotation and bending of bonds are the main types of molecular motion detected, with associated energy from IR absorbance being converted into these motions. A combination of vibrational and other rotational movements lead to the creation of the absorbance bands most commonly found in the region 4000 – 400 cm^{-1} of the IR spectrum.

FTIR spectrometry has many advantages over other dispersive techniques. Measurements can be achieved quickly due to frequencies measured simultaneously and sensitivity is greater due to increased sensitivity of detectors, a higher optical throughput (reducing noise), and signal averaging.

2.2.2.1 Experimental Procedure

A Thermo Scientific Nicolet 8700 (Loughborough, UK), equipped with a DTGS-KBr detector and controlled by Omnic 8.1 software, was used to collect spectra of PCL during transmission experiments. For this technique, a Linkam THM600 (Surrey, UK) hot-stage cell was loaded into the spectrometer and an infra-red beam passed through the sample. A Linkam PR600 thermometric stage was attached to the spectrometer to monitor temperature control and a Bibby Scientific Techne TE-10D (Stone, UK) water bath was attached for cooling.

a)



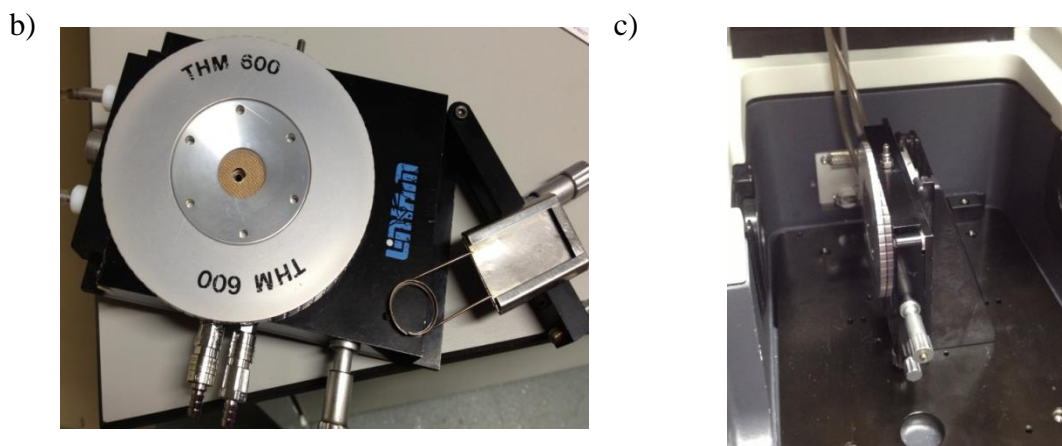


Figure 2.6 – ThermoScientific Spectrometer (a) and Linkham Hotstage (b) fitted in the FTIR spectrometer (c)

2.2.2.2 Sample Preparation

Pre-dried KBr powder was pressed into 16 mm diameter discs, using a Specac (Slough, UK) die-press at 15 tons. One background disc of 300 mg and two sample discs of 150 mg were produced. Drops of polymer solution, which was made up of 1 polymer pellet and 25 ml of dichloromethane solvent, were placed on the surface of a KBr disc and allowed to evaporate under an extractor fan. The sample was then blast-heated to ensure all solvent had evaporated. The thickness of the sample was adjusted to maintain an absorbance less than 1, so that the absorbance band could be determined accurately. The second sample disc was then placed on top to sandwich the sample between both discs.

2.2.2.3 Isothermal Crystallisation

A background spectrum was initially measured along with a sample spectrum which was measured against this background trace so to eliminate absorbance bands characteristic of water vapour and carbon dioxide present in the atmosphere. For

isothermal studies, the PCL thin film was heated from room temperature to 70 °C at a rate of 80 °C/min and held in the melt for 2 min to remove any trace of crystallinity. The sample was then rapidly cooled to the isothermal hold temperature and spectra were recorded at a resolution of 4 cm⁻¹ in sets of 100 scans across 1000 min.

2.2.2.4 Peak Resolution of FTIR Spectra

In order to analyse the crystallisation kinetics of the samples, it was necessary to separate the overlapping regions of the carbonyl peak, which was chosen as the analysis peak as this gave the strongest absorbance value. The baseline was corrected to the extremes of the wavelength range for this peak. The overlapping carbonyl bands were attributed to amorphous and crystalline regions and appeared at 1735 and 1725 cm⁻¹ respectively. The amorphous region was determined by taking a spectrum whilst in the melt, where a single amorphous band was present.

The process of resolving the peaks could be done automatically via a function within the Omnic software, but some variables could be adjusted manually to improve accuracy. An example of the peak resolution process is depicted in Figure 2.7. The two main peaks, the amorphous peak at 1735 cm⁻¹ and the crystalline peak at 1725 cm⁻¹, were set and fixed at the wavenumber of the peak maxima. By altering noise peaks either side of the amorphous and crystalline bands to produce the best match with the sample spectrum, it was possible to reduce the error calculated between the resolution trace and the sample trace. Using the 'Fit Peaks' function adjusted the Lorentzian values of the peaks and provided details of the heights of the two main bands. Locking all of the noise peaks into position enabled the same resolution to be used across all spectra within the series, producing details of changes in peak height of the amorphous

and crystalline regions over time. This information could then be used to determine crystallinity and kinetic parameters.

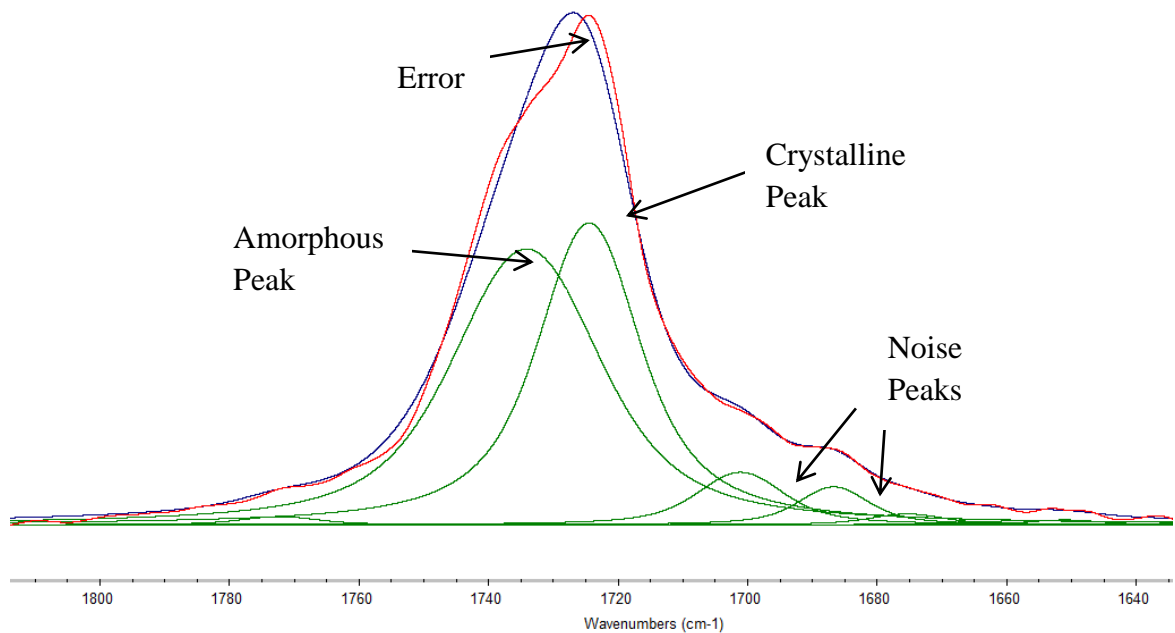


Figure 2.7 – Example of peak resolution within Omnic

2.2.3 Hot Press

A Moore E1127 hydraulic hot-press (Birmingham, UK) was used to press 35 g of PCL into plaques of size 180 x 150 x 1 mm. The polymer pellets were initially contained within two plates, which were heated between two platons at 150 °C for 3 min. The polymer was then compressed and held under load of 10 ton for a further 4 min, before being released and water cooled to room temperature. Dog bones and DSC samples were cut and placed in different storage temperatures for annealing studies.

Initial testing of plaques was carried out using DSC (see section 2.2.1.4) and Instron mechanical tester (see section 2.5) so any changes in crystallinity and mechanical properties could be monitored over time.

2.2.4 Instron Mechanical Tester

Tensile load-extension experiments were carried out on an Instron 5566 (High-Wycombe, UK) controlled by Merlin software, linked to a computer.



Figure 2.8 – Instron Mechanical Tester

Tensile dog-bone shaped test pieces were stamped out from a hot-pressed plaque (see section 2.4) and stored at different temperatures (see section 2.2.1.4). These had a gauge length of 25 mm and a width of 4 mm. The thickness of the samples was calculated as an average of three measurement points taken across the gauge length.

Specimens were clamped vertically within the tensometer and a cross-head speed of 20 mm/min was applied, with the response of the sample recorded graphically as a stress-strain curve.

Engineering stress was determined according to

$$\sigma = \frac{F}{A_0}$$

where F is the applied load and A_0 is the initial cross-sectional area of the test piece.

Strain was determined according to

$$\varepsilon = \frac{l}{l_0}$$

where l is the sample length on extension and l_0 the original sample length. The yield stress was taken as the stress at the point of yield, and the modulus was calculated prior to the proportional limit, using the following mathematical phrase;

$$E = \frac{\sigma}{\varepsilon}$$

All results were averaged over five repeat tests on the same samples.

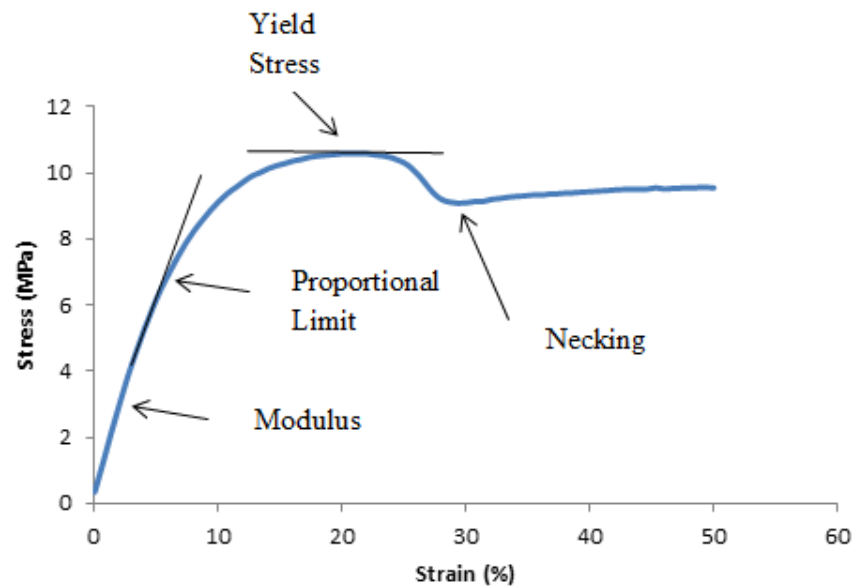


Figure 2.9 – Illustration of a typical stress-strain curve, highlighting its main components

2.3 References

1. Product data sheet (www.perstorp.com)
2. Van de Velde, K. & Kiekens, P. (2002), Biopolymers: overview of several properties and consequences on their applications, *Polymer Testing*, **21**, 433-442
3. Labet, M. & Thielemans, W. (2009), Synthesis of polycaprolactone: a review, *Chemical Society Reviews*, **38**, 3484-3504
4. Sinha, V. R., Bansal, K., Kaushik, R., Kumria, R. & Trehan, A. (2004), Poly- ϵ -caprolactone microspheres and nanospheres: an overview, *International Journal of Pharmaceutics*, **278**, 1-23
5. Dhanvijay, P. U., Shertukde, V. V. & Kalkar, A. K. (2012), Isothermal and nonisothermal crystallisation kinetics of poly(ϵ -caprolactone), *Journal of Applied Polymer Science*, **124**, 1333-1343

6. Liu, P., Hu, A., Wang, S., Shi, M., Ye, G. & Xu, J. (2011), Evaluation of nonisothermal crystallisation kinetic models for linear poly(phenylene sulfide), *Journal of Applied Polymer Science*, **121**, 14-20
7. Kong, Y. & Hay, J. N. (2002), The measurement of the crystallinity of polymers by DSC, *Polymer*, **43**, 3873-3878
8. Lu, X. F. & Hay, J. N. (2001), Isothermal crystallisation kinetics and melting behaviour of poly(ethylene terephthalate), *Polymer*, **42**, 9423-9431
9. He, Y., Fan, Z., Hu, Y., Wu, T., Wei, J. & Li, S. (2007), DSC analysis of isothermal melt-crystallisation, glass transition and melting behaviour of poly(L-lactide) with different molecular weights, *European Polymer Journal*, **43**, 4431-4439
10. Kong, K. & Hay, J. N. (2003), The enthalpy of fusion and degree of crystallinity of polymers as measured by DSC, *European Polymer Journal*, **39**, 1721-1727
11. Hoffman, J. D. & Weeks, J. J. (1962), Melting processes and equilibrium melting temperature of polychlorotrifluoroethylene, *Journal of Research of the National Bureau of Standards Section A: Physics and Chemistry*, **66A**, 13-28
12. Koenig M. F. & Huang S. J. (1995), Biodegradable blends and composites of polycaprolactone and starch derivatives, *Polymer*, **36**, 1877-1882
13. Smith, B. C. (1996), *Fundamentals of Fourier Transform Infrared Spectroscopy*, CRC Press, Florida: USA

Chapter 3. – Thermal Analysis of PCL by DSC

Differential Scanning Calorimetry (DSC) is a common method used for the thermal analysis of polymers, and has been used by many authors on most polymeric materials [1-5]. As a technique it has numerous uses including measurement of glass transitions, melting points and crystallisation kinetics [6-11].

The focus of this work is on the study of crystallisation kinetics and an appreciation of the limitations of the technique in a study of crystallisation kinetics.

3.1. Results and Discussion.

3.1.1 Isothermal Crystallisation

PCL samples were held in the melt for 2 min before being cooled at 180 °C/min to the crystallisation temperature. The DSC responses for these samples are shown in Figure 3.1, with the crystallisation beginning when there is a change in the baseline of the DSC trace. This represents the evolution of heat as a result of the phase transition. Crystallisation is an exothermic reaction, where energy is released in the form of heat.

The relative crystallinity was calculated as a function of time for each isothermal temperature from the area under the curve, obtained by integrating the curve from the onset of crystallisation to time t and dividing it by the total area, i.e.

$$X_t = \int_0^t \frac{dH}{dt} dt / \int_0^{\infty} \frac{dH}{dt} . dt \quad \text{Equation 3.1}$$

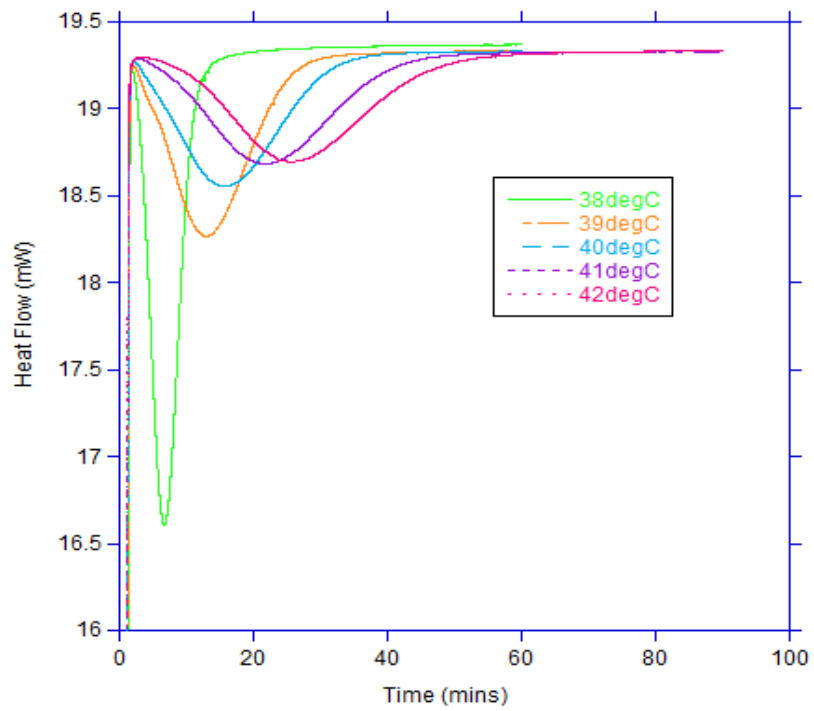


Figure 3.1 – Change in heat flow with time during crystallisation at 38-42 °C

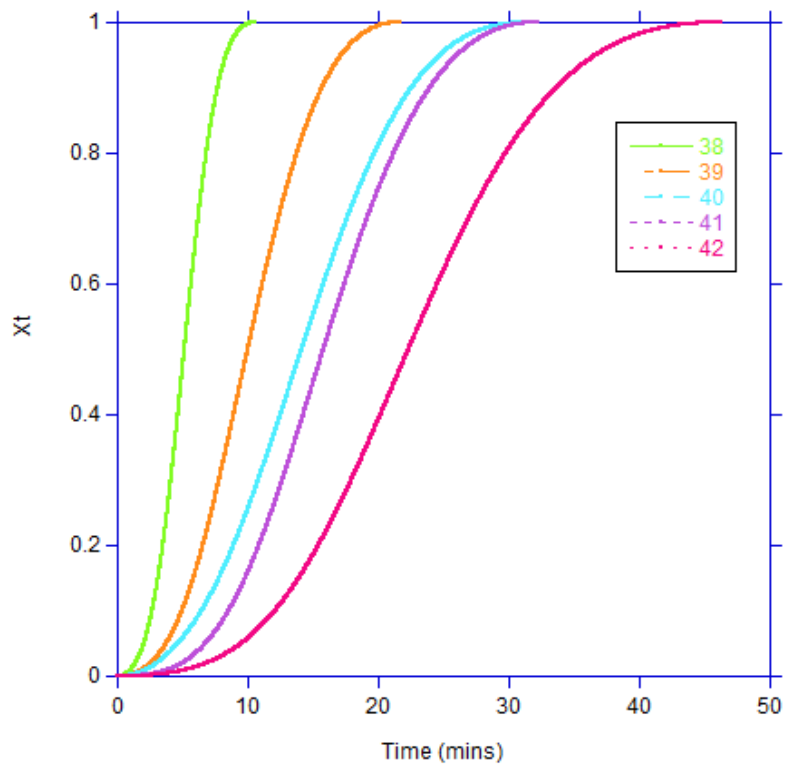


Figure 3.2 – Growth of relative crystallinity with time during crystallisation at 38-42 °C

where dH/dt is the relative heat flow rate. The results of these integrations are shown in Figure 3.2 where the development of the relative change in crystallinity is presented against time; it exhibits the increase in rate of crystallisation with decreasing temperature.

The initial exponential dependence of the relative crystallinity on time is described by the Avrami equation [12-13] which is given as

$$1 - X_t = \exp(-Zt^n) \quad \text{Equation 3.2}$$

where X_t is the fractional extent of crystallisation at time t , Z is a rate constant incorporating time dependent characteristics of nucleation and growth, and n is the Avrami exponent, which takes different values depending on the crystallisation mechanism involved.

The results are presented as a double-log plot from which the rate constant Z , half-life $t_{1/2}$ and n values are determined since

$$\log[-\ln(1 - X_t)] = n \log t - \log Z \quad \text{Equation 3.3}$$

A plot of $\log[-\ln(1-X_t)]$ against $\log(t)$ should be linear with a slope of n and an intercept at $\log(t) = 0$ of $\log(Z)$; this is shown in Figure 3.3 and the degree of fit of the equation to the data is represented by the linearity of the plots. Typically, a change in gradient is noticed towards the end of crystallisation, demonstrating that two consecutive processes are present; primary and secondary crystallisation. This deviation from the straight line caused Hay [14] to note that the Avrami equation was not appropriate for analysis of the latter stages of the crystallisation process. However, analysis can be limited to the primary process by selecting an appropriate value for X_∞ ,

at which it terminates. Equation 3.3 was modified to be only applicable to the primary process;

$$\left[\frac{1-X_t}{X_\infty}\right] = \exp(-Zt^n) \quad \text{Equation 3.4}$$

and
$$\log[-\ln\{1-X_t/X_\infty\}] = n \log t - \log Z \quad \text{Equation 3.5}$$

using X_∞ as an adjustable parameter whose value can be found by linearising the fit of equation 3.5 to the data. The best estimated X_∞ value was used to mark the end of the primary process and the linearity of equation 3.5 to the data can be seen from the straight line plots shown in Figure 3.3. The Avrami exponent, n , and the rate constant, Z , were determined from the slope and intercept at $t=1$, see Table 3.1. The half-life, $t_{1/2}$, was determined from these values since,

$$Z = \ln 2 / t_{1/2}^n \quad \text{Equation 3.2}$$

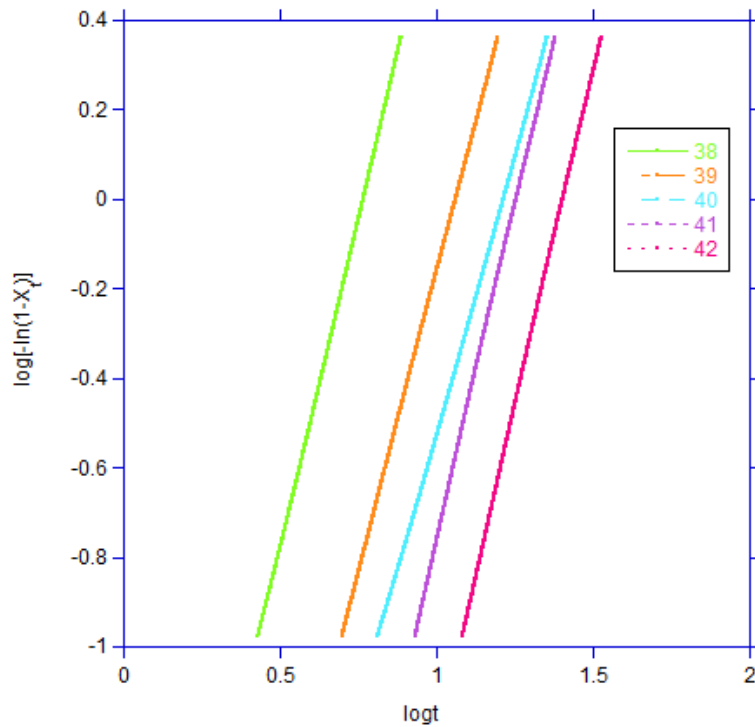


Figure 3.3 – Avrami double-log plot for isothermal crystallisation at 38-42 °C

The value of the exponent varied between 2.5 and 3.1 which in terms of the crystallisation models adopted by Avrami was consistent with growth of spherical particles from heterogeneous nuclei, for which $n=3.0$ and in particular to growth of spherulites. Hay [15] suggests that the Avrami equation is only a valid description of the overall crystallisation process when nucleation is sporadic or predetermined (with a constant radial growth rate). These situations would give an n value of 4 and 3 respectively. In this model the exponent value is an integer, but as can be seen from the results of this project, that is not the case. Fractional n values close to acceptable integer values have been commonly observed in the crystallisation of polymers and may be produced due to variation in nucleation density across the sample. Multiple investigations, from numerous polymers, support this description [9, 16-21], and this includes other studies on PCL. [22-24].

The variation in half-life ($t_{1/2}$) with temperature is illustrated in Figure 3.4 and exhibits a marked dependence on temperature, increasing exponentially with increasing crystallisation temperature. As crystallisation temperature decreases, nucleation and growth rates increase, which produces faster rates of crystallisation at lower temperatures, so reducing the half-lives. This was found by Zhang and Zeng [25], who recorded a higher nucleation density for a shorter time at lower crystallisation temperatures. This also correlates with the nucleation theory suggested by Hoffman and Lauritzen [26-28].

The variation in the growth rate constant, Z , is shown in Figure 3.5. Since Z is a reciprocal function of $t_{1/2}$, it exhibits strong temperature dependence but decreases with increasing crystallisation temperature. This is consistent with nucleation control of crystallisation.

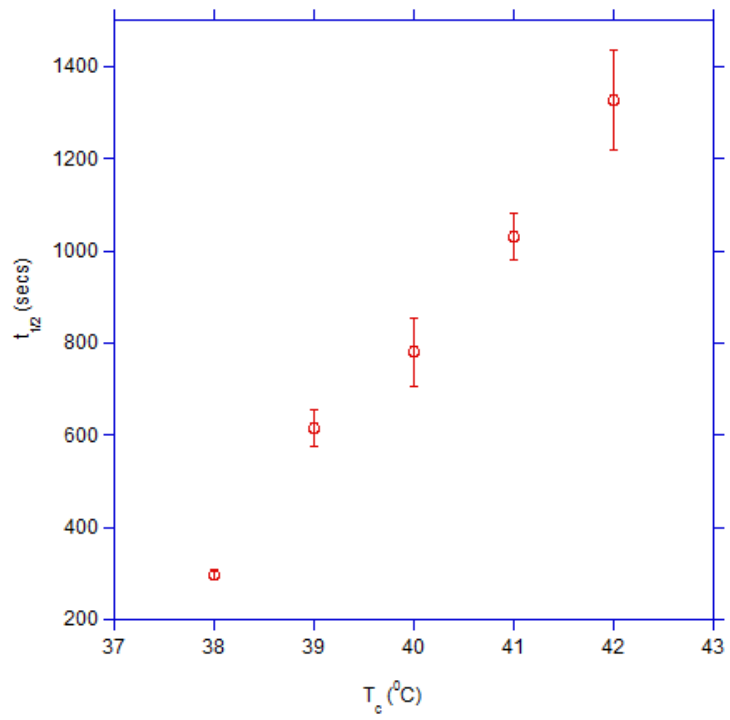


Figure 3.4 – Variation in half-life with crystallisation temperature

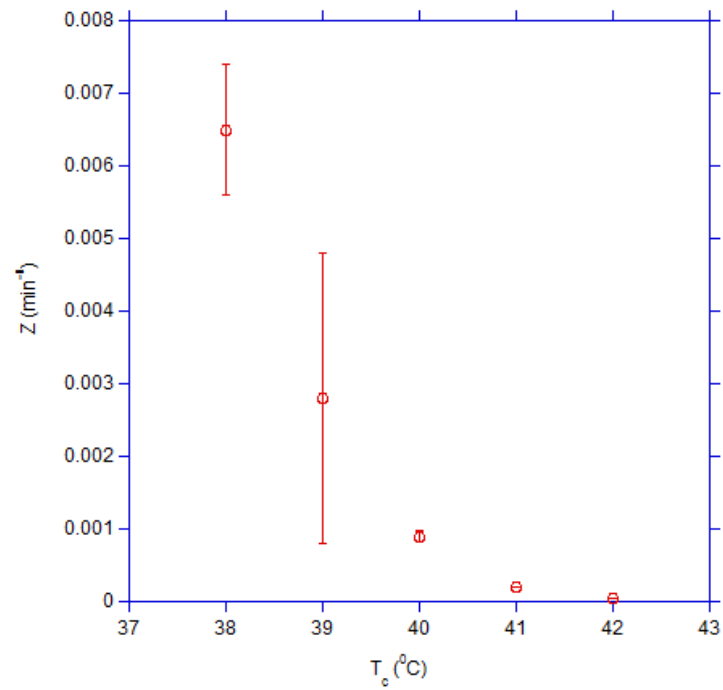


Figure 3.5 – Variation in growth rate (Z) with crystallisation temperature

T_c (°C)	n
38	2.9 ± 0.06
39	2.5 ± 0.26
40	2.6 ± 0.08
41	2.9 ± 0.06
42	3.1 ± 0.10

Table 3.1 - Avrami Rate Parameters

3.1.2 Nonisothermal Crystallisation

Similar procedures were adopted to measure the nonisothermal crystallisation kinetics of PCL as those implemented for measuring the isothermal kinetics in that the samples were held in the melt for 2 min, but then the samples were allowed to cool at different cooling rates until the crystallisation was complete and the calorimeter had returned to the baseline. As observed in the isothermal results, crystallisation was marked by the change in heat evolution, as the sample underwent a phase transition from the melt region into a region of increased crystallinity. The results of these experiments are presented in Figure 3.6 and show a strong relationship between temperature and cooling rate, with the temperature range over which the sample crystallises shifting to lower values as the cooling rate increases. The crystallisation peak temperature, which marks the maximum rate of crystallisation, shifted to a lower temperature as cooling rate increases, as did the onset of crystallisation indicating that at

lower cooling rates the crystallisation process started earlier and may be due to the increased time spent at each temperature as the sample was cooled.

The relative crystallinity of the sample was measured by integrating the heat flow curves with temperature, not time as used before. These are plotted for each cooling rate as a function of temperature in Figure 3.7 as a series of sigmoidal shaped curves. Each curve has an induction period before the onset of crystallisation followed by a period of increasing rate. This was followed by regions of relatively constant rate of crystallisation before falling off as the crystallisation stopped. This cut off was steeper than observed in isothermal crystallizations and occurred at higher X_{∞} values. We would attribute this last stage to impingement of the spherulites.

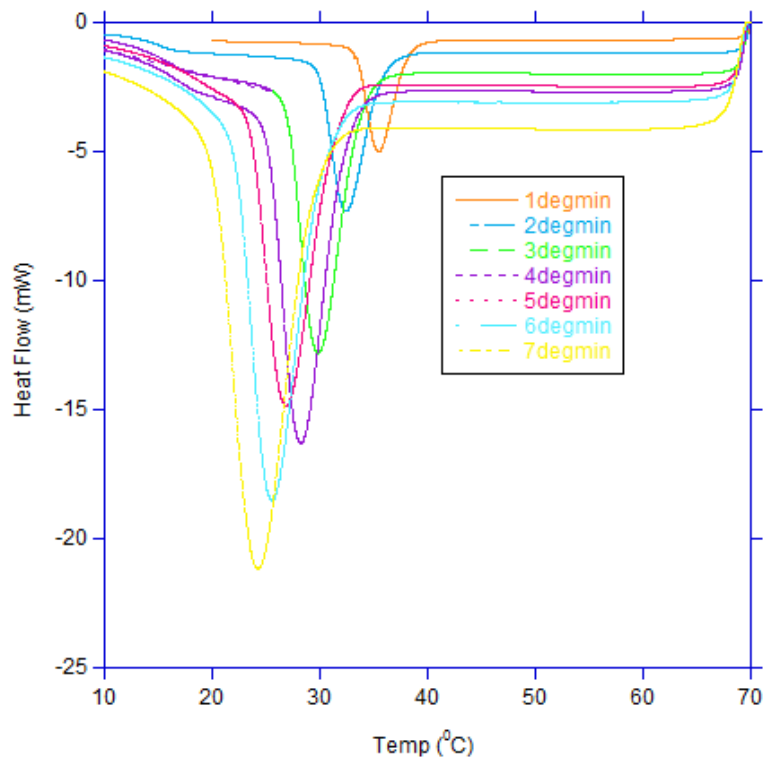


Figure 3.6 – Change in heat flow with temperature for cooling rates of 1-7 °C

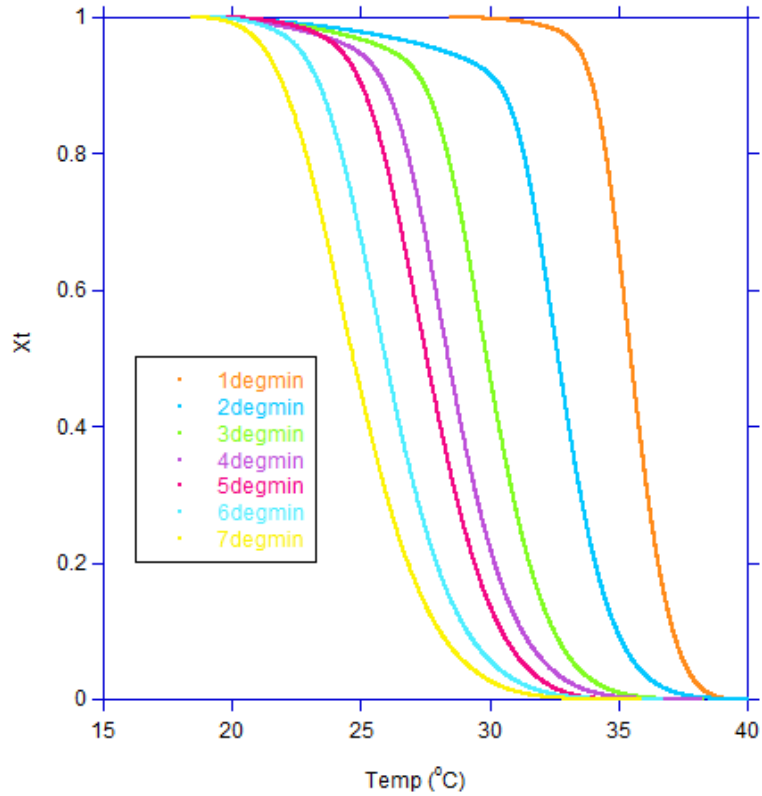


Figure 3.7 – Development of relative crystallinity with temperature for cooling rates of 1-7 °C

Several kinetic equations have been derived to describe the time and temperature dependence of crystallisation in nonisothermal conditions [29-32]. Ozawa's [33] is the most commonly used and was derived from Evans' model of crystallisation as expanding raindrops and their impingement on the surface of a pool, which lead to the Ozawa equation;

$$1 - X_T = \exp\left(\frac{-K(T)}{\Phi^m}\right) \quad \text{Equation 3.3}$$

where X_T is the relative crystallinity at a certain crystallisation temperature, $K(T)$ is the cooling function at a certain crystallisation temperature, Φ is the cooling rate and m is the Ozawa exponent, the value of which depends on the type of nucleation and growth mechanism occurring within the sample.

Ozawa's equation is limited in its application to constant cooling rate is assumed and in order to produce the double-log plot the relative crystallinity at fixed temperatures for different cooling rates is required. The method of analysis described by Ozawa also ignores secondary crystallisation, although as the Avrami equation for isothermal results in this thesis was limited to the primary process, this is not a consideration during comparison. It has also been argued that, as the temperature is continuously lowered on cooling, fold length should be considered as this is a function of crystallisation temperature. [34].

From the Ozawa equation it follows that

$$\log[-\ln(1 - X_T)] = \log K(T) - m \log \phi \quad \text{Equation 3.4}$$

and a plot of $\log [-\ln(1 - X_T)]$ against $\log(\Phi)$ should be linear with a slope of m and an intercept of $\log K(T)$, see Figure 3.9. The plot was produced by reading off the relative crystallinity at fixed temperature from the cooling curves shown in Figure 3.7 were linear with degree of fit, R^2 , of 0.98 (a perfect linear fit would have been 1.00). The Ozawa plots at five selected temperatures, from 33 to 37 °C, are shown in Figure 3.8 and from the double-log plots the Ozawa parameters m and $K(T)$ were determined.

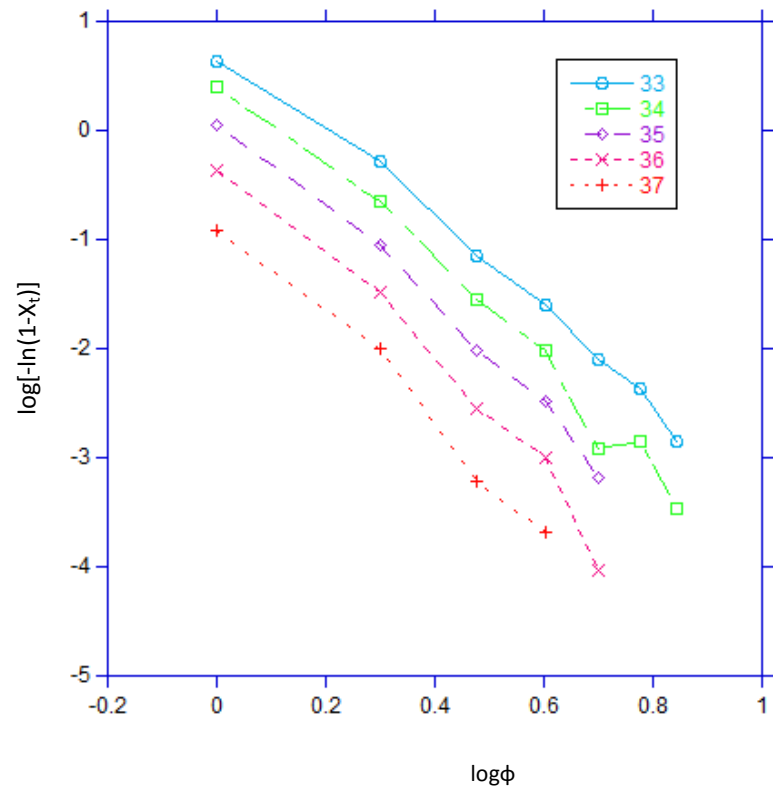


Figure 3.8 - Ozawa plots at fixed temperatures from 33 to 37 °C.

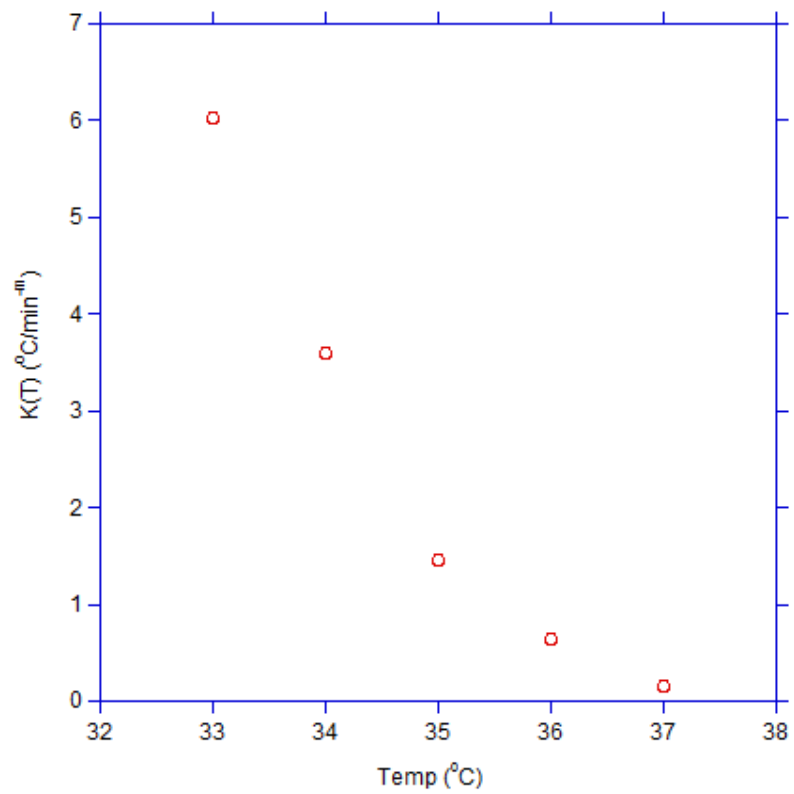


Figure 3.9 – Variation in $K(T)$ with temperature

T_f (°C)	m
33	4.1
34	4.5
35	4.6
36	5
37	4.7

Table 3.2 – Ozawa exponent ‘m’ values

The values for the Ozawa parameters were determined from the slope and intercept of the double log plots and are listed in Table 3.2. The values of the exponent ‘m’ lay between 4 and 5. A value of 4 can be explained if the nucleation density is temperature dependent and linearly dependent on time. It would then have the characteristics of sporadic nucleation. The m value would change from 3.0 to 4.0 to account for the time dependence of nucleation.

If nucleation is time dependent then the growth rate would be expected also to be time dependent and if it is assumed that it increases linearly with time on cooling the corresponding m value would be 7.0, by analogy to Avrami’s models for the crystallization of sporadically nucleated spherulites. 5.0 was the highest value of m observed and so the assumption of linear increase in rate of growth and nuclei numbers cannot be valid and a more realistic approach to the change in these rates with temperature is required. The assumption of Ozawa in deriving his equivalent of the Avrami equation that fractional crystallinity obtained at the same temperature but at

different cooling rates can be compared is clearly not valid; each system has a different thermal history in spending different time intervals at each decrement in temperature and producing a distribution of lamellae and morphology.

Although seemingly suitable as a method of analysis for this data as exemplified by the high degree of fit, the rate parameters are of little value in describing the crystallisation kinetics for the nonisothermal crystallisation. Several other investigations have found that the Ozawa equation fails to describe the nonisothermal melt crystallisation kinetics, although this is often due to non-linearity of the double-log plot. This has been explained by non-constant m values which change with temperature on cooling indicating that the crystallisation mechanism may differ depending on the undercooling [35-36]. This is particularly evident at a high degree of cooling and has led to the conclusion that the Ozawa equation is only valid over a narrow range of cooling rates [37-38]. This has resulted in the increased use of alternative kinetic equations. Wang et al (2005) [39] were able to produce nonisothermal crystallisation kinetic results for PCL that could be satisfactorily described by the Ozawa equation and gave meaningful m values of 2.3 ± 0.1 . However, the higher molecular weight material used and the lower crystallisation temperatures investigated in comparison to those adopted in this thesis may account for the difference in conclusion concerning the suitability of the Ozawa in kinetic analysis.

In order to understand the effect of cooling rate on the time scale over which crystallisation occurred the half-life of the isothermal crystallisations, obtained above by DSC, were plotted against the temperature and plotted against the reciprocal degree of super-cooling, $1/\Delta T$ in Figure 3.10. This produced a linear relationship which enabled $t_{1/2}$ values to be determined by linear extrapolation at the fixed temperatures chosen for

analysis of the nonisothermal data, i.e. Ozawa's analysis. The half-lives, shown in Figure 3.11 are small, 30 to 90 s. For the crystallisation to occur in such a short time it is difficult to believe that the heat of crystallisation can be completely dissipated from the sample into the calorimeter and that during the maximum rate of crystallisation thermal lags will develop across such a poor thermal conductor. It is possible that crystallisation may predominately occur at some constant temperature during most of the crystallisation and that the rate is controlled by heat losses from the sample. A balance between heat generated by the crystallisation and lost from the sample will determine the crystallisation temperature; too fast a crystallisation would generate an increase in temperature and too slow a rate would result in a drop in temperature. If the heat lost and the heat generated is equal then a constant temperature condition results.

Accordingly the kinetic data was analysed assuming that the nonisothermal crystallisations had been carried out isothermally at an unknown fixed temperature, and could be analysed in terms of the Avrami equation in order to compare with the results obtained isothermally at known temperatures.

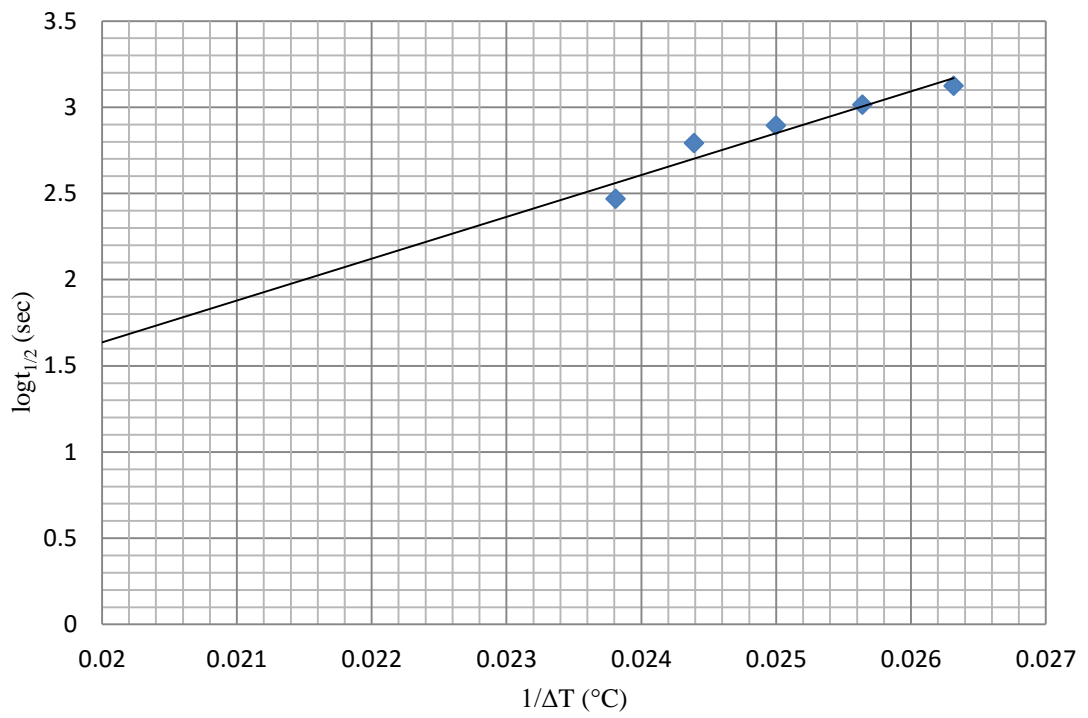


Figure 3.10 – Linear extrapolation of isothermal $t_{1/2}$ data

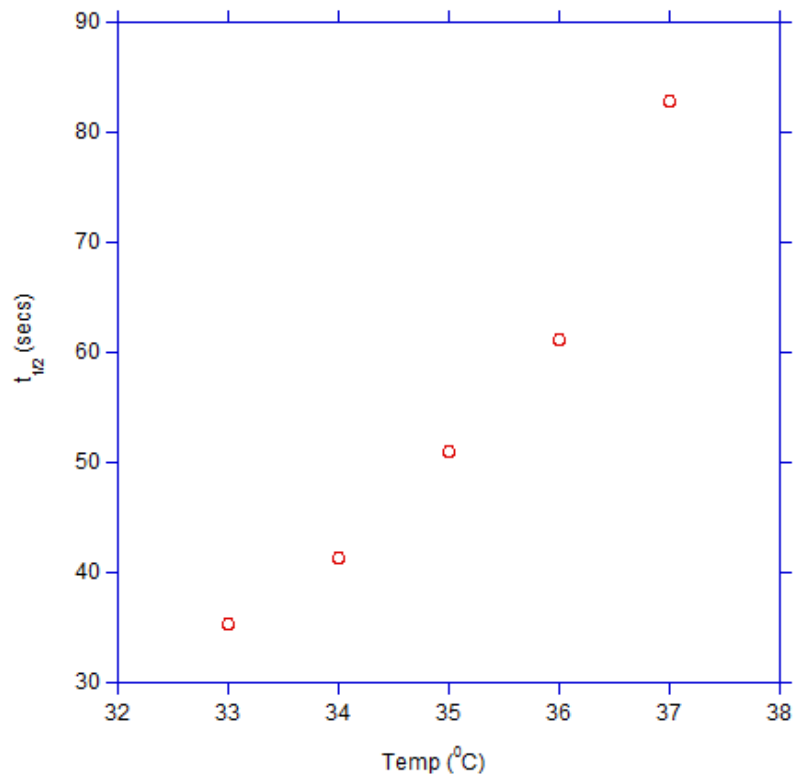


Figure 3.11 – $t_{1/2}$ values for nonisothermal fixed temperatures of 33-37 $^{\circ}C$ determined from extrapolated data

Initial trials on this hypothesis were conducted on the data collected from the original cooling rates studies. The Avrami equation was applied after the data was converted to relative crystallinity, X_t , against time, t , and analysed as before using Equation 3.3 as shown in Figure 3.12 but the Avrami rate parameters determined, listed in Table 3.3, exhibited no relationship to those determined for the isothermal crystallisation given in Table 3.1. The values of n were more in line with those determined from using the Ozawa procedure and suggested that at the low cooling rates adopted, 1-7 °C/ min the sample was crystallising on cooling. It was decided to use higher cooling rates to see at what point the sample would not cool at the rate of the DSC and still evolve the heat of crystallisation. A fast cooling rate must eventually produce a condition under which the crystallisation rate will become limited by rate of loss of heat from the sample, and the crystallisation would then occur under constant melt temperature conditions. At this point the sample will be crystallising under isothermal conditions, as the heat evolved by the sample on crystallisation counter-acts the cooling mechanism imposed by the DSC.

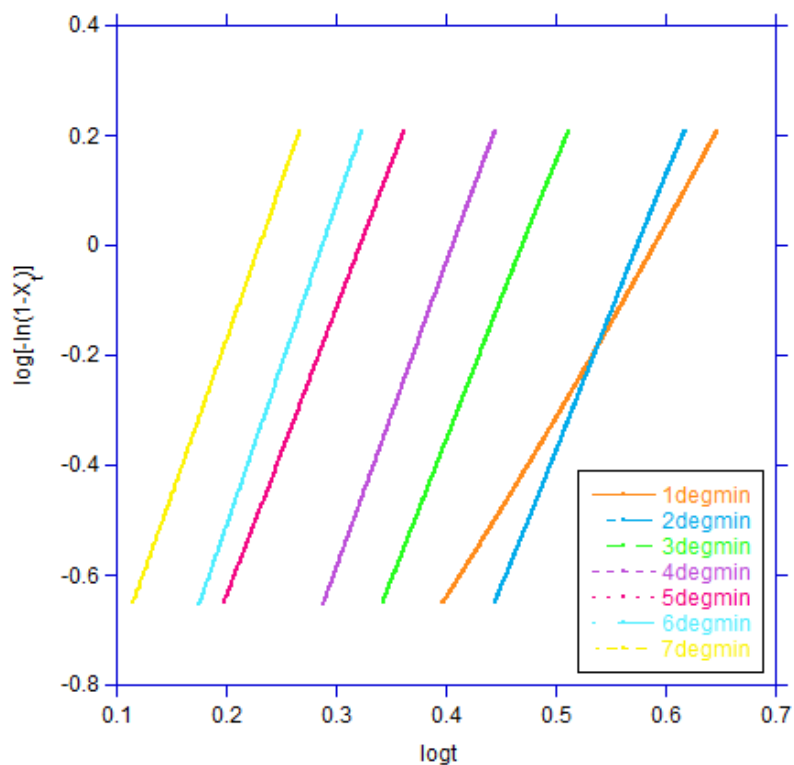


Figure 3.12 – Double-log plot produced from application of the Avrami equation to nonisothermal data

Rate of Cooling($^{\circ}\text{C min}^{-1}$)	n	Z (min^{-n})	$t_{1/2}$ (sec)
1	3.6 ± 0.17	0.008 ± 0.003	200 ± 10.20
2	4.9 ± 0.34	0.003 ± 0.002	206 ± 22.63
3	5.1 ± 0.06	0.003 ± 0.0006	168 ± 4.90
4	5.4 ± 0.34	0.005 ± 0.0008	150 ± 4.90
5	5.2 ± 0.14	0.03 ± 0.01	116 ± 5.66
6	5.8 ± 0.13	0.02 ± 0.008	114 ± 8.49
7	5.6 ± 0.13	0.05 ± 0.008	98 ± 2.83

Table 3.3 – Avrami parameters for nonisothermal data considered as crystallising at constant temperature

3.1.3 High Cooling Rates

Nonisothermal crystallisation experiments were conducted on samples of PCL at higher rates of cooling; from 10 to 30 °C/min. A Mettler DSC 1/500 was used in preference to the Perkin Elmer DSC 7 due to the improved ability to maintain cooling at these rates to lower temperatures. The procedure used was the same as previous; samples were heated to 70 °C and held in the melt for 2 min before being cooled at varying rates down to a temperature at which the DSC trace returned to baseline.

The relative crystallinity was calculated as a function of time rather than temperature and the Avrami equation applied assuming that the crystallisation had been carried out at constant temperature, using Equation 3.2 and Equation 3.3 respectively. The results of these calculations are shown in Figure 3.13 and Figure 3.14 and again exhibit the same characteristics observed with nonisothermal data. The rate parameters do not appear to match with the isothermal results, i.e. n values between 4 and 5 and half-lives of less than 90 s. These were inconsistent with the isothermal rate data and the hypothesis that at a certain rate of cooling, i.e. above 10 °C/min, the DSC could not compensate for the levels of heat being produced by the crystallisation of the sample, and so creating an 'isothermal environment' for crystallisation.

Due to limitations of the cooler in the DSC it was not possible to achieve sustained cooling rates above 30 °C/min since the DSC rapidly lost controlled cooling. No further work on the effect of cooling rate was carried out.

An n value of between 4 and 5, as shown in Table 3.4, indicates that the crystallization was proceeding with a similar mechanism to that discussed above for nonisothermal crystallisation, i.e. crystallisation by growth from sporadically nucleated

spheres such that the number of spherulites increased as the crystallisation temperature decreased.

It is interesting to speculate that the drop in n value at the highest cooling rate achieved might suggest partial success in that the isothermal conditions may have been achieved at the higher rates of crystallisation, and reflect the variation of temperature across the crystallising sample. Clearly work is required on this to verify these speculative conclusions.

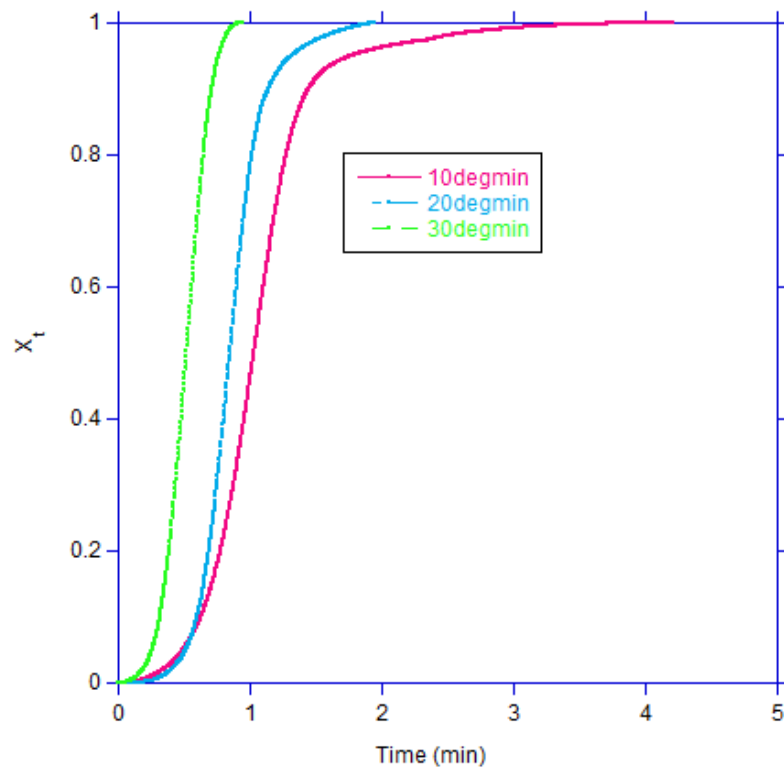


Figure 3.13 – Growth in relative crystallinity for samples tested at higher cooling rates

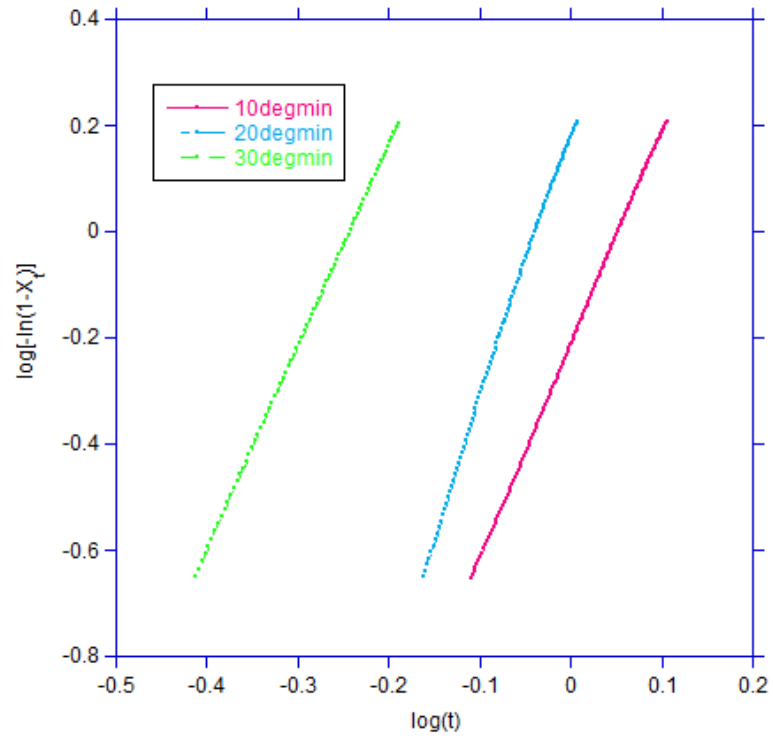


Figure 3.14 – Avrami double-log plot for samples tested at higher cooling rates
(time in min)

Rate of Cooling (°C/min)	n	Z (min ⁻ⁿ)	t _{1/2} (s)
10	4.2 ±	0.4636 ± 0.15	67 ± 6
20	4.9 ±	2.1385 ± 1.09	55 ± 6
30	4.1 ±	10.8531 ± 1.72	36 ± 6

Table 3.4 – Avrami parameters for higher cooling rates of 10-30 °C

3.2 Conclusions

Studies into the crystallisation kinetics of PCL were conducted under isothermal and nonisothermal conditions. In isothermal conditions the crystallisations were analysed using the Avrami equation and produced n values of around 3, indicating a crystal growth mechanism of three-dimensional pre-determined spheres. Nonisothermal crystallisation kinetics were analysed using the Ozawa equation, which was found to be an unsuitable method of analysis as the rate parameters obtained had little meaning and details suggested crystal growth via an undetermined mechanism. It was suggested that, particularly at high rates of cooling, samples crystallised in nonisothermal conditions would exhibit an isothermal crystal growth mechanism as the sample cannot cool as quickly as the DSC would indicate due to a poor dissipation of heat created on crystallisation. The data was therefore analysed using the Avrami equation, which produced an Avrami exponent value that did not support this hypothesis; a value of n between 4 and 5 was recorded, suggesting a changing number of nuclei resulting from the changing temperatures experienced during cooling. However, limitations of the equipment prevented cooling rates of above 30 °C/min from being tested, and so it is possible that the original hypothesis was still correct.

Further experiments should be carried out at even higher cooling rates to investigate whether such cooling conditions would produce an environment within the sample of maintained isothermal temperature. This could be done on a Mettler Toledo Flash DSC, as the use of a much smaller sample enables control at much higher cooling rates (up to 800 °C/min). Other investigation to increase support for this hypothesis could be conducted using an optical microscope to measure the spherulite radial growth rates as a function of temperature, as they should accelerate on cooling but stay constant

if the temperature remains constant, particularly under these high cooling rate conditions.

3.3 References

1. Chen, Z., Hay, J. N. & Jenkins, M. J. (2013), The effect of secondary crystallisation on melting, *European Polymer Journal*, **49**, 2697-2703
2. Lu, X. F. & Hay, J. N. (2001), Isothermal crystallisation kinetics and melting behaviour of poly(ethylene terephthalate), *Polymer*, **42**, 9423-9431
3. Van der Wal, A., Mulder, M. M. & Gaymans, R. J. (1997), Fracture of polypropylene: 2. The effect of crystallinity, *Polymer*, **39**, 5477-5481
4. Asadinezhad, A., Jafari, S. H., Khonakdar, H. A., Böhme, F., Hässler, R. & Häussler, L. (2007), Kinetics of isothermal crystallisation and subsequent melting behaviour of PTT/PA12 blend, *Journal of Applied Polymer Science*, **106**, 1964-1971
5. Jenkins, M. J. & Harrison, K. L. (2006), The effect of molecular weight on the crystallisation kinetics of polycaprolactone, *Polymers for Advanced Technologies*, **17**, 474-478
6. Dhanvijay, P. U., Shertukde, V. V. & Kalkar, A. K. (2012), Isothermal and nonisothermal crystallisation kinetics of poly(ϵ -caprolactone), *Journal of Applied Polymer Science*, **124**, 1333-1343
7. Liu, P., Hu, A., Wang, S., Shi, M., Ye, G. & Xu, J. (2011), Evaluation of nonisothermal crystallisation kinetic models for linear poly(phenylene sulfide), *Journal of Applied Polymer Science*, **121**, 14-20
8. Kong, Y. & Hay, J. N. (2002), The measurement of the crystallinity of polymers by DSC, *Polymer*, **43**, 3873-3878

9. Lu, X. F. & Hay, J. N. (2001), Isothermal crystallisation kinetics and melting behaviour of poly(ethylene terephthalate), *Polymer*, **42**, 9423-9431
10. He, Y., Fan, Z., Hu, Y., Wu, T., Wei, J. & Li, S. (2007), DSC analysis of isothermal melt-crystallisation, glass transition and melting behaviour of poly(L-lactide) with different molecular weights, *European Polymer Journal*, **43**, 4431-4439
11. Kong, K. & Hay, J. N. (2003), The enthalpy of fusion and degree of crystallinity of polymers as measured by DSC, *European Polymer Journal*, **39**, 1721-1727
12. Avrami, M. (1940), Kinetics of phase change II transformation – time relaxations for random distribution of nuclei, *Journal of Chemical Physics*, **8**, 212-224
13. Avrami, M. (1941), Kinetics of phase change and microstructure kinetics of phase change III, *Journal of Chemical Physics*, **9**, 177-184
14. Hay, J. N. (1971), Application of the modified Avrami equations to polymer crystallisation kinetics, *British Polymer Journal*, **3**, 74-82
15. Hay, J. N. (1979), Crystallisation from the melt, *Flow-Induced Crystallisation*, Gordon and Breach Science Publishers Ltd: London; Great Britain
16. Xu, Y., Shang, S. & Huang, J. (2011), Two-stage crystallisation kinetics equation and nonisothermal crystallisation analyses for PTEG and filled PTEG, *Journal of Materials Science*, **46**, 4085-4091
17. Razavi-Nouri, M. & J. N. Hay (2007), Isothermal crystallisation kinetics and melting behaviour of metallocene-catalysed polyethylenes, *Iranian Polymer Journal*, **16**, 105-112

18. Hay, J. N. & Mills, P. J. (1982), The use of differential scanning calorimetry to study polymer crystallisation kinetics, *Polymer*, **23**, 1380-1384
19. Xu, Y., Ye, S. R., Bian, J. & Qian, J. W. (2004), Crystallisation kinetics analysis of poly(trimethylene terephthalate) including the secondary crystallisation process, *Journal of Materials Science*, **39**, 5551-5555
20. Sabino, M. A., Feijoo, J. L. & Müller, A. J. (2000), Crystallisation and morphology of poly(*p*-dioxanone), *Macromoleculuar Chemical Physics*, **201**, 2687-2698
21. Chen, E. C. & Wu, T. M. (2007), Isothermal crystallisation kinetics and thermal behaviour of poly(ϵ -caprolactone)/multi-walled carbon nanotube composites, *Polymer Degradation and Stability*, **92**, 1009-1015
22. Su, H. H., Chen, H. L., Díaz, A., Casas, M. T., Puiggali, J., Hoskins, J. N., Grayson, S. M. Pérez, R. A. & Müller, A. J. (2013), New insights on the crystallisation and melting of cyclic PCL chains on the basis of a modified Thomson-Gibbs equation, *Polymer*, **54**, 846-859
23. Atanase, L. I., Glaied, O. & Riess, G. (2011), Crystallisation kinetics of PCL tagged with well-defined positional triazole defects generated by click chemistry, *Polymer*, **52**, 3074-3081
24. Zhu, G., Ling, J. & Shen, Z. (2003), Isothermal crystallisation of random copolymers of ϵ -caprolactone with 2,2-dimethyltrimethylene carbonate, *Polymer*, **44**, 5827-5832
25. Zhang Z. & Zeng, H. (1993), Nucleation and crystal growth of PEEK on carbon fiber. *Journal of Applied Polymer Science*, **48**, 1987-1995

26. Lauritzen, J. I. & Hoffman, J. D. (1960), Theory of formation of polymer crystals with folded chains in dilute solution, *Journal of Research of the National Bureau of Standards Section A: Physics and Chemistry*, **64**, 73-102
27. Lauritzen, J. I. & Hoffman, J. D. (1973), Extension of theory of growth of chain-folded polymer crystals to large under-coolings, *Journal of Applied Polymer Physics*, **44**, 4340-4352
28. Hoffman, J. D., Frolen, L. J., Ross, G. S. & Lauritzen, J. I. (1975), Growth rate of spherulites and axialites from the melt in polyethylene fractions: Regime-1 and Regime-2 crystallisation, *Journal of Research of the National Bureau of Standards Section A: Physics and Chemistry*, **79**, 671-699
29. Nakamura, K., Katayama, K. & Amano, T. (1973), Some aspects of nonisothermal crystallisation of polymers. II. Consideration of the isokinetic condition, *Journal of Applied Polymer Science*, **17**, 1031-1041
30. Liu, S., Yu, Y., Cui, Y., Zhang, H. & Mo, Z. (1998), Isothermal and nonisothermal crystallisation kinetics of nylon-11, *Journal of Applied Polymer Science*, **70**, 2371-2380
31. Mubarak, Y., Harkin-Jones, E., Martin, P. & Ahmad, M. (2001), Modeling of nonisothermal crystallisation kinetics of isotactic polypropylene, *Polymer*, **42**, 3171-3182
32. Jeziorny, A. (1978), Parameters characterising the kinetics of the non-isothermal crystallisation of poly(ethylene terephthalate) determined by DSC, *Polymer*, **19**, 1142-1144
33. Ozawa, T. (1971), Kinetics of non-isothermal crystallisation, *Polymer*, **12**, 150-158

34. Lopez, L. & Wilkes, G. (1989), Non-isothermal crystallisation kinetics of poly(ρ -phenylene sulphide), *Polymer*, **30**, 882-887
35. Oburođlu, N., Ercan, N., Durmus, A. & Kaşgöz, A. (2012), Effects of filler type on the nonisothermal crystallisation kinetics of poly(butylene terephthalate) (PBT) composites, *Journal of Applied Polymer Science*, **123**, 77-91
36. Liu, T., Mo, Z., Wang, S. & Zhang, H. (1997), Nonisothermal melt and cold crystallisation kinetics of poly(aryl ether ether ketone ketone), *Polymer Engineering and Science*, **37**, 568-575
37. Yang, F. & Qiu, Z. (2011), A comparative study of crystallisation kinetics of a miscible biodegradable poly(butylene succinate-co-butylene adipate) blend with poly(hydroxyl ether biphenyl A) and its neat component, *Thermochimica Acta*, **523**, 200-206
38. Sajkiewicz, P., Carpaneto, L. & Wasiak, A. (2001), Application of the Ozawa model to non-isothermal crystallisation of poly(ethylene terephthalate), *Polymer*, **42**, 5365-5370
39. Wang, Y., Rodriguez-Perez, M., Reis, R. & Mano, J. (2005), Thermal and thermomechanical behaviour of polycaprolactone and starch/polycaprolactone blends for biomedical applications, *Macromolecular Materials and Engineering*, **290**, 792-801

Chapter 4. – FTIR Spectroscopic Analysis of PCL on Crystallisation

4.1 Principles of 2D Infrared Spectroscopy

Two-dimensional (2D) infrared spectroscopy is used to simplify complex spectra consisting of many overlapped peaks, and enhance their spectral resolution by spreading peaks over a second dimension. This helps to establish the assignment of peaks to certain functional groups within the molecule through correlation of bands. The mathematical procedure involved in obtaining 2D correlation spectra from time or temperature dependent complex spectra has been explained by Noda and Ozaki [1-4] in some detail.

If $y(\nu, t)$ defines the perturbation-induced variations in intensities of spectra observed at fixed intervals of time or temperature (or an alternative external variable), t between t_{\min} and t_{\max} , then the dynamic spectrum of the system, $\tilde{y}(\nu, t)$ is defined as

$$\tilde{y}(\nu, t) = y(\nu, t) - \bar{y}(\nu) \text{ for } t_{\min} \leq t \leq t_{\max} \quad \text{Equation 4.1}$$

where $\bar{y}(\nu)$ is the initial or reference spectrum of the system.

The intensity of the 2D correlation spectrum $X(\nu_1, \nu_2)$ is then represented as

$$X(\nu_1, \nu_2) = \langle \tilde{y}(\nu_1, t) \cdot \tilde{y}(\nu_2, t') \rangle \quad \text{Equation 4.2}$$

where $X(\nu_1, \nu_2)$ is a quantitative measure of comparative similarities or differences in the intensities. $\tilde{y}(\nu, t)$ is measured at two separate variables; ν is the wavenumber and t is either time or temperature at fixed intervals. The symbol $\langle \rangle$ is the cross-correlation function and is designed to compare the two dependences of the spectra at t .

When the model from Noda is simplified, $X(\nu_1, \nu_2)$ becomes a complex number function, such that

$$\mathbf{X}(\nu_1, \nu_2) = \Phi(\nu_1, \nu_2) + i\Psi(\nu_1, \nu_2) \quad \text{Equation 4.3}$$

This function includes both real and imaginary components, which are recognised as synchronous and asynchronous 2D correlation intensities.

The synchronous 2D correlation intensity, $\Phi(\nu_1, \nu_2)$, is a symmetrical spectrum with respect to a diagonal line of $\nu_1 = \nu_2$ and represents the overall similarity or coincidental trends between two separate intensity variations measured at different spectral variables as the value of t is scanned from t_{\min} to t_{\max} . This is the in-phase character of the system. The asynchronous 2D correlation intensity, $\Psi(\nu_1, \nu_2)$, is anti-symmetric with respect to the diagonal and is considered to measure out-of-phase character of the spectral intensity variations. The intensity of an asynchronous spectrum represents sequential or successive, but not coincidental, changes of spectral intensities measured separately at ν_1 and ν_2 .

4.2 Analysing 2D spectral features

2D infra-red spectra may display different features depending on changes occurring within the material. When a peak exhibits two separate but overlapping absorption bands of the same magnitude change in intensity, one increasing and the other decreasing, the synchronous correlation presents a *four-leaf-clover* pattern. This cluster of 2D peaks is made up of two auto-peaks and two negative cross peaks; it is common for this pattern to be asymmetric due to the changing magnitudes of the two absorption bands not being equal. This produces auto-peaks of differing sizes.

The corresponding asynchronous spectrum shows two well resolved cross peaks. These provide sequential order information and the lack of any other feature indicates that there is no peak shift or broadening occurring. This also makes this spectral correlation a reliable indicator that there are two overlapping absorption bands present, as there can be no other contributing factors.

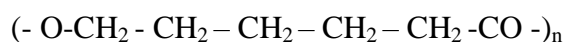
A single band may also be analysed using 2D correlation spectroscopy. When the band position shifts to a higher wavenumber and the intensity of the peak increases, the synchronous spectrum will present an *angel* pattern. This is not a symmetrical cluster of peaks as the magnitude of intensity changes is uneven and so results in one auto-peak being disproportionately larger than the other, with cross peak ‘wings’. As a similar angel pattern is more commonly observed when there are two overlapping bands accompanied with changes in intensity, this synchronous pattern is less reliable for use as a specific indicator for distinguishing positional shifts coupled with intensity changes and two overlapping bands with intensity changes [2, 5].

The asynchronous spectrum is distorted from the usual butterfly shape, usually seen when only a shift in band position occurs, where the cross peaks near the diagonal are elongated and distributed closer to the position of the larger auto-peak seen in the synchronous correlation. This spread covers both positive and negative synchronous correlation intensities. The presence of weaker secondary cross peaks indicates that there is a change in intensity of the peak clusters as well as the shift in band position, although these may not always be obvious due to their small magnitude in comparison with the strength of the main cross peaks. Adjustment of the contour level in the 2D mapping can increase the evidence of these peaks.

4.3 Results and Discussion

4.3.1 FTIR Spectrum of PCL

The FTIR spectrum of partially crystalline PCL is given in Figure 4.1. The absorption bands have been assigned and are shown in Table 4.1; they are entirely consistent with the molecular structure of a linear aliphatic ester, for which the repeat unit is



Functional group assignments of the IR absorption bands have been made in Table 4.1 from standard assignment lists [6-7].

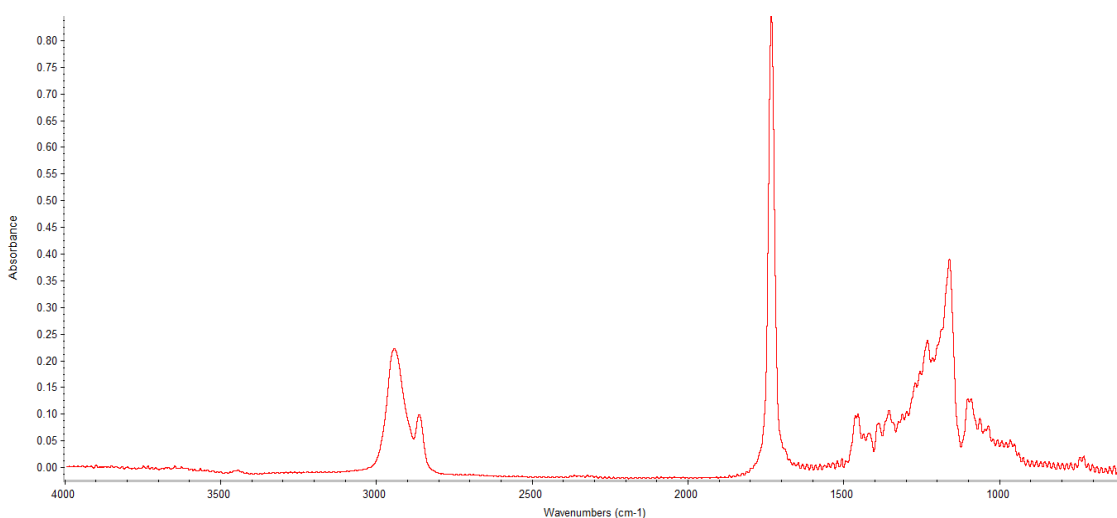


Figure 4.1 – The FTIR spectrum of PCL

The doublet absorption band at 3000-2800 cm^{-1} is attributed to the aliphatic methylene bonds stretching, the 1730 cm^{-1} band to the ester carbonyl bond stretching, and the remaining bands to methylene and ester group vibrations.

Reversible changes to the spectrum were observed to occur on heating and cooling between 30 and 70 °C through the melting point. These were attributed to phase change and assignments of the absorption bands to the crystalline or amorphous phase made according to whether they appeared or disappeared on melting and crystallizing, see Figure 4.2 and Table 4.1. Since these changes were quite varied for convenience they are discussed according to wavenumber and group functionality.

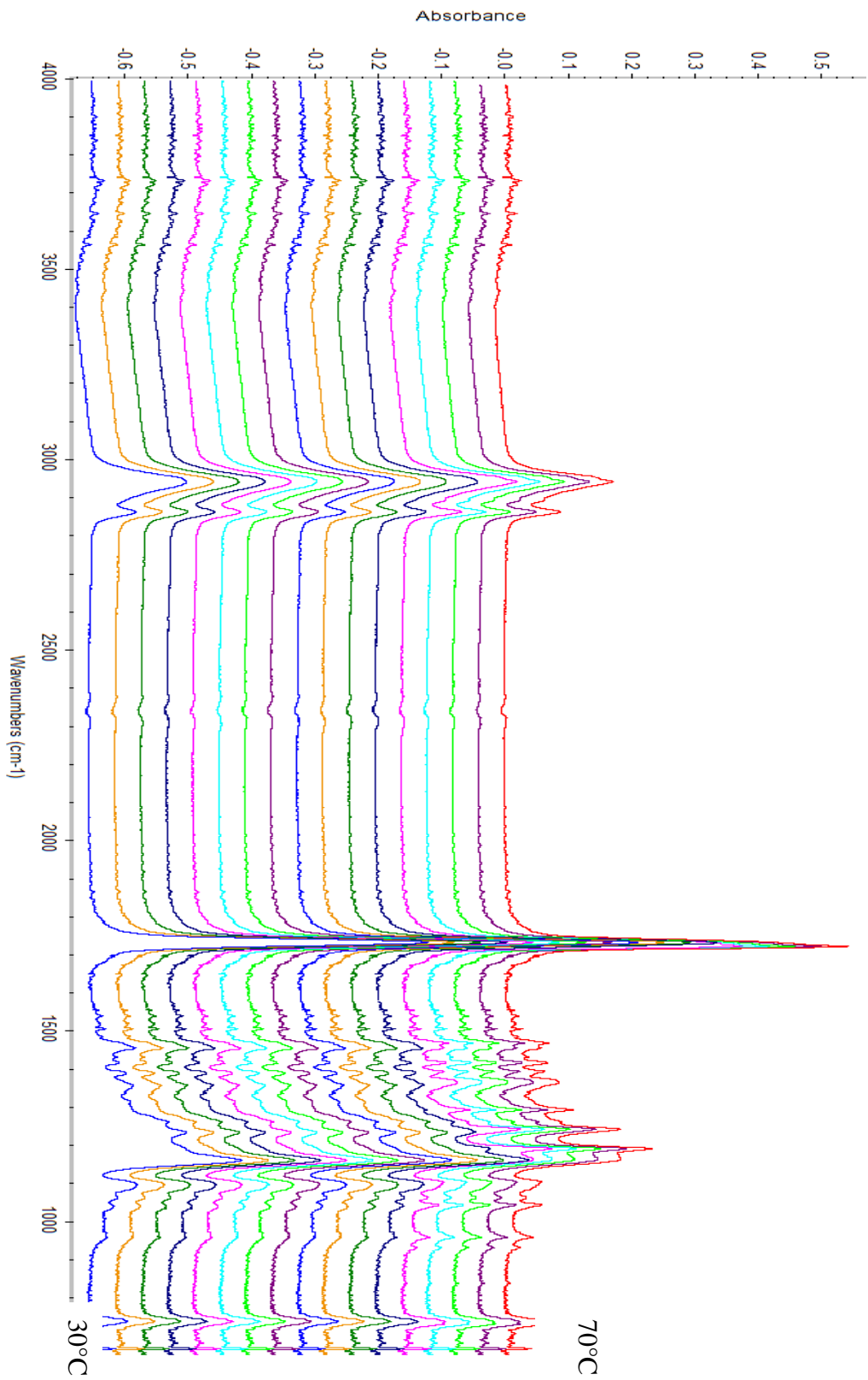


Figure 4.2 – Changes to the FTIR spectrum on heating from 30 to 70 °C

Table 4.1 – Molecular assignment of the characteristic IR bands – change on crystallisation

Wavenumber /cm ⁻¹	Vibrational Assignment	Intensity	Comments
2960 2945 2900 2865	Asymmetric Stretching of >CH ₂ Symmetric Stretching of >CH ₂	vw m vw m	Crystalline Amorphous Crystalline Amorphous
1735 1724	>C=O Stretching	s s	Amorphous Crystalline
1471 1458	>CH ₂ Bending	vw vw	Crystalline Amorphous
1396 1390	>CH ₂ Wagging	w w	Crystalline Amorphous
1295 1245 1237	Asymmetric Stretching of C-O-C Symmetric Stretching of C-O-C Symmetric Stretching of C-O-C	w m w w	Crystalline Crystalline Amorphous Amorphous
1193 1163 1107 1066 1047	>CH ₂ Deformation >CH ₂ Deformation	w w w	Crystalline Amorphous No change No change No change
960 950 735	-C-O Stretching	w w w	Crystalline Amorphous No change

s: strong, m: medium, w: weak and vw: very weak intensity

4.3.2 Analysis of FTIR Spectrum of PCL

Many of the absorption bands split on melting or re-crystallisation can be associated with differences in the force fields of the amorphous and crystalline domains or due to differences in chain configuration, e.g. cis and trans; in these regions the crystalline being limited to trans and the amorphous is in thermal equilibrium between cis and trans. To simplify these complex changes the analysis was carried out on the separate functional absorption bands.

4.3.2.1 Methylene Stretching Region - 3000-2600 cm^{-1}

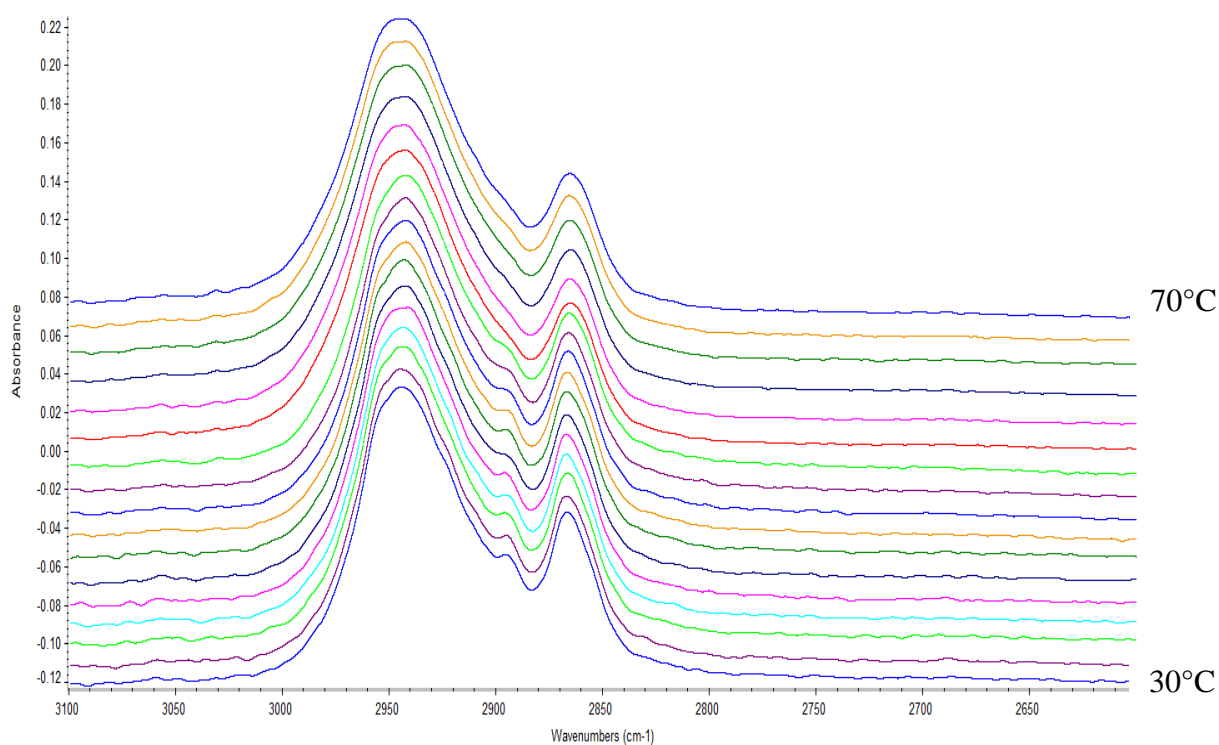


Figure 4.3 – Changes to the FTIR spectrum of PCL on heating from 30 to 70°C in the region 2750-3000 cm^{-1}

The change in the doublet on heating from 30 to 70°C can be seen in Figure 4.3. The bands are due to the asymmetric and symmetric stretching of the methylene $>CH_2$ bonds. On crystallisation the asymmetric band sharpens and a minor band develops at 2900 cm^{-1} with a shoulder at 2960 cm^{-1} which are attributed to the symmetric and asymmetric stretching of the crystalline band, since its appearance and disappearance were observed to be reversible on crystallization and melting. The intensities of the crystalline bands were too small for 2D IR correlation analysis to be carried out on these minor changes.

4.3.2.2 Carbonyl Region - $1850\text{-}1600\text{ cm}^{-1}$

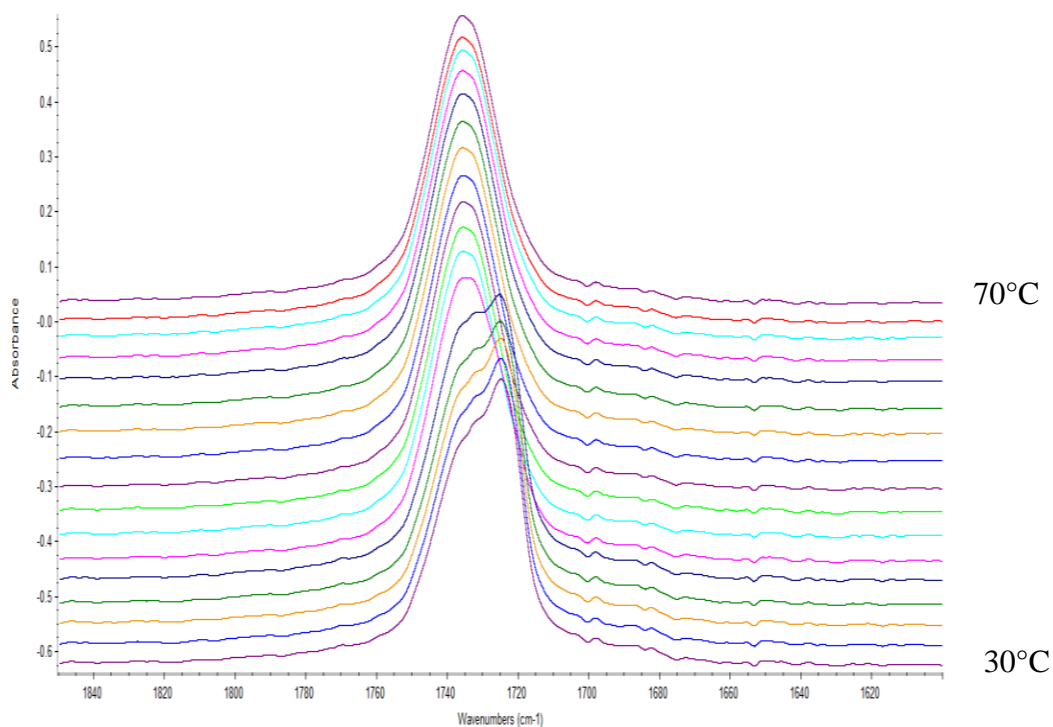


Figure 4.4 – Change to the carbonyl absorption band on cooling from 70 °C – 30 °C

Significant changes occurred to the carbonyl band centred at 1735 cm^{-1} during crystallisation at around $43\text{ }^{\circ}\text{C}$, as illustrated in Figure 4.4. The broader band exhibited in the melt shifted and became narrower, presenting a maximum at 1725 cm^{-1} . These broad and narrow bands were attributed to amorphous and crystalline regions of PCL respectively.

3D and 2D correlation maps of the carbonyl absorption band are shown in Figure 4.5 and Figure 4.6. The three-dimensional synchronous correlation map given in Figure 4.5A shows a large peak at high wavenumber which progressively decreases in intensity, and a second peak which develops simultaneously at a lower wavenumber. Although it is difficult to show clearly in the 3D illustration, there is a coupling between the two. The two-dimensional correlation map shown in Figure 4.5B shows the characteristic angel pattern of a single absorption band that shifts position from higher to lower wavenumber, coupled with a change in intensity. The pattern comprises of two positive auto-peaks and two negative cross peaks. One auto-peak is disproportionately large compared to the other due to the difference in breadth of the two absorption bands, with the amorphous band being much broader than the narrow crystalline band. The maximum intensity of the two auto-peaks can be used to define the wavenumber of the initial and final peak; 1735 and 1725 cm^{-1} respectively. The asynchronous spectra are shown in Figure 4.6. The 2D correlation exhibits a two-way pattern indicating the simultaneous decrease in intensity of the higher wavelength band and increase in intensity of the lower wavelength band. Both the angel pattern presented via the synchronous spectrum and the two-way pattern illustrated via the asynchronous spectrum are characteristic of two component bands, attributed to amorphous and crystalline regions, both of which show changes in intensity but in opposite directions.

These changes make the ratio of the two carbonyl absorption bands a convenient method of measuring the fractional crystallinity [8].

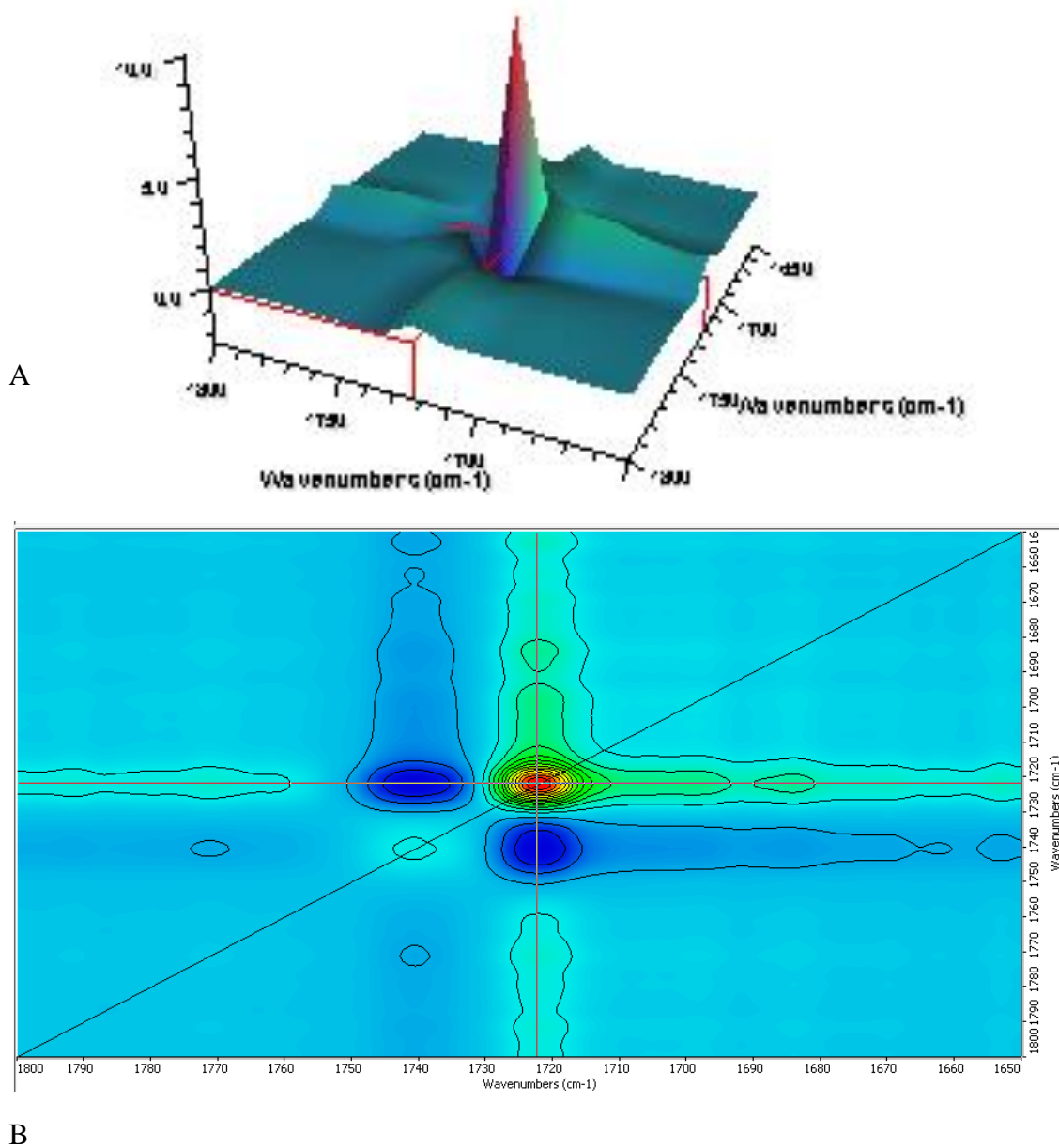
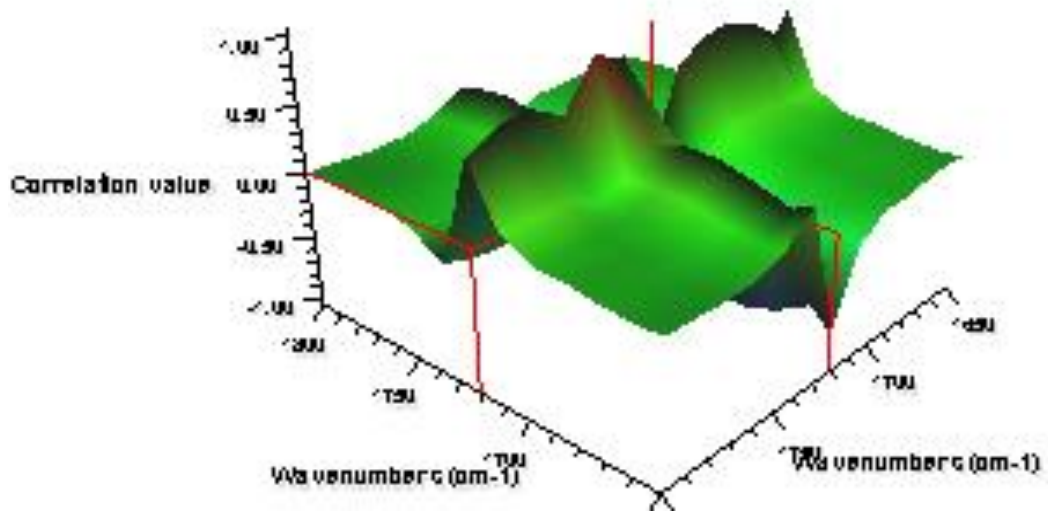
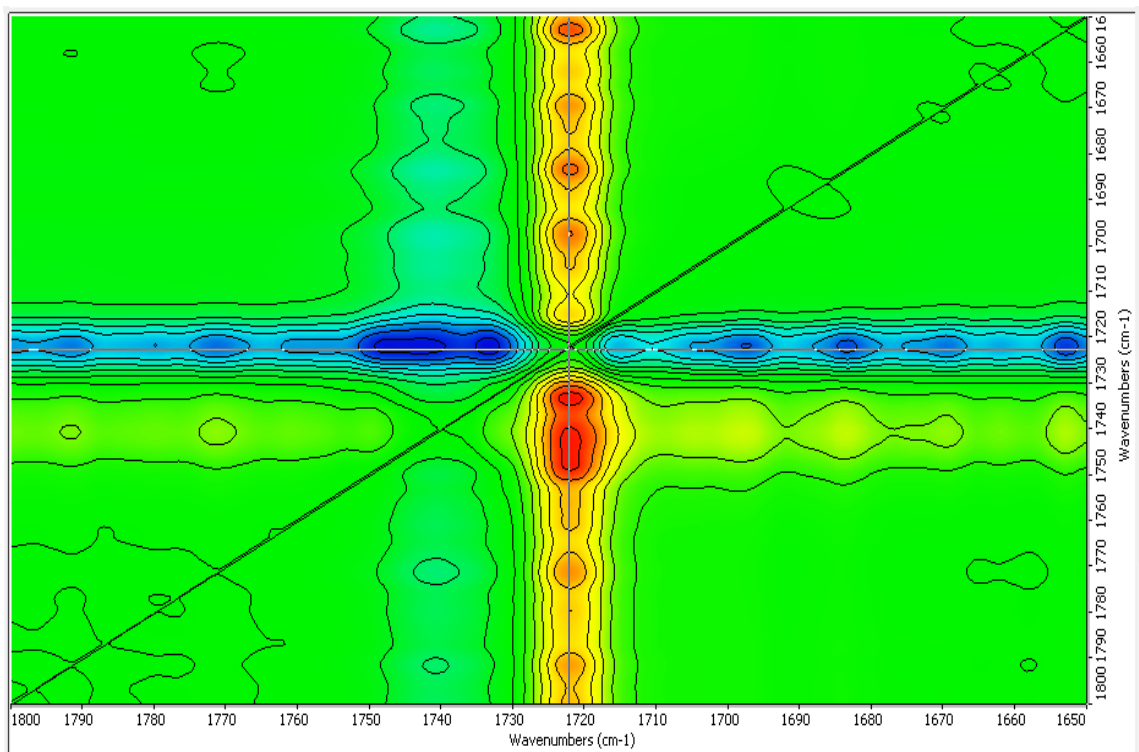


Figure 4.5 – 3D (A) and 2D (B) synchronous correlation intensity contour map of the carbonyl band in region 1800-1650 cm⁻¹



A



B

Figure 4.6 – 3D (A) and 2D (B) asynchronous correlation map of the carbonyl absorption band in region 1800-1650 cm^{-1}

4.3.2.3 Methylene Groups – 1400-1350 cm^{-1}

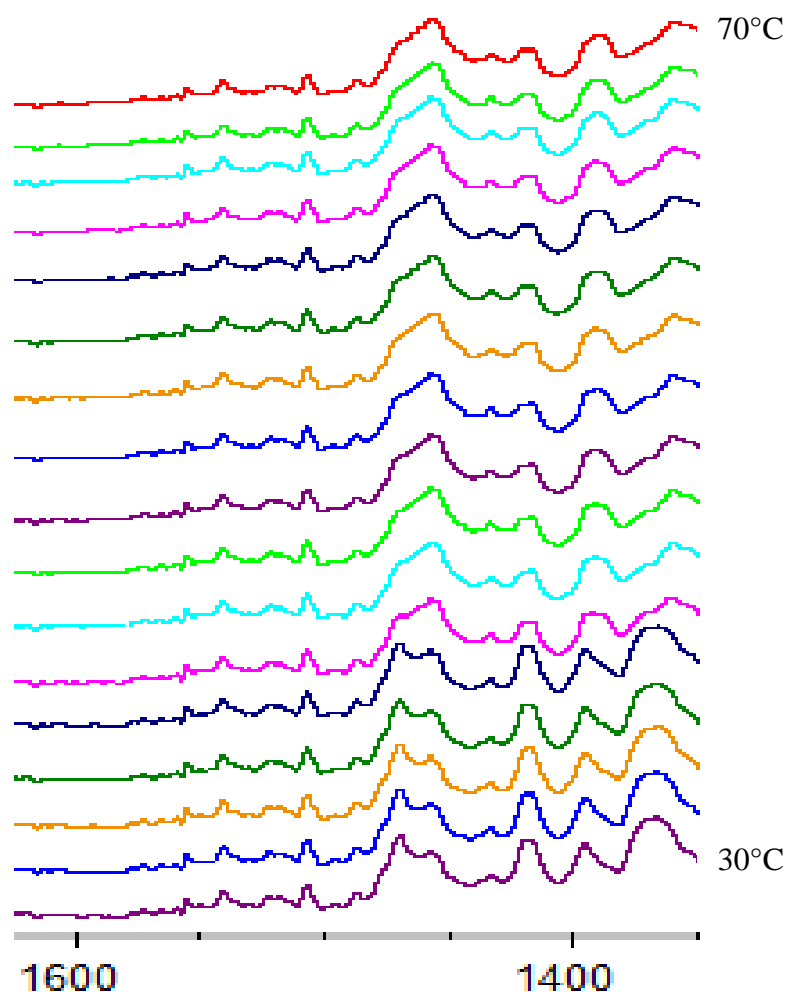


Figure 4.7 – Changes to the FTIR spectrum on heating from 30 to 70°C in the region 1350-1600 cm^{-1}

The change in the bending and wagging modes of the methylene group, as assigned in Table 4.1 are shown in Figure 4.7 and while it was possible to assign them to crystalline and amorphous regions from the change on melting and crystallising the intensities of the bands were too low for correlation analysis to be meaningful.

4.3.2.4 Ester Group - 1250-1000 cm^{-1}

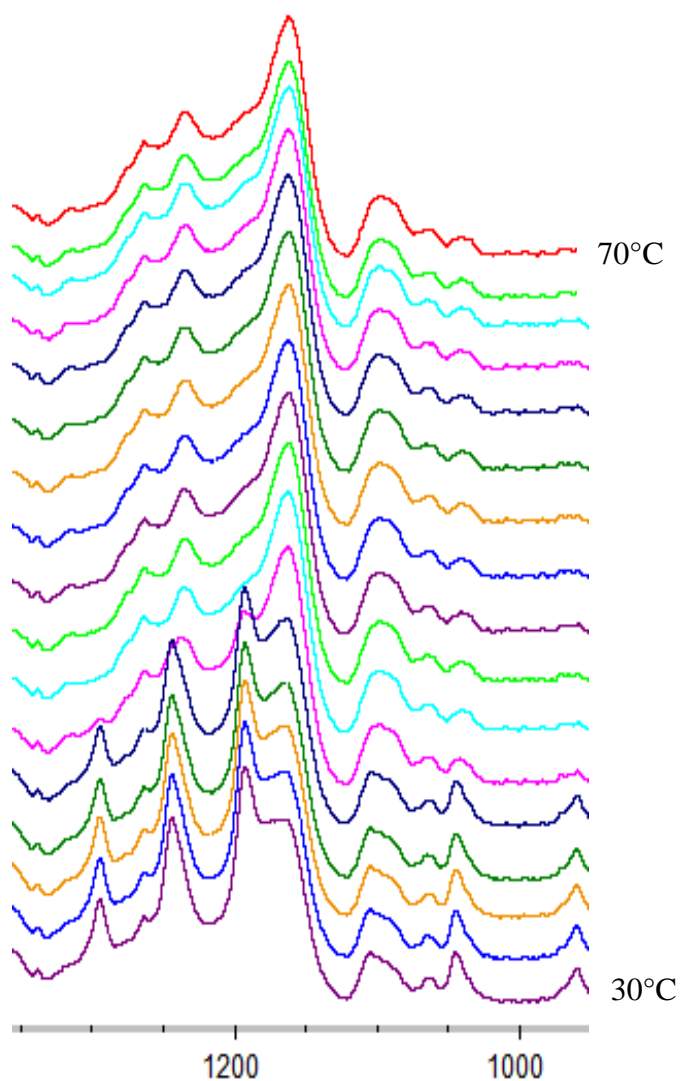


Figure 4.8 – Change to the FTIR spectrum of heating from 30 to 70°C in the region 1000-1350 cm^{-1}

The asymmetric and symmetric stretching bands are clearly sensitive to environment as well as change in intensity and wavenumber on melting such that they can be assigned to crystalline and amorphous regions from these changes. However the presence of many overlapping peaks makes the measurement of intensity dependent on baseline determination and accordingly they were not analysed further. This was also true with the methylene group deformation peaks at 1163 and 1194 cm^{-1} although they

are a very good example of the change in the spectra from crystalline to amorphous material.

4.4 Conclusions

The FTIR spectrum of PCL exhibits many peaks, which can be assigned to the rotational-vibrational movement of difference absorption bands, which have been given in Table 4.1. Changes in band position and intensity occur during crystallisation and melting, with the most notable change in PCL occurring in the carbonyl peak at 1728 cm^{-1} . Here a broad amorphous band located at 1735 cm^{-1} reduces in intensity simultaneously with an increase in the crystalline band at 1725 cm^{-1} . This has been analysed using 2D spectroscopy and the resulting *angel* pattern confirms the presence of two overlapping component bands attributed to amorphous and crystalline phases, with a simultaneous intensity change and shift in band position. This indicates that this group's absorption can be used to measure the fractional crystallinity and follow its development with time in a kinetic study. Other absorption bands may also be used but baseline problems produced by overlapping with adjacent bands and low intensity make them less desirable for this purpose.

4.5 References

1. Noda, I. (1989), Two-dimensional infra-red spectroscopy, *Journal of the American Chemical Society*, **111**, 8116-8118
2. Noda, I. & Ozaki, Y. (2004), *Two-Dimensional Correlation Spectroscopy – Applications in Vibrational and Optical Spectroscopy*, John Wiley & Sons, Chichester: UK

3. Noda, I. (2006), Kernel analysis for two-dimensional (2D) correlation spectroscopy, *Journal of Molecular Structure*, **799**, 34-40
4. Noda, I. (2006), Cyclical asynchronicity in two-dimensional (2D) correlation spectroscopy, *Journal of Molecular Structure*, **799**, 41-47
5. Morita, S., Shinzawa, H., Noda, I. & Ozaki, Y. (2006), Effect of band position shift on moving-window two-dimensional correlation spectroscopy, *Journal of Molecular Structure*, **799**, 16-22
6. Zhu, B., Li, J., He, Y., Yoshie, N. & Inoue, Y. (2003), Hydrogen-bonding interaction and crystalline morphology in the binary blends of poly(ϵ -caprolactone) and polyphenol catechin, *Macromolecular Bioscience*, **3**, 684-693
7. Elzein, T., Brogly, M. & Schultz, J. (2003), Quantitative calculation of the orientation angles of adsorbed polyamides nanofilms, *Polymer*, **44**, 3649-3660
8. Chen, Z., Hay, J. N. & Jenkins, M. J. (2013), The kinetics of crystallisation of poly(ethylene terephthalate) measured by FTIR spectroscopy, *European Polymer Journal*, **49**, 1722-1730

Chapter 5. – Isothermal Crystallisation

Kinetics as measured by FTIR Spectroscopy.

The use of Fourier Transform Infra-Red Spectroscopy (FTIR) is becoming more common in the study of crystallisation kinetics as the use of DSC does not enable any appreciable investigation of the development of secondary crystallisation with time [1-3]. FTIR spectroscopy can be used to measure directly the degree of crystallinity and study its development over extended periods of time well into the secondary crystallisation process. This use of this technique to measure the crystallisation kinetics of PCL is the subject of this chapter.

5.1 Results and Discussion

5.1.1 Changes in FTIR Spectrum of PCL during Crystallisation

As noted in the previous chapter many changes occur in the FTIR spectrum of PCL with time during crystallisation and melting; this includes shift in the position as well as intensities of the absorption bands. These have been attributed to conformational changes in the polymer chain with temperature as well as on crystallising. This can be seen most noticeably in the PCL carbonyl peak at 1728 cm^{-1} . This led to the use of this peak to follow the development of crystallinity in PCL, and later to evaluate the kinetics of crystallisation of PCL. A comparison will be made with the kinetic rate parameters determined by DSC.

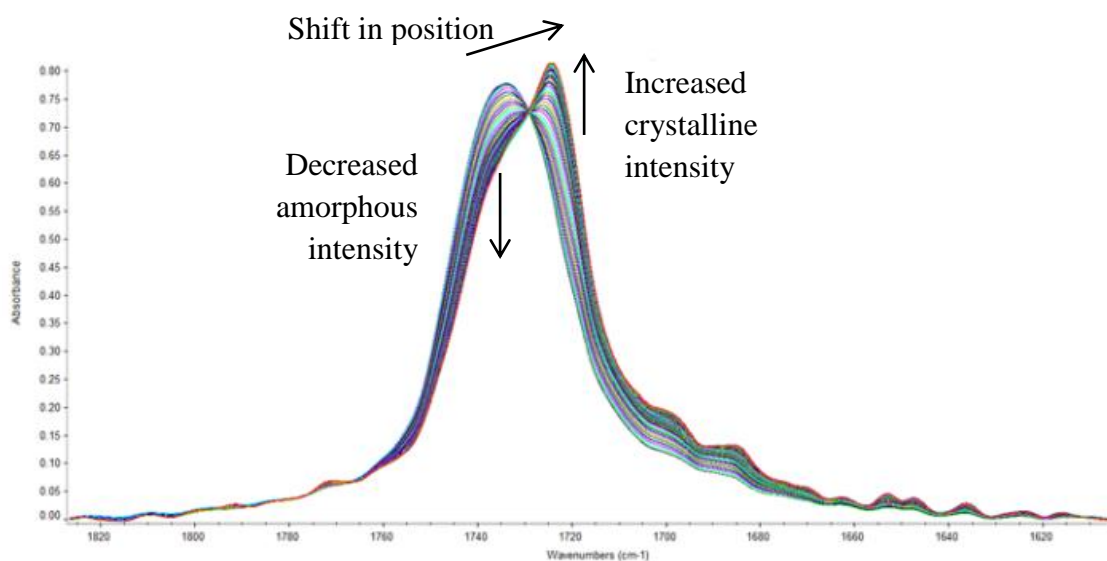


Figure 5.1 – Change in peak position and intensity of amorphous and crystalline bands with time

An example of how the carbonyl peak shifts and the intensity of the crystalline (at 1725 cm^{-1}) and amorphous (at 1735 cm^{-1}) peaks increase and decrease respectively over time can be seen in Figure 5.1. These changes occur simultaneously, illustrated by the isobestic point at 1728 cm^{-1} . This particular illustration of isothermal crystallisation was carried out at $43\text{ }^{\circ}\text{C}$, although similar observations have also been made in the isothermal crystallisation temperature range of $43\text{-}47\text{ }^{\circ}\text{C}$.

The regions of the spectra shown in Figure 5.1 were baseline corrected at two fixed wavenumbers either side of the carbonyl peak and the intensities auto-smoothed. The carbonyl peak was then de-convoluted into two absorption bands by Omnic software to achieve the best possible fit, as detailed in section 2.2.2.3. This is represented diagrammatically in Figure 5.2. The result of resolving the carbonyl peak into its two absorbance bands as a function of time is given in Figure 5.3.

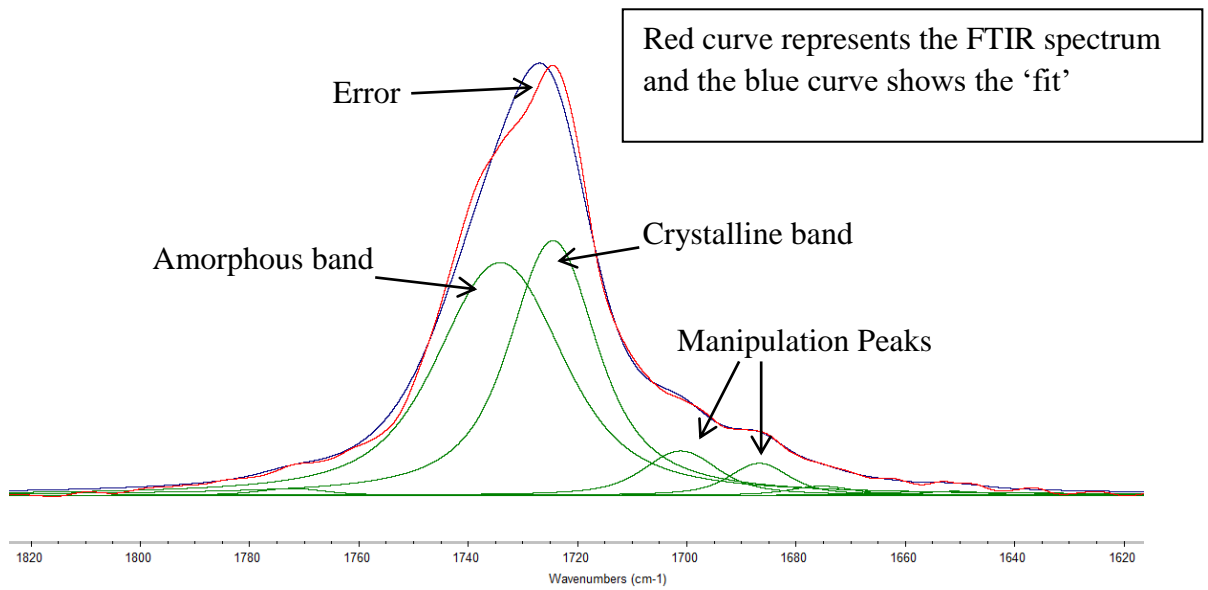


Figure 5.2 – Illustration of the deconvolution of the carbonyl band into its component parts

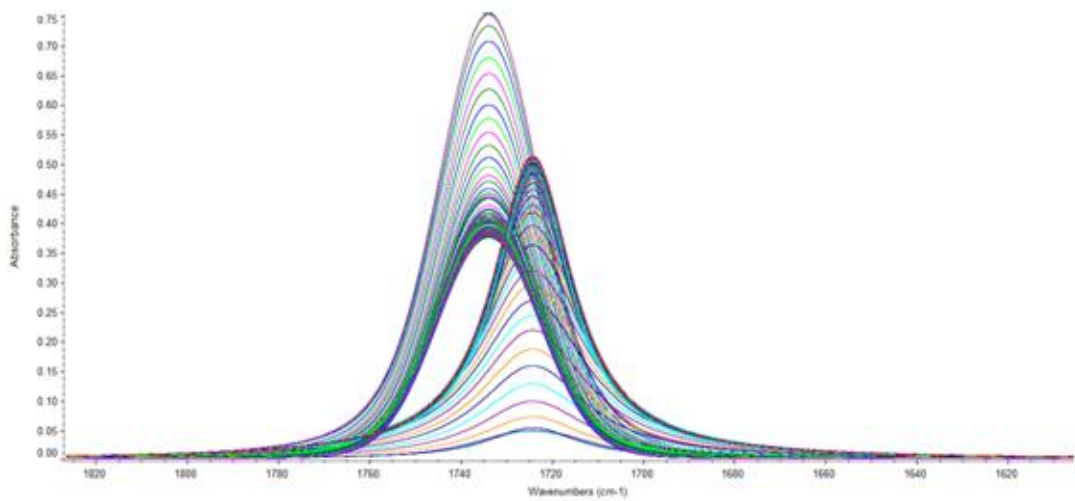


Figure 5.3 – Result of resolving the carbonyl absorption band into its two component parts on crystallisation

The development of the crystalline intensity with the logarithm of time for each isothermal temperature is presented in Figure 5.4 and shows the characteristic time dependence, which is commonly seen during the development of crystallinity. It compares favourably with that monitored by DSC [4-9] and discussed in Chapter 3. The initial exponential increase in crystallinity with time, attributed to primary crystallisation, was followed by a logarithmic dependence on time attributed to secondary crystallisation. Secondary crystallisation, however, could not be measured by DSC to any appreciable extent. Clearly DSC lacked the sensitivity to detect the small changes in heat flow from this process over the long time scale involved. FTIR spectroscopy, by measuring the change in intensity of a crystalline peak, does not have this problem; if one is prepared to wait changes will be observed.

The amorphous band showed the reverse dependence on the logarithm of time, with the intensity decreasing with time. Again two regions were present: The initial decrease in intensity followed the temperature drop on cooling to the crystallisation temperature. Once the isothermal temperature has been reached there was an induction period during which the absorbance was constant before it decreased exponentially as crystallisation developed. After this the rate slows but intensity continues to decrease logarithmically with time. Again these regions are recognised as primary and secondary crystallisation respectively and are illustrated in Figure 5.5.

The differences in the absorbance at each temperature reflect the thickness of film used in the analysis. All were chosen to value maximum absorbances below 1.0.

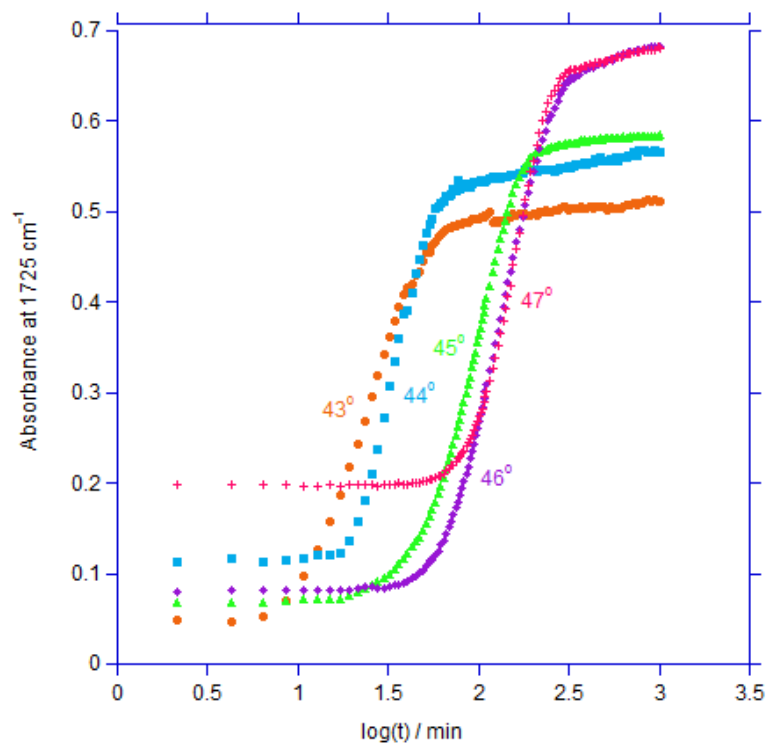


Figure 5.4 – Increase in absorbance of the crystalline band at 1725 cm⁻¹ with log(t)

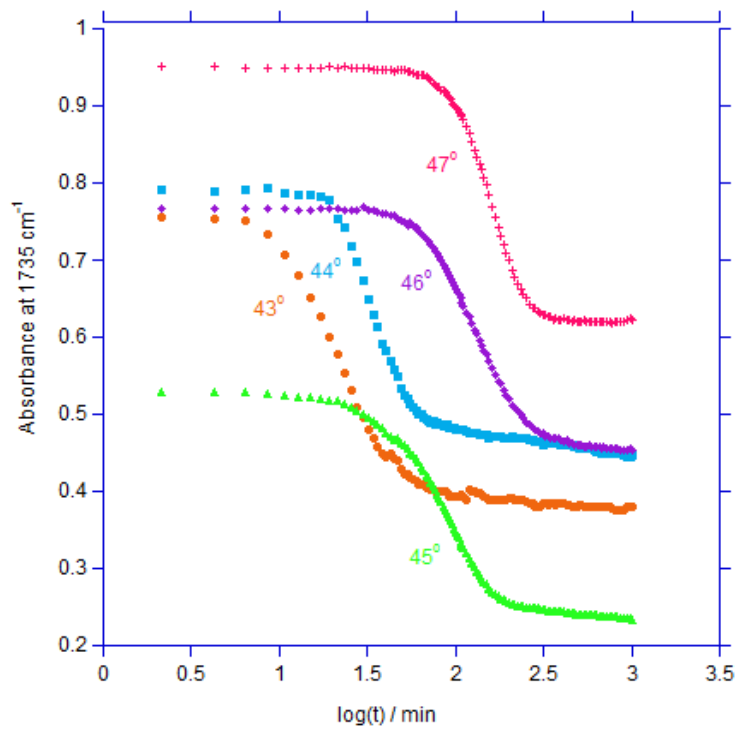


Figure 5.5 - Decrease in absorbance of the amorphous band at 1735 cm⁻¹ with log(t)

A crystallising polymer is considered to follow a two-phase model, whereby the amorphous weight fraction, $X_{a,t}$, is related to the crystalline weight fraction, $X_{c,t}$, at time, t , such that

$$X_{a,t} + X_{c,t} = 1 \quad \text{Equation 5.1}$$

with $X_{a,t}$ defined as $A_{a,t}/A_{a,0}$, $A_{a,t}$ is the amorphous band absorbance at time, t , and $A_{a,0}$ is the amorphous band absorbance at time t_0 , where no crystallinity has developed. It therefore follows that

$$X_{c,t} = 1 - (A_{a,t}/A_{a,0}) \quad \text{Equation 5.2}$$

Since $A_{a,t}/A_{a,0} + A_{c,t}/A_{a,0} = 1$, Equation 5.3

Then $A_{c,t} = A_{c,0} - A_{a,t} (A_{c,0}/A_{a,0})$ Equation 5.4

And also $A_{a,t} = A_{a,0} - A_{c,t} (A_{a,0}/A_{c,0})$ Equation 5.5

The linear relationship described above is illustrated in Figure 5.6 for each isothermal temperature, and was used to support this interpretation of spectral changes exhibited during crystallisation measured by FTIR spectroscopy. The plots of $A_{c,t}$ against $A_{a,t}$ and $A_{a,t}$ against $A_{c,t}$ gave intercepts of $A_{c,0}$ and $A_{a,0}$. These values were used to calculate the fractional crystallinity and the amorphous content with time. These followed the same dependence as observed with the intensities of the absorption bands and are given in Figure 5.7 and Figure 5.8 respectively.

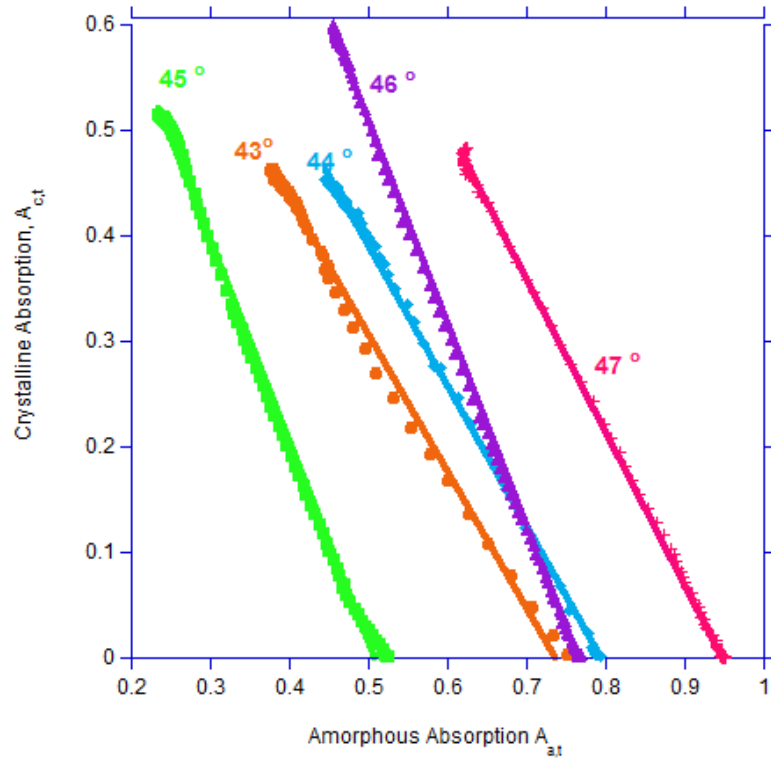


Figure 5.6 – Dependence of the crystalline on amorphous absorption with crystallisation temperature

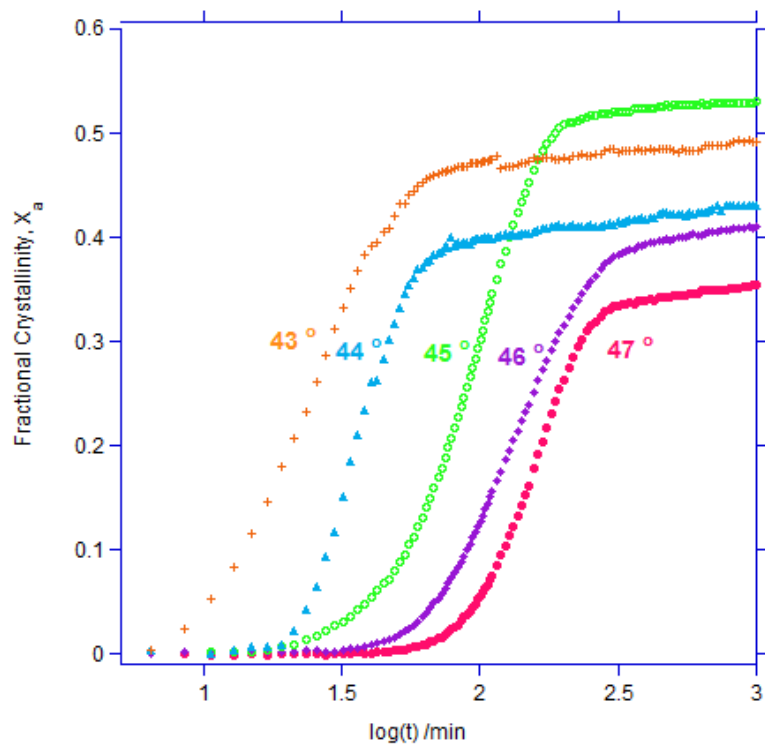


Figure 5.7 - Development of fractional crystallinity with log(t)

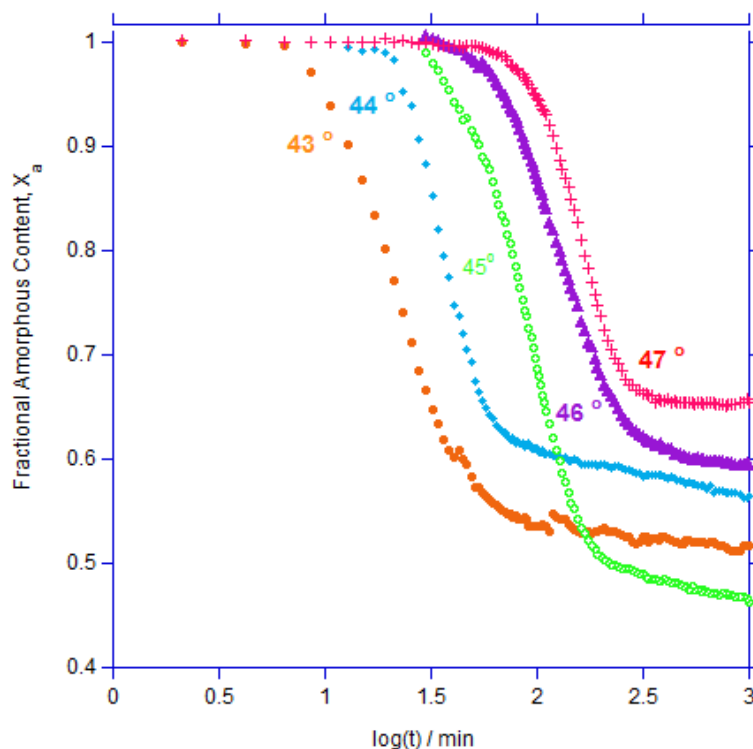


Figure 5.8 - Decrease in fractional amorphous content with $\log(t)$

The development of the fractional crystallinity, X_c , and the decrease in the amorphous content, X_a , with time were summed and compared with the assumption given above that the total of the two values should be equal to 1. This indicated an average error of $\pm 0.5\%$ in the measurements and is illustrated in Figure 5.9. The fractional crystallinity obtained from the amorphous content, $(1-X_a)$ was compared directly with that determined directly from the crystalline band, X_c , see Figure 5.10, at each crystallization temperature. In every case the degree of agreement in fractional crystallinity between the two sets of data was better than ± 0.01 . These curves were used to analyse the kinetics of the phase transition using the Avrami equation.

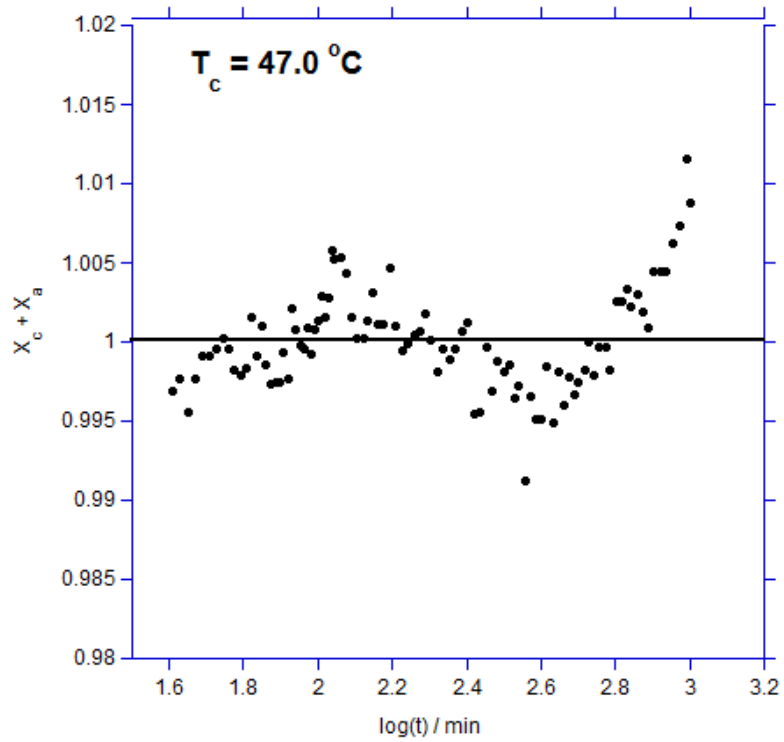


Figure 5.9 - Consistency of the data with Equation 5.1 over the total crystallisation process

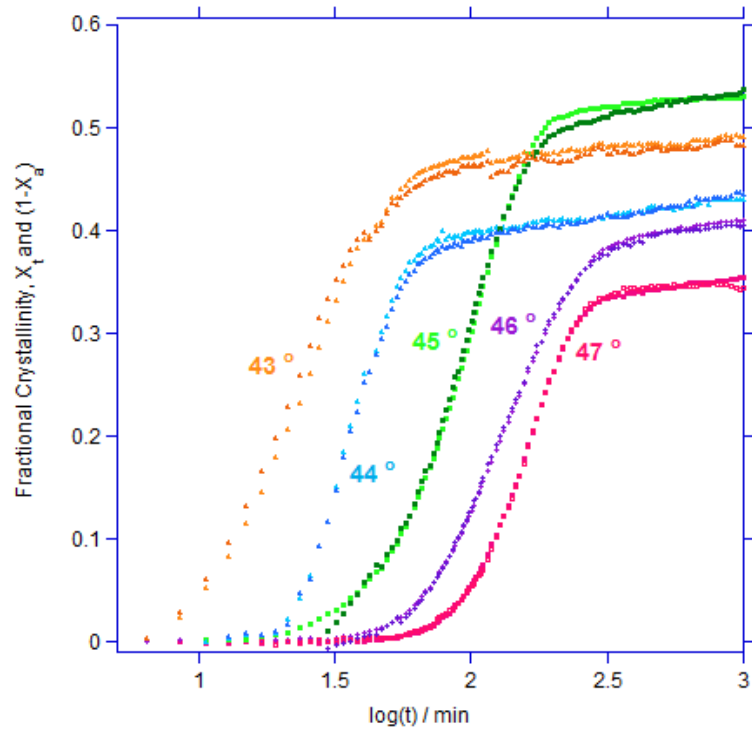


Figure 5.10 - Comparison of the fractional crystallinity determined from the absorption of the crystalline and amorphous bands

5.1.2 Kinetic Analysis of Crystallisation from FTIR Spectroscopy

5.1.2.1 Primary Crystallisation

The development of the crystalline fraction with time was calculated for each crystallisation temperature and used to measure the crystallisation kinetics of the primary and secondary processes of the phase transition. The change in fractional crystallinity as a function of $\log(t)$ is presented in Figure 5.7 for a range of isothermal crystallisation temperatures between 43 and 47 °C.

The characteristic initial exponential dependence is present and illustrates that the fractional crystallinity with time follows an Avrami equation [10-11], given by

$$1 - X_t = \exp(-Zt^n) \quad \text{Equation 5.6}$$

where X_t is the fractional crystallinity at time t , Z is a rate constant incorporating the time dependent characteristics of nucleation and growth, and n is the Avrami exponent,. n takes different values depending on the crystallisation mechanism. A linear increase with $\log(t)$, attributed to secondary crystallisation [1,2,12], is seen to follow this.

The analysis was conducted assuming a two-phase crystallisation model; a primary stage in which crystals grow until impingement occurs and a secondary stage in which further development of crystallinity occurs within the boundaries of the crystalline regions.

These two stages follow a different time dependency and so are described by modified Avrami equations. The primary stage was limited to the initial stages up to a point, $X_{p,\infty}$, at which secondary crystallisation was considered to dominate the increase in crystallinity. The Avrami equation was modified to include the two, so

$$X_{p,t} = X_{p,\infty} [1 - \exp(-Z_p(t - t_i)^{n_p})] \quad \text{Equation 5.7}$$

where $X_{p,t}$ is the crystalline fraction developed at time t , Z_p and n_p are the rate constant and the Avrami exponent for the primary process respectively and t_i is the induction time. The parameters $X_{p,\infty}$ and t_i were adjustable and represented the end of the primary process and the initial onset of crystallisation respectively. The optimum values of these parameters were selected as those that provided the best linear fit to the Avrami plot, using the regression coefficient R^2 , and were taken from the intersection of the primary and secondary processes. These along with the primary crystallisation rate parameters determined from this analysis are presented in Table 5.1 with the linear plot of $\log [-\ln (1-X_{p,t}/X_{p,\infty})]$ against $\log(t)$ given in Figure 5.11. The effect of varying the induction time, t_i , on the linearity of the Avrami plot and the sum of the squares of the residuals, R^2 , are presented in Figure 5.12 and Figure 5.13 and enabled the optimum values of n and t_i to be determined.

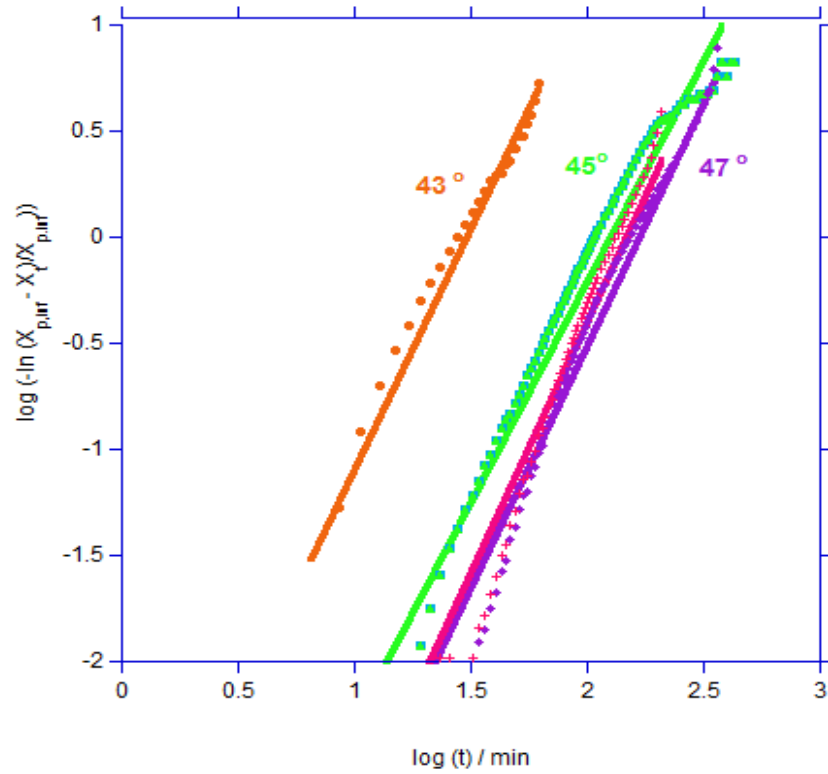


Figure 5.11 – Avrami double-log plot for the primary process of crystallisation between 43-47 °C

Table 5.1 – Avrami parameters for primary crystallisation.

Temp (°C)	$X_{p,\infty}$	$n \pm 0.2$	t_i (min)	$t_{1/2}$ (min)	Z_p (min ⁻ⁿ) $\times 10^6$
43	0.455	2.36	0	20	8150
44	0.395	3.12	5	30	171
45	0.500	2.61	10	74	10.2
46	0.390	2.30	15	108	14.6
47	0.330	2.63	20	130	1.91

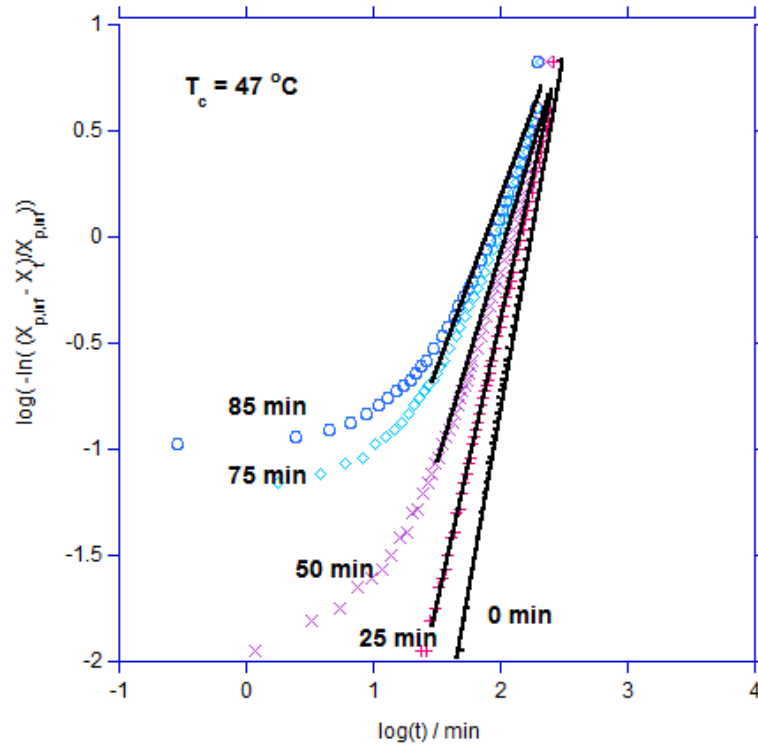
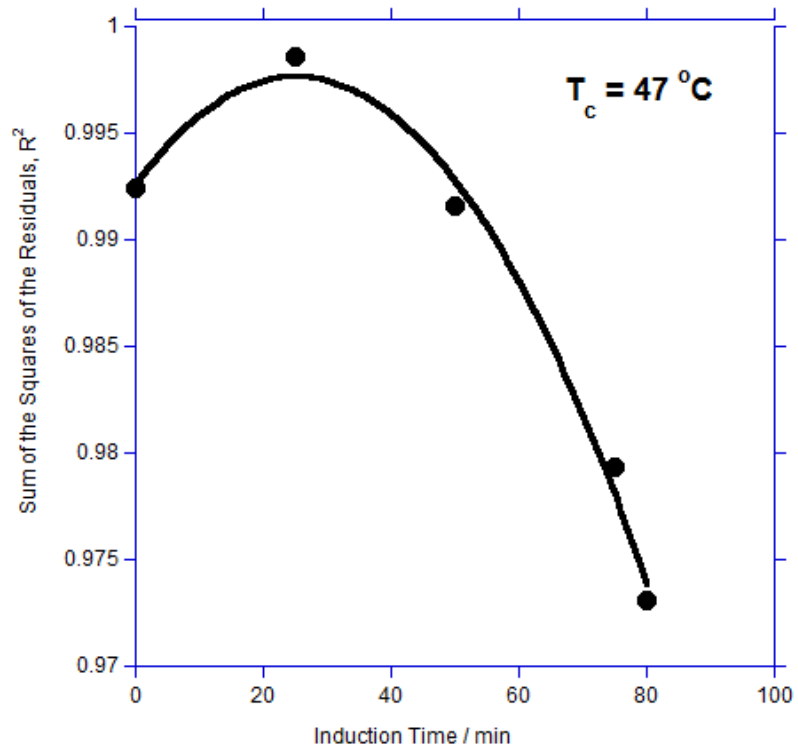
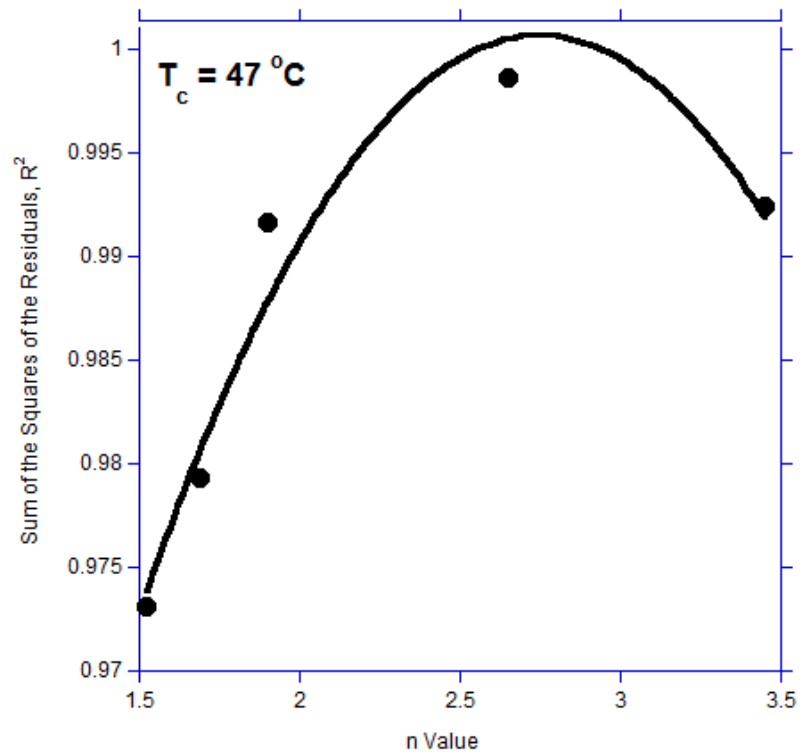


Figure 5.12 - The effect of induction time on the linearity of the $\log(-\ln(X_{p,inf} - X_t)/X_{p,inf})$ plots



A



B

**Figure 5.13 – Effect of induction time on
A – degree of fit and B – n value**

The crystallisation rate parameters for the primary process are listed in Table 5.1 and show strong dependence in both half-life, $t_{1/2}$, and the rate constant, Z_p , with temperature. The $t_{1/2}$ values were taken to be the time at $X_{p,\infty}/2$ and exhibited an exponential increase with crystallisation temperature. Z_p was calculated from

$$Z_p = \ln 2 / (t_{1/2})^n \quad \text{Equation 5.8}$$

This decreased exponentially with increasing crystallisation temperature and is characteristic of nucleation controlled crystallisation. The best fit values of $X_{p,\infty}$ indicate the primary process was restricted to the first 27-35% crystallinity, and this percentage increased with increasing temperature.

The observed n values of 2.4 and 3.1 ± 0.2 are in line with those previously determined for PCL [13-16], and with those values observed previously in this thesis from the DSC experiments. Chen and Wu (2007) [13] found that the primary crystallisation of PCL exhibited n values of 2.6 – 2.9 whilst Atanase et al (2011) [15] obtained n values of 2.5 – 3.1; both adopted isothermal temperatures similar to those used in this thesis and their results are in good agreement with the results listed in Table 5.1. The values of n have been attributed to predetermined nucleation of spherulites as required by the Avrami equation for which n should be 3.0. Many reasons for the observation of fractional values have been cited in the literature, and these involve non-uniform nucleation and non-negligible volume of nuclei [17-18].

5.1.2.2 Secondary Crystallisation

Secondary crystallisation processes occur consecutively to primary crystallisation and is deemed to begin after the primary stage has finished. Several kinetic equations have been developed to follow the development of secondary crystallisation with time, but the most widely accepted is that it obeys an Avrami equation with an n value of 1.0.

If primary and secondary crystallisation are consecutive processes, then the fractional crystallinity, X_t , at time, t, is the sum of the two Avrami equations, where

$$\mathbf{X_t = X_{p,t} + X_{s,t}} \quad \mathbf{Equation\ 5.9}$$

If these two processes have final values of $X_{p,\infty}$ and $X_{s,\infty}$, the fractional crystallinity at the end of primary and secondary crystallisation respectively, then

$$\mathbf{X_t = X_{p,\infty} [1-(\exp(-Z_p t^{n_p}))] + X_{s,\infty} [1-(\exp(-Z_s(t - t_{p,\infty})^{n_s}))]} \quad \mathbf{Equation\ 5.10}$$

At the end of the primary process, at $X_{p,\infty}$, the first term is constant and if the secondary process is analysed when $X_t > X_{p,\infty}$ then

$$\mathbf{X_t = X_{p,\infty} + X_{s,\infty} [1-(\exp(-Z_s(t - t_{p,\infty})^{n_s}))]} \quad \mathbf{Equation\ 5.11}$$

Avrami plots for the secondary process are given in Figure 5.14 and the kinetic parameters obtained are presented in Table 5.2. The best fit values of n_s were determined in the linear region of dependence on $\log(t)$.

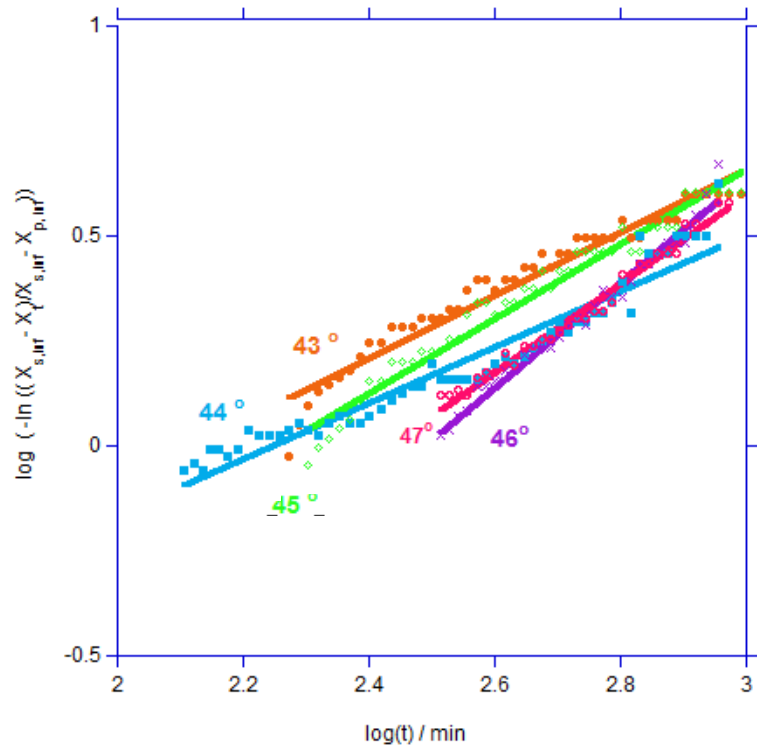


Figure 5.14 – Avrami fit to secondary crystallisation

Temp (°C)	$t_{1/2}$ (min)	$n \pm 0.1$	$-\log Z_s$ (min^{-n_s})	R^2	$X_{p,\infty}$	$X_{s,\infty} - X_{s,\infty}$
43	79	0.75	1.58	0.950	0.45	0.081
44	103	0.67	1.51	0.933	0.40	0.086
45	121	0.89	2.01	0.966	0.47	0.056
46	230	1.25	3.11	0.978	0.34	0.071
47	186	1.05	2.51	0.982	0.35	0.066

Table 5.2 –Avrami parameters for secondary crystallisation

As can be seen from Figure 5.14, the plots are linear and exhibit a successful fit of the Avrami equation to the data. In most cases the lines are parallel, with an average n value of 1.0 ± 0.3 , and there was no systematic change with crystallisation temperature; differences were only noticed with choice of $X_{p,\infty}$ and $t_{p,\infty}$. Values of the half-life were calculated from the Z_s value since

$$t_{1/2} = (\ln 2 / Z_s)^{1/n} \quad \text{Equation 5.12}$$

These increased with temperature, consistent with nucleation control of crystallisation.

5.1.2.3 Temperature Dependence of Crystallisation Growth Rates

The temperature dependence of crystallisation can be estimated over a wide range of temperatures using an expression based on the theory of Hoffman & Lauritzen [19] which was modified by Chan & Isayev [20]. This equation assumes that the number of nucleation sites is dependent on temperature and that all sites are activated at the same time, and describes the overall rate of crystallisation as a function of temperature. The spherulite growth rates, g and g_0 from the Hoffman-Lauritzen expression were substituted for $(1/t_{1/2})$ and $(1/t_{1/2})_0$ respectively to give the overall function

$$\left(\frac{1}{t_{1/2}}\right) = \left(\frac{1}{t_{1/2}}\right)_0 \exp\left[\frac{-U^*}{R(T - T_\infty)}\right] \exp\left[\frac{-K_g}{T(\Delta T)}\right] \quad \text{Equation 5.13}$$

where U^* is the activation energy of viscous flow and taken to be 6284 J mol^{-1} [21], T_∞ is the thermodynamic glass transition temperature, K_g the nucleation constant, T the crystallisation temperature, and ΔT the super-cooling from the equilibrium melting point, T_m^0 .

Figure 5.15 shows plots of $\ln (1/t_{1/2})+U^*/R(T-T_\infty)$ against $1/(T\Delta T)$ for both primary and secondary crystallisation, with both sets of data exhibiting linear relationships. The slopes of the lines were 1.84 and $1.01 \times 10^5 \text{ K}^2$ respectively, corresponding to the nucleation regimes I and II. Primary crystallisation occurs under Regime I and secondary crystallisation occurs under Regime II, since the ratio of K is around 2:1 [1].

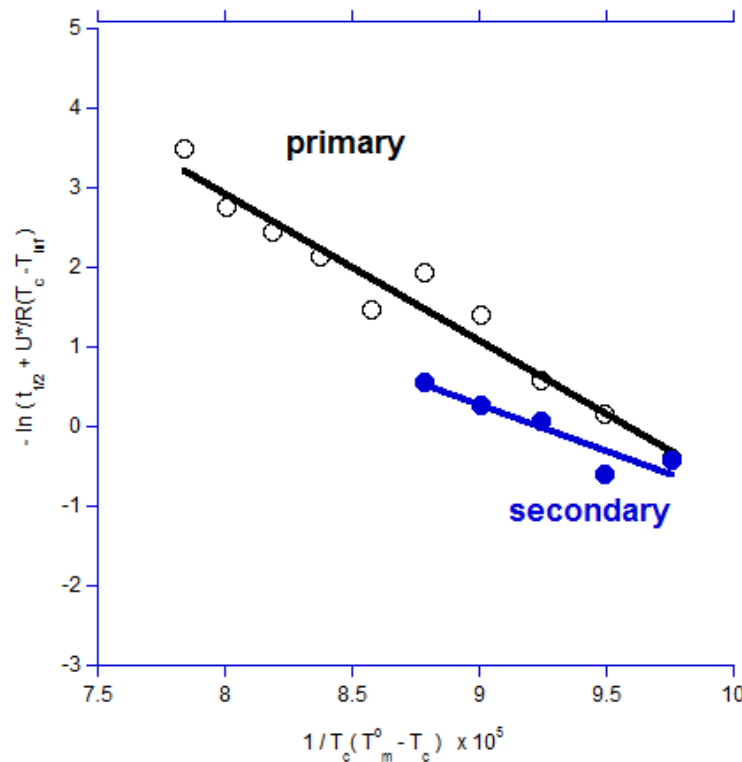


Figure 5.15 – Dependence of half-life on the degree of super-cooling

Following Hoffman and Lauritzen's theory of nucleation, Regime I is considered to occur at low degrees of super-cooling, i.e. at high crystallisation temperatures. Secondary nucleation of the growth surface is rate determined since the first act of nucleation is slow compared with coverage of the surface, and there is a

delay before the next layer is nucleated. For this model the growing surface is smooth and

$$K_I = 4b\sigma\sigma_e T_m^0 / \Delta H_v k \quad \text{Equation 5.14}$$

where b is the monomolecular layer thickness, taken to be the perpendicular separation of (010) planes. σ is free energy of the side surface of the polymer crystal, σ_e the fold surface free energy, k is the Boltzmann constant and ΔH_v the enthalpy of fusion per unit volume. The equilibrium melting point, T_m^0 , of PCL was taken to be 80 °C, plotting experimental data of T_m against T_c and extrapolating the line to intersect $T_m = T_c$. This procedure is described by Hoffman and Weeks and is outlined in Section 1.6.

Regime II is normally observed at lower temperatures, where there are higher degrees of super-cooling, and secondary nucleation is considered to be much quicker where it occurs before the surface layer is covered. For this model, the surface is rough and there are numerous secondary nuclei;

$$K_{II} = 2b\sigma\sigma_e T_m^0 / \Delta H_v k \quad \text{Equation 5.15}$$

where all parameters are the same as above.

Using the crystallographic unit cell dimensions of $a = 7.496 \times 10^{-8}$ cm, $b = 4.974 \times 10^{-8}$ cm and $c = 17.277 \times 10^{-8}$ cm and with 4 monomer units per unit cell [22], the heat of fusion per unit volume, ΔH_v , was calculated to be 118.7 J cm^{-3} and the crystalline density, 1.174 g cm^{-3} .

σ was estimated [19,23-24] from

$$\sigma = 0.11\Delta H_v (ab)^{1/2} \quad \text{Equation 5.16}$$

From this calculation σ was determined to be 7.97×10^{-3} and $\sigma_e 5.49 \times 10^{-2} \text{ J cm}^{-2}$.

5.2 Conclusions

The carbonyl absorbance band in the infra-red spectrum of PCL is sensitive to changes in crystalline content and can be used to determine the degree of crystallinity as a function of time. The fractional crystallinity is directly measured via deconvolution of the absorption band into two components; amorphous and crystalline. An accuracy of $\pm 1\%$ is sufficient for kinetic studies to be carried out on samples during crystallisation. The advantage of this method is that both primary and secondary crystallisation processes can be measured to a similar degree of accuracy and the kinetics can be investigated at higher temperatures and for longer periods than by other analytical methods such as DSC. This enables the secondary crystallisation stage to be studied in greater detail than is possible by DSC.

The overall crystallisation identified two consecutive processes exhibiting different time dependencies, and was attributed to primary and secondary crystallisation. Modified versions of the Avrami equation were applied to each process, producing separate Avrami exponents, n , assigned to each; 3.0 ± 0.4 for the primary phase and attributed to the growth and impingement of spherulites; 1.0 ± 0.2 for the secondary phase and attributed to the thickening of lamellae in a one-dimensional growth which was confined to the amorphous regions between crystals.

Primary crystallisation was found to be initiated by secondary nucleation in Regime I as outlined by Hoffman and Lauritzen. This suggests slow secondary nucleation and rapid cover of the growth face before further nucleation occurs, providing a smooth growth surface. Secondary crystallisation was found to be initiated

in Regime II where multiple nucleation of the growth face occurs and hence produces a rough face to the growth surface. This is due to an increased difficulty in building material on the surface of the lamellae as the melt is constrained between them.

5.3 References

1. Chen, Z., Hay, J. N. & Jenkins, M. J. (2013), The kinetics of crystallisation of poly(ethylene terephthalate) measured by FTIR spectroscopy, *European Polymer Journal*, **49**, 1722-1730
2. Lu, X. F. & Hay, J. N. (2001), Isothermal crystallisation kinetics and melting behaviour of poly(ethylene terephthalate), *Polymer*, **42**, 9423-9431
3. Kong, Y. & Hay, J. N. (2003), Multiple melting behaviour of poly(ethylene terephthalate), *Polymer*, **44**, 623-633
4. Kalkar, A. K., Deshpande, V. D. & Vatsaraj, B. S. (2013), Poly(butylene terephthalate)/montmorillonite nanocomposites: effect of montmorillonite on the morphology, crystalline structure, isothermal crystallisation kinetics and mechanical properties, *Thermochimica Acta*, **568**, 74-94
5. Kai, J., Liu, M., Wang, L., Yao, K., Li, S. & Xiong, H. (2011), Isothermal crystallisation kinetics of thermoplastic starch/poly(lactic acid) composites, *Carbohydrate Polymers*, **86**, 941-947
6. Zhou, B., He, W. N., Jiang, X. Y., Tong, Z. Z., Xu, J. T. & Fan, Z. Q. (2014), Effect of molecular weight on isothermal crystallisation kinetics of multi-walled carbon nanotubes-graft-poly(ϵ -caprolactone), *Composites Science and Technology*, **93**, 23-29

7. Martins, J. A., Zhang, W., Carvalho, V., Brito, A. M. & Soares, F. O. (2003), Evaluation of the sample temperature increase during the quiescent and shear-induced isothermal crystallisation of polyethylene, *Polymer*, **44**, 8071-8079
8. Park, S. H., Lee, S. G. & Kim, S. H. (2013), Isothermal crystallisation behaviour and mechanical properties of polylactide/carbon nanotube nanocomposites, *Composites Part A: Applied Science and Manufacturing*, **46**, 11-18
9. Martíne-x-Palau, M., Franco, L. & Puiggalí, J. (2007), Isothermal crystallisation of poly(glycolic acid-alt-6-hydroxyhexanoic acid) studied by DSC and real time synchrotron SAXS/WAXD, *Polymer*, **48**, 6018-6028
10. Avrami, M. (1940), Kinetics of phase change II transformation – time relaxations for random distribution of nuclei, *Journal of Chemical Physics*, **8**, 212-224
11. Avrami, M. (1941), Kinetics of phase change and microstructure kinetics of phase change III, *Journal of Chemical Physics*, **9**, 177-184
12. Dharivijay, P. U., Shertukde, V. V. & Kalkar, A. K. (2012), Isothermal and nonisothermal crystallisation kinetics of poly(ϵ -caprolactone), *Journal of Applied Polymer Science*, **124**, 1333-1343
13. Chen, E. C. & Wu, T. M. (2007), Isothermal crystallisation kinetics and thermal behaviour of poly(ϵ -caprolactone)/multi-walled carbon nanotube composites, *Polymer Degradation and Stability*, **92**, 1009-1015
14. Su, H. H., Chen, H. L., Díaz, A., Casas, M. T., Puiggalí, J., Hoskins, J. N., Grayson, S. M., Pérez, R. A. & Müller, A. J. (2013), New insights on the crystallisation and melting of cyclic PCL chains on the basis of a modified Thomson-Gibbs equation, *Polymer*, **54**, 846-859

15. Atanase, L. I., Glaied, O. & Riess, G. (2011), Crystallisation kinetics of PCL tagged with well-defined positional triazole defects generated by click chemistry, *Polymer*, **52**, 3074-3081
16. Zhu, G., Ling, J. & Shen, Z. (2003), Isothermal crystallisation of random copolymers of ϵ -caprolactone with 2,2-dimethyltrimethylene carbonate, *Polymer*, **44**, 5827-5832
17. Long, Y., Shanks, R. A. & Stachurski, Z. H. (1995), Kinetics of polymer crystallisation, *Progress in Polymer Science*, **20**, 651-701
18. Banks, W. & Sharples, A. (1963), The Avrami equation in polymer crystallisation, *Makromolekulare Chemie*, **59**, 233-236
19. Hoffman, J. D., Davis, G. T. & Lauritzen, J. I. (1973), *Treatise on Solid State Chemistry: Crystalline and Non-Crystalline Solids, Vol 3, JB Hannaby Edition*, Plenum Publishing, New York: USA
20. Chan, T. W. & Isayev, A. I. (1994), Quiescent polymer crystallisation: modelling and measurements, *Polymer Engineering and Science*, **34**, 461-471
21. Lauritzen, J. I. & Hoffman, J. D. (1960), Theory of formation of polymer crystals with folded chains in dilute solution, *Journal of Research of the National Bureau of Standards Section A: Physics and Chemistry*, **64**, 73-102
22. Bittiger, H., Marchessault, R. H. & Niegisch, W. D. (1970), Crystal structure of poly- ϵ -caprolactone, *Acta Crystallographica*, **B26**, 1923
23. Hoffman, J. D., Frolen, L. J., Ross, G. S. & Lauritzen, J. I. (1975), Growth rate of spherulites and axialites from the melt in polyethylene fractions: Regime-1 and Regime-2 crystallisation, *Journal of Research of the National Bureau of Standards Section A: Physics and Chemistry*, **79**, 671-699

24. Miller, R. L. & Boyer, R. F. (1978), Chain folding and cross-sectional area per chain, *Journal of Polymer Science: Polymer Physics Edition*, **16**, 371-374

Chapter 6. – Ageing in PCL

Ageing measurements were carried out on bulk samples of PCL moulded and slow cooled in a heated press, as outline in Chapter 2. These moulded plaques were stored in an oven at 50°C, at room temperature (20°C), in a conventional fridge at 5°C and in a freezer at -18°C for up to 6 months. Samples were removed at frequent time intervals; dumb-bell shaped specimens had been cut from these and were used for conventional tensile tests along with discs for DSC testing to measure the heat of fusion and the melting points.

6.1 Results

6.1.1 Mechanical Properties

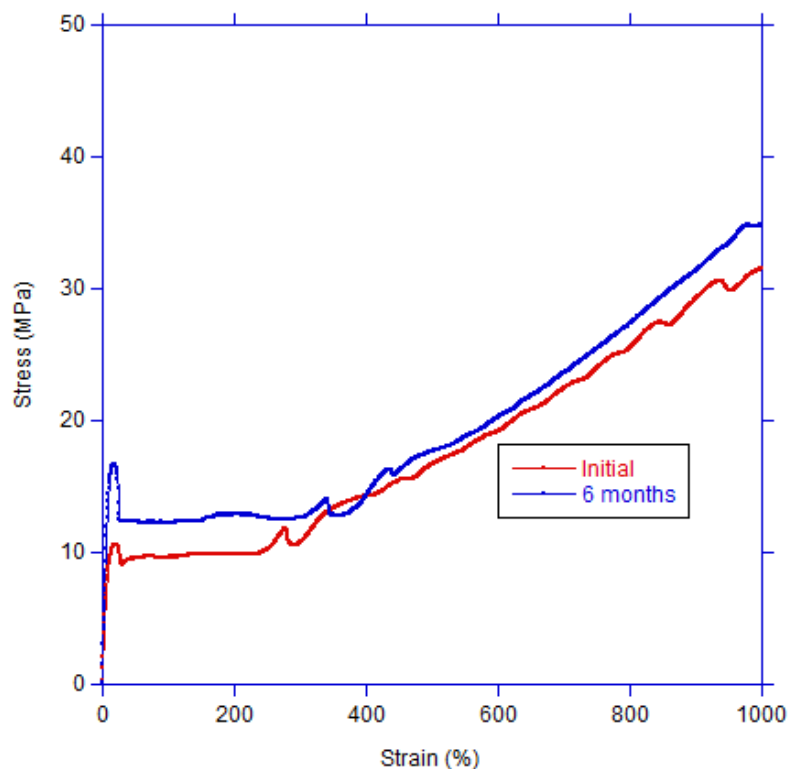


Figure 6.1 – Engineering stress-strain curve as initially produced and after 6 months at room temperature

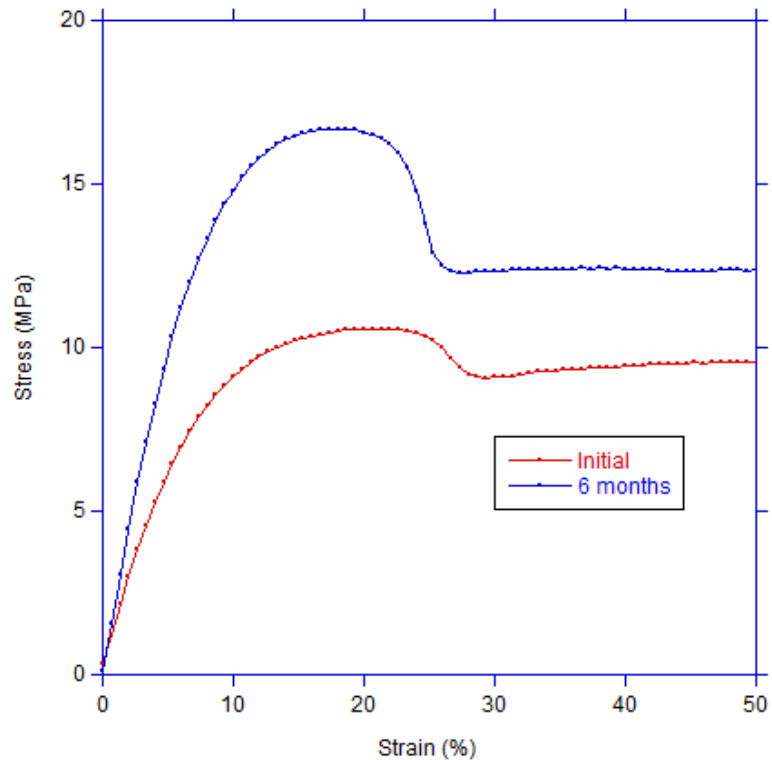


Figure 6.2 –As in Figure 6.1 up to 50% strain

Figure 6.1 and Figure 6.2 show the stress-strain curves of samples at room temperature as initially produced and after 6 months of storage at room temperature. The engineering stress/strain behaviour is characteristic of a ductile polymer which yields with the formation of a neck at about 20% strain followed by a region in which the sample uniformly draws to above 200%. The final rise in stress before ductile failure above 1000% strain was attributed to the shape of the contoured ends of the specimens. The localised yielding and the reduction in cross-sectional area in the necked region of the specimen means that the stress displayed in the figures was not true stress but engineering stress, i.e. F/A_0 where F is the load in Newtons and A_0 is the cross-sectional area of the original specimen. The initial elastic modulus, taken as the gradient of the line from zero stress until the curve deviated from a straight line, and the yield stress,

taken as the maximum point of the elastic deformation, were considered to be characteristic properties of the aged material. These were assessed using the regression coefficient, R^2 , and values of both yield stress and modulus for all samples, along with the standard deviation error, are listed in Table 6.1. The engineering stress-strain curves appear to have the same general shape, with the sample exhibiting necking at the yield stress. However the sharpness of the neck profile at the yield point is greater in the samples that have been stored for longer periods and as a result the drawing stress increased with time. The yield stress also increased and necking occurred at progressively lower strains with time, see Figure 6.3 and Figure 6.4. On drawing beyond the yield point further minor necks were observed which gave rise to spikes in the stress-strain curves as these drew into the yielded zone of the specimen. All the specimens drew to the limit of the crosshead and no ductile fracture was observed. The trend in mechanical properties on ageing is that of producing more brittle material with increased modulus and yield stress.

These trends, particularly that of increased yield stress with time was seen at all storage temperatures but to different extents; the freezer samples showed very little change in yield stress over time, but at all other temperatures an increase in yield stress, as well as an increase in the rate of increase, was observed. This can be seen in Table 6.1 and Figure 6.3 to Figure 6.6. The room temperature samples did however show a greater increase in yield value than the oven samples, though this may have been due to the oven condition being within the melting range of the polymer.

The modulus also increased with increasing storage time, and again exhibited the same temperature dependence as the yield stress. The values with time and storage temperatures can be seen in Table 6.1 along with the calculated error from five repeat

experiments. The general trends exhibited by both the yield stress and the modulus are shown in Figure 6.5 and Figure 6.6.

Time (hour)	Yield Stress (MPa)						Modulus (MPa)							
	OT	SD	RT	SD	FT	SD	OT	SD	RT	SD	FT	SD	F:FT	SD
0	10.65	0.45	10.65	0.45	10.65	0.45	134.4	6.34	134.4	6.34	134.4	6.34	134.4	6.34
1	12.28	0.34	11.1	0.56	10.87	0.31	149.7	11.35	136.1	8.85	131.3	10.23	130.1	9.98
4	12.3	0.12	11.84	0.34	10.59	0.51	147.4	4.77	150.3	3.72	129.8	13.33	137.1	10.28
8	12.37	0.57	12.4	0.17	11.36	0.48	147.3	3.64	159.4	9.14	138.3	7.11	132.3	5.43
16	13.06	0.26	11.6	0.2	11.38	0.25	147.5	8.44	143.9	10.21	139.6	7.21	136.1	3.69
24	13.55	0.29	13.68	0.41	12.6	0.57	161.7	2.09	173.6	8.18	158.4	5.56	154.2	5.91
48	13.74	0.45	14.08	0.12	12.52	0.22	151	5.99	176.6	3.1	156.5	3.94	145.1	5.25
72	14	0.37	14.22	0.31	12.55	0.08	155.6	3.16	178.6	5.18	157.4	3.27	151.6	5.22
96	13.87	0.51	14.49	0.16	12.81	0.25	150.5	6.84	182.9	5.48	160.8	1.1	149.6	3.45
120	14.12	0.28	14.65	0.31	12.95	0.15	155.6	3.56	188.2	3.5	162.7	3.29	148.8	3.38
144	14.02	0.08	14.58	0.22	12.78	0.19	150.8	3.62	179	3.45	158.2	4.01	143	4.83
168	13.97	0.66	14.67	0.25	13.38	0.25	168.6	4.29	183.4	8.06	170	5.77	156.3	3.61
336	14.56	0.19	16.09	0.44	13.56	0.19	167.1	7.05	200.1	6.95	184	3.38	154.3	4.63
504	14.79	0.32	15.56	0.38	13.3	0.11	167.2	7.37	194.3	6.36	169.3	3.98	153.8	3.19
672	14.79	0.25	15.94	0.51	13.52	0.2	166.3	4.37	212.4	5.34	183.6	3.76	168.9	8.53
1344	15.34	0.37	16.06	0.28	14.04	0.26	173.4	5.4	213.1	7.98	184.1	6.97	175.9	6.46
2016	14.92	0.1	16.04	0.3	13.92	0.16	161.5	6.28	217.1	5.83	180.8	5.34	158.5	3.62
4032	14.88	0.13	16.43	0.19	14.72	0.11	170.8	4.78	215.4	5.06	197.2	8.85	159.4	4.33

Table 6.1 – The change in yield stress and modulus and the standard deviation (SD) with time at different storage temperatures

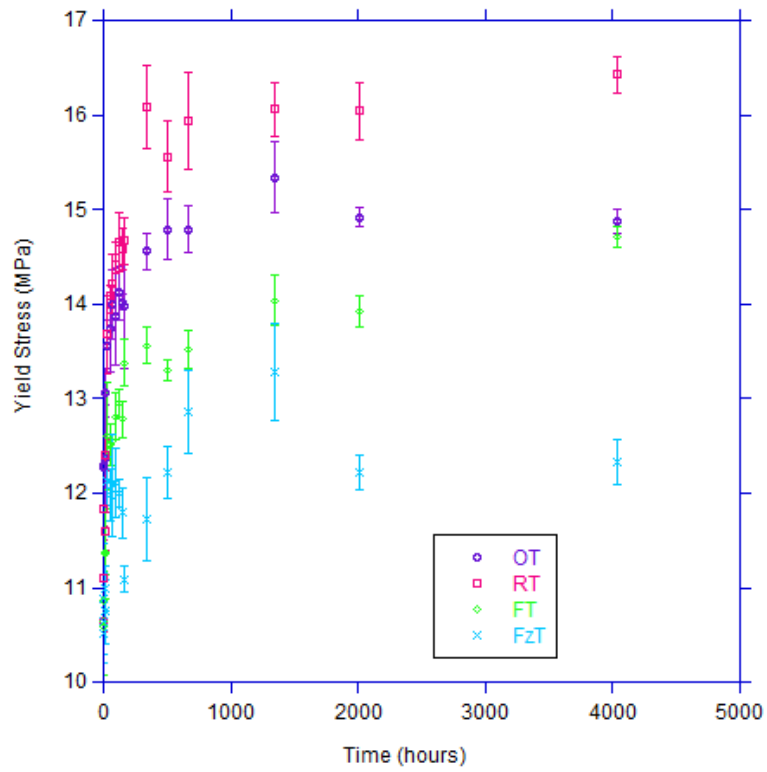


Figure 6.3 – Development of yield stress with ageing time

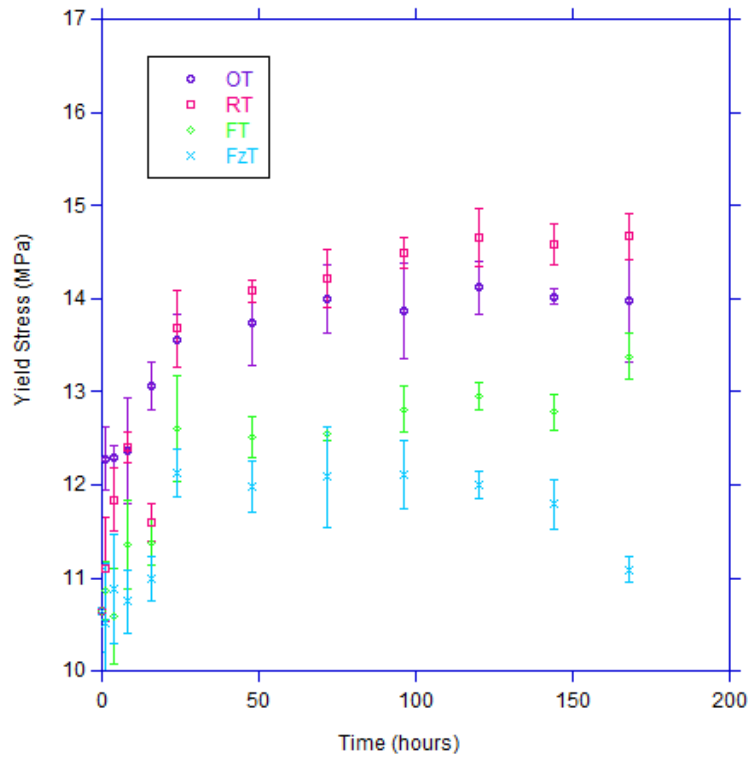


Figure 6.4 – Development of yield stress over the first 200 hours of ageing

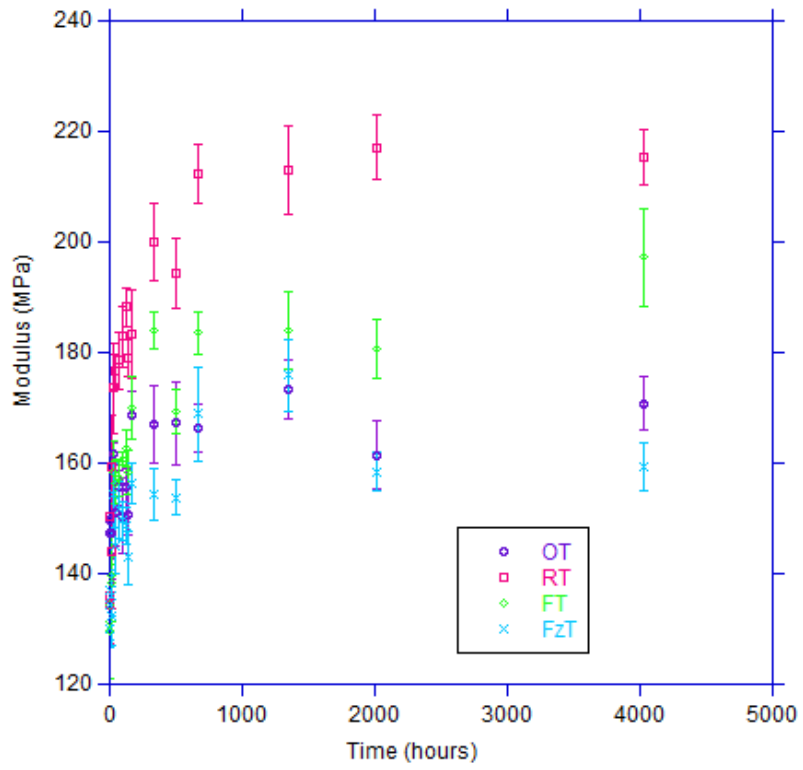


Figure 6.5 – Variation of modulus with ageing time

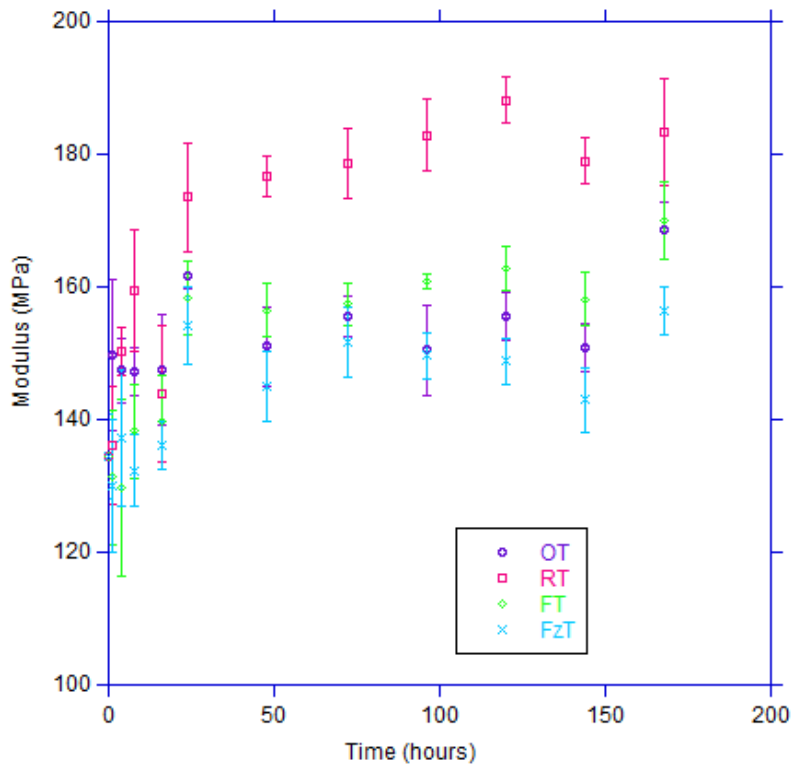


Figure 6.6 – Variation of modulus over the first 200 hours of ageing

6.1.2 Effect of Ageing on Melting

Figure 6.7 shows the melting endotherms of samples aged at -18°C for 24, 168, 2520 and 3696 hours in comparison with the un-aged material. All samples were heated at $10^{\circ}\text{C min}^{-1}$ from room temperature to 70°C with the same sample mass. There is comparatively little difference between all of the endotherms in that the peak temperatures, T_{max} , aged for 0, 24 and 3696 hours have the same values within experimental error and overall T_{max} changes by only $\pm 1.0^{\circ}\text{C}$. However, a low melting peak develops which is only apparent after ageing for 168 hours and moves with increasing storage time to higher temperatures. This must be due to the development of thin lamellae which grow within the amorphous layers between the lamellae present in the original sample and thickened with time. Specimens aged above 2520 hours do not show this low melting peak.

The melting endotherms of the specimens aged at 5°C are shown in Figure 6.8 over the same time scale. There is a greater change in T_{max} and a more obvious trend of the melting endotherms to higher temperatures with increased storage time. A low melting endotherm becomes apparent after storing for 24 hours but the trend seen at -18°C is less apparent here, with some samples showing a low melting peak at lower temperatures as storage time increases; this may be due to sample variation. However, the lower temperature peak is not present in the endotherms of the material aged for more than 2352 hours.

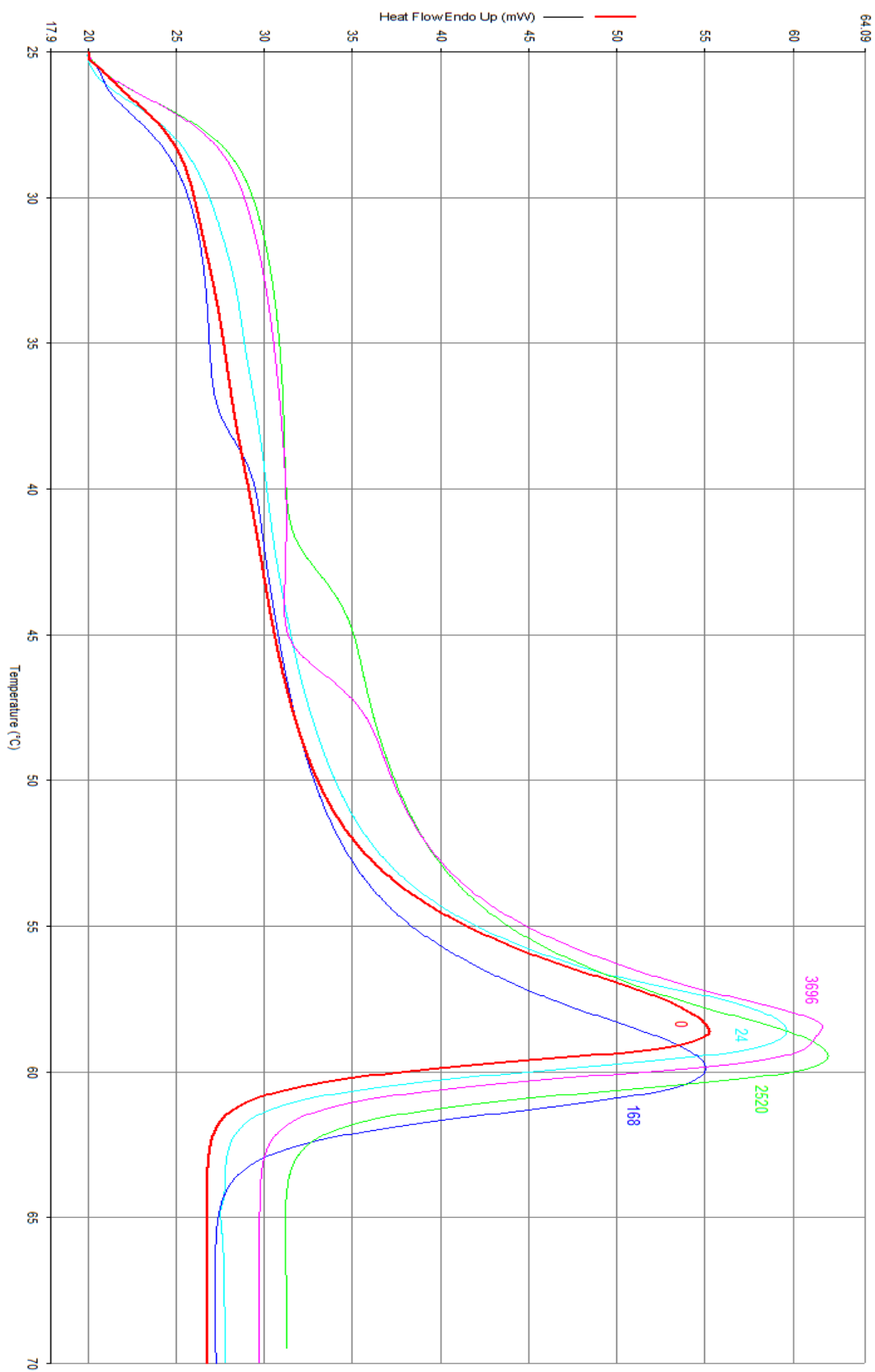


Figure 6.7 - Melt endotherms for samples stored at -18°C at 0, 24, 168 2520 and 3696 hours

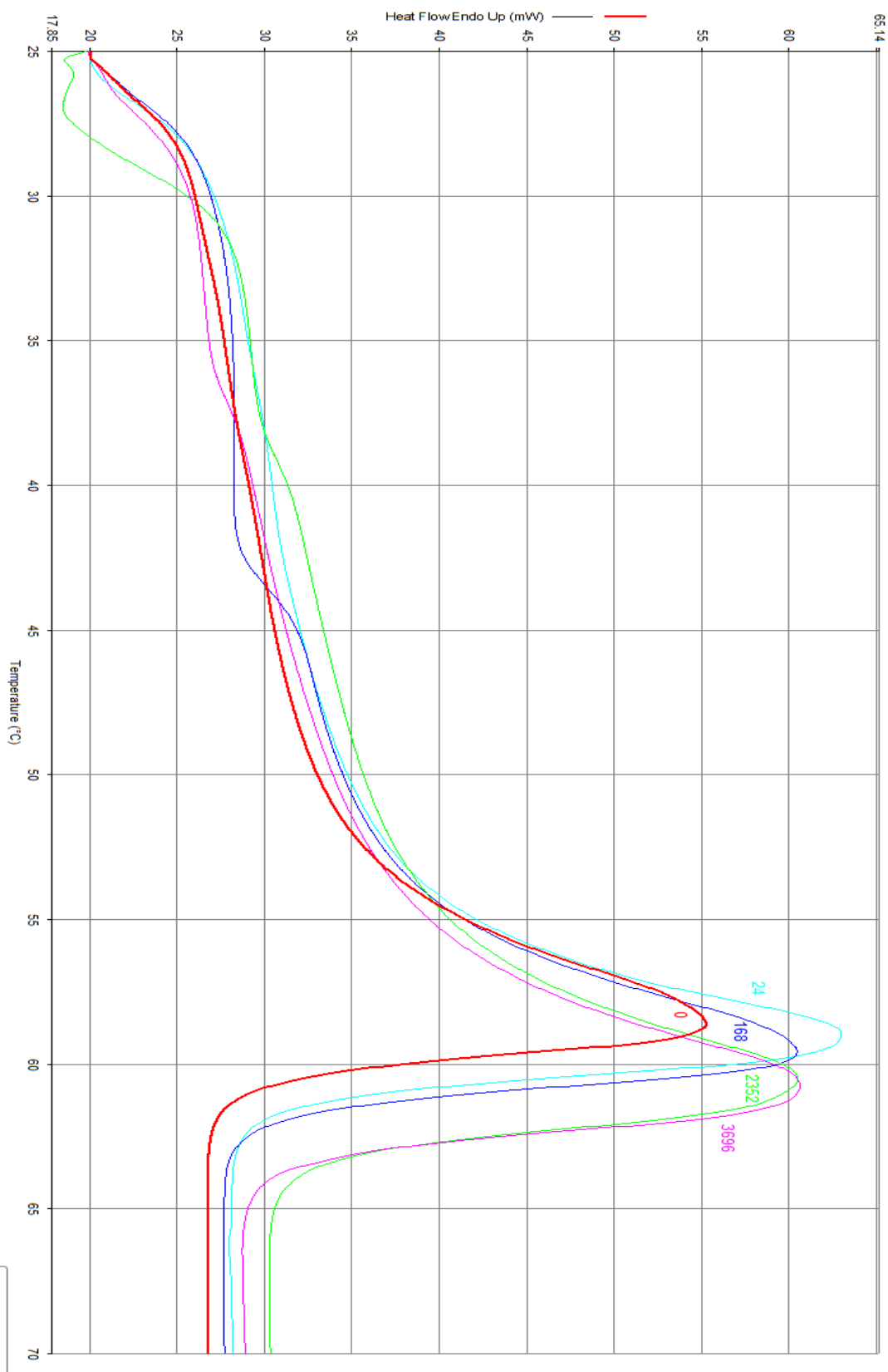


Figure 6.8 - Melt endotherms for samples stored at 5°C at 0, 24, 168 2352 and 3696 hours

The endotherms for the specimens aged at 20°C are shown in Figure 6.9. There is clear separation between them and a progressive shift to higher temperatures with storage time. After 24 hours a lower melting peak is apparent but this is not present in any of the other isotherms, presumably because it has moved into the main endotherm.

The melt endotherms of the specimens aged at 50°C are shown in Figure 6.10 along with that of the un-aged specimen for comparison. It is clear that some partial melting must occur prior to ageing at 50°C followed by recrystallization at this raised temperature since the crystallinity of the sample has increased on ageing. There is a large increase in T_{\max} after 24 hours and a progressive increase with storage time.

A melting point for the aged specimens was defined by T_{\max} since this represented the temperature at which most of the crystallites in the specimens were melting. It was also reproducible and convenient to measure. T_{\max} was plotted against storage time at each ageing temperature in Figure 6.11. In every case, with the possible exception of ageing at -18°C where little change was observed, the melting point increased rapidly over the first 500 hours and then linearly with time; the linear rate also increased with temperature. The increase with temperature indicates that ageing of PCL cannot simply involve re-crystallisation since this is a nucleation controlled process, but instead it has the characteristics of a thermally activated process such as diffusion whose rate increases with temperature.

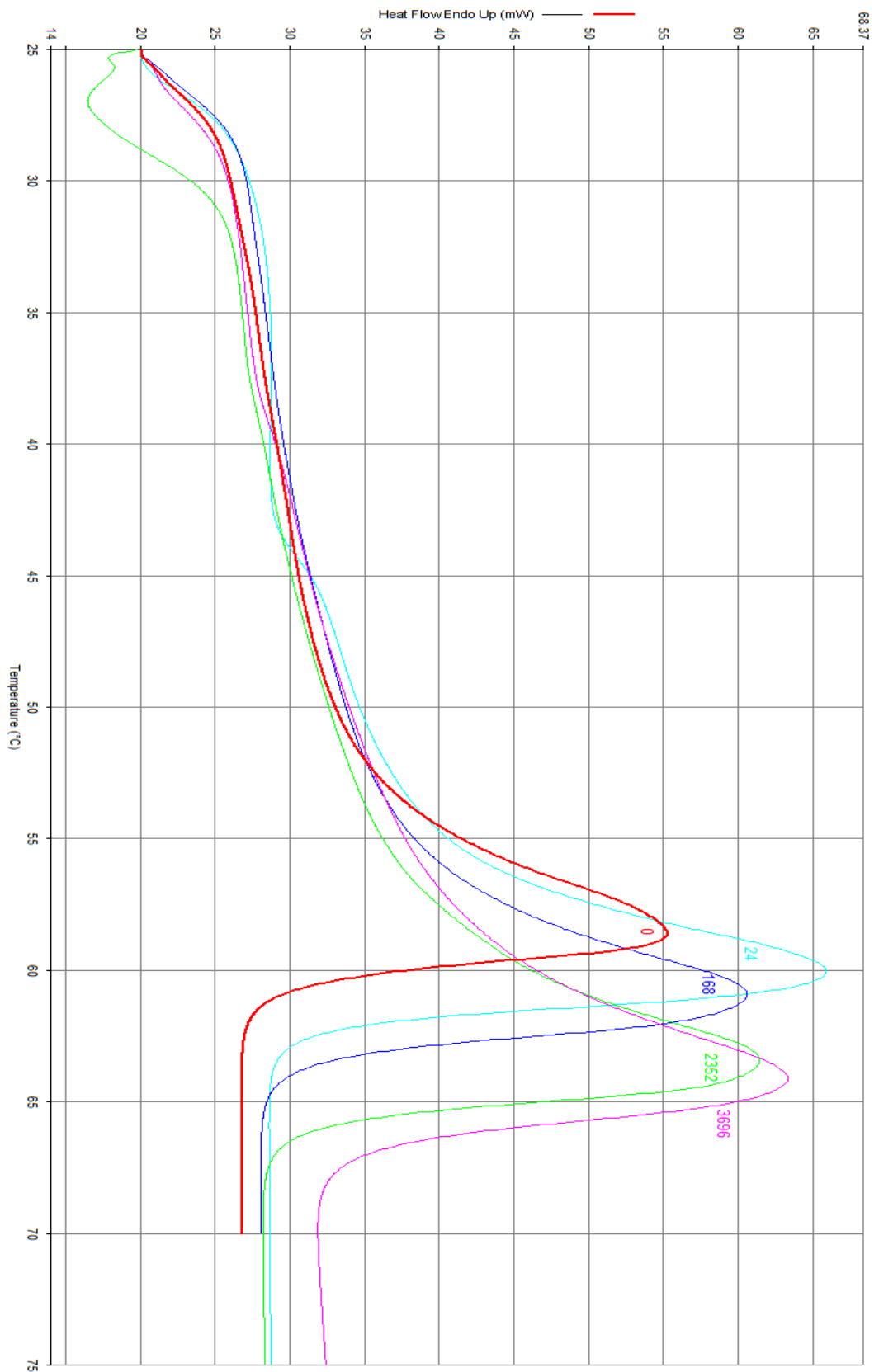


Figure 6.9 - Melt endotherms for samples stored at 20°C at 0, 24, 168 2352 and 3696 hours

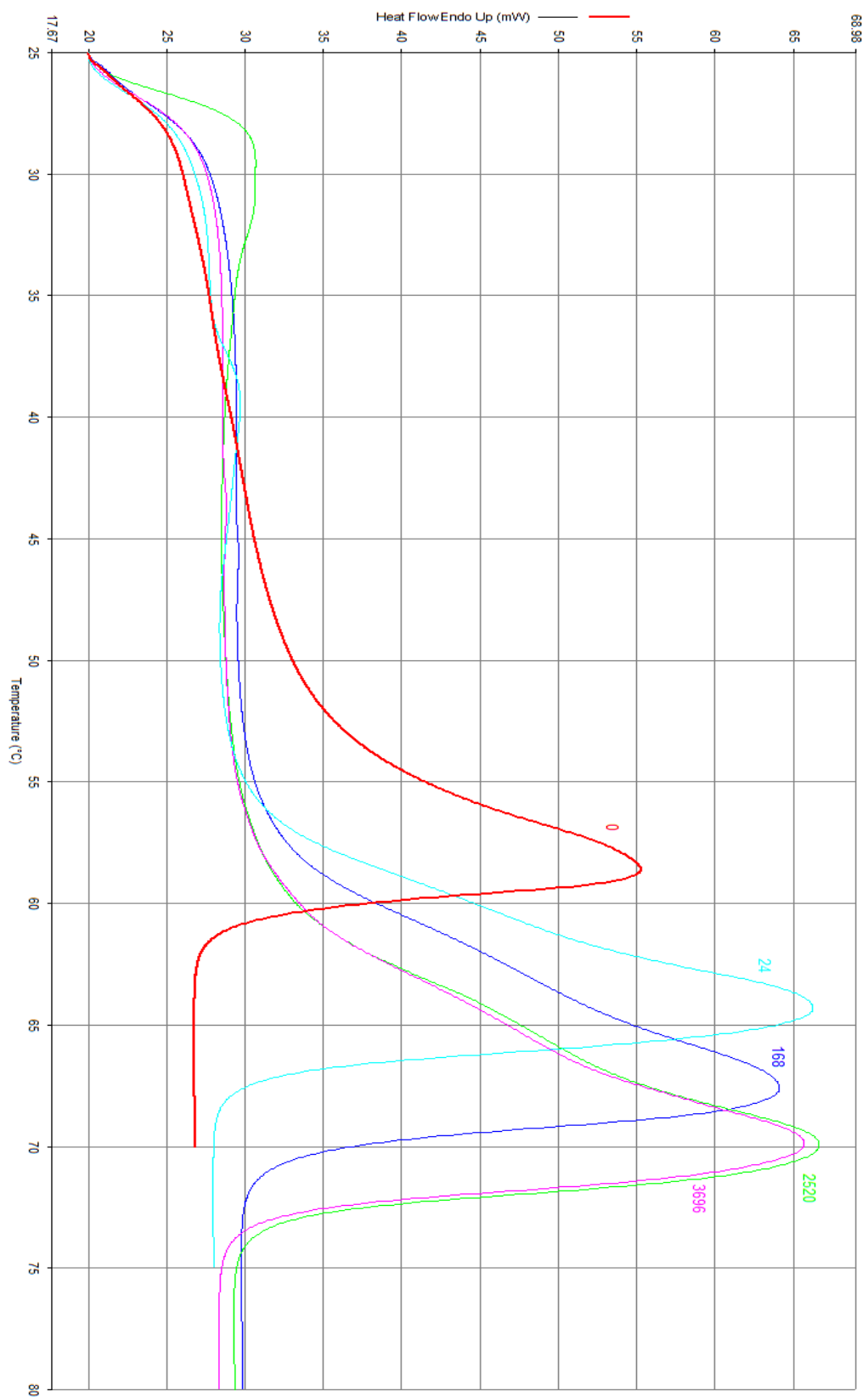


Figure 6.10 - Melt endotherms for samples stored at 50°C at 0, 24, 168 2520 and 3696 hours

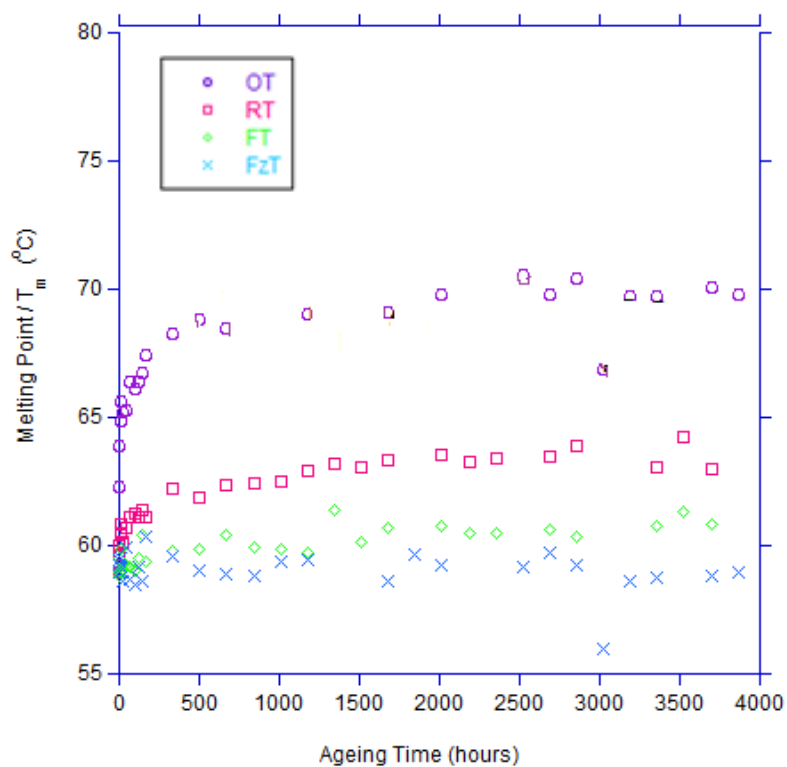


Figure 6.11 - Effect of time on the peak melting point

6.1.3 Effect of Ageing on Crystallinity

The heat of fusion was determined from the area under the melting endotherm and above the specific heat baseline drawn from the flat portion of the melting curves to above the final trace of melting. The difficulty in drawing a reproducible baseline made measurement of the heat of fusion inaccurate and produced a variation of $\pm 5\%$ and some considerable scatter in the data, see Figures 6.12 and 6.13.

From the heat of fusion, ΔH_f , the percentage crystallinity was determined using a value for the heat of fusion of completely crystalline PCL of 139.3 J g^{-1} [1] since

$$X = \Delta H_f / \Delta H_f^0 \quad \text{Equation 6.1}$$

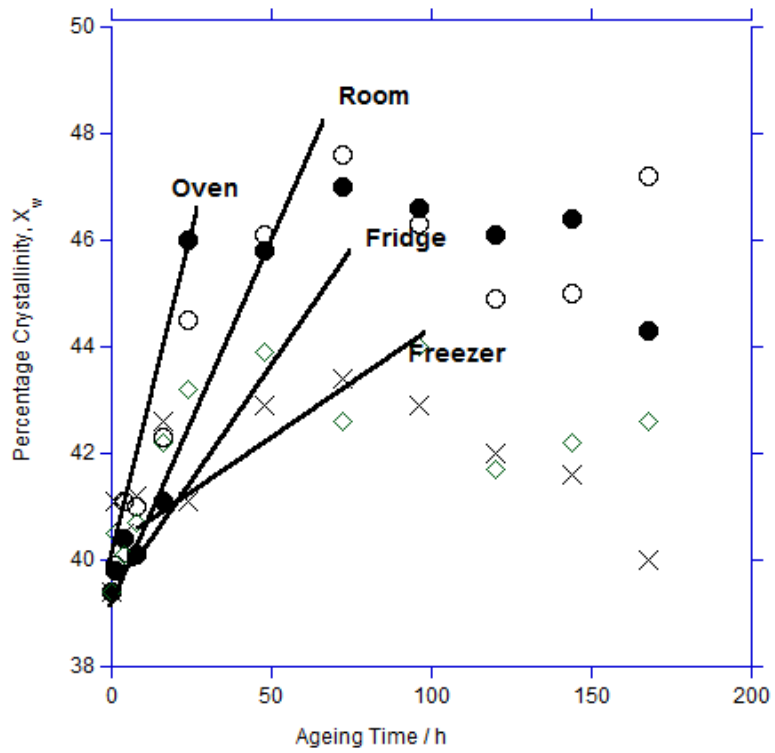


Figure 6.12 – Change in the percentage crystallinity on ageing up to 200 hours

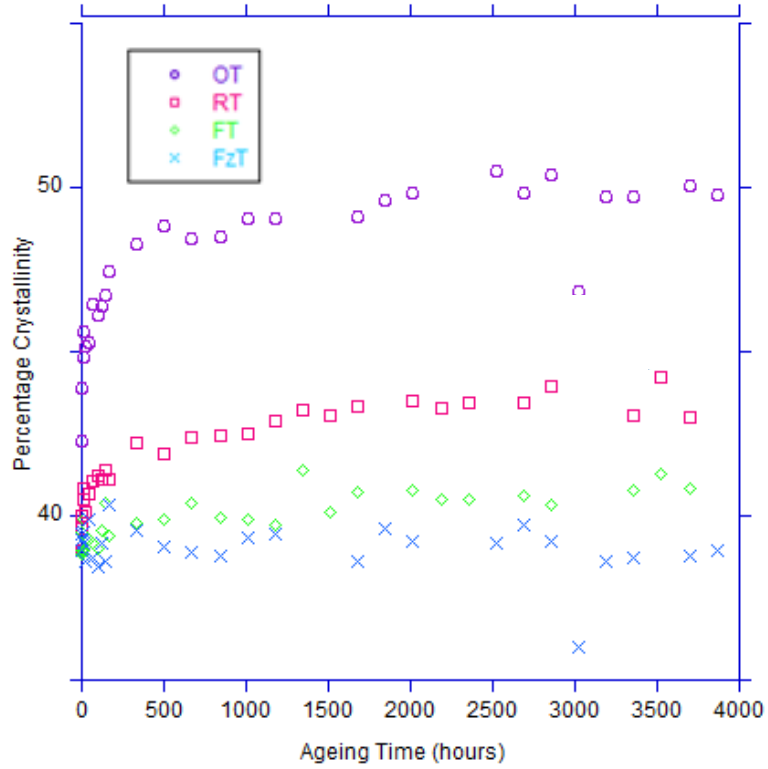


Figure 6.13 – Change in the percentage crystallinity on ageing up to 4000 hours

Figure 6.12 shows the change in the percentage crystallinity with time over a short initial period and then over a more extended period, given in Figure 6.13. Despite the large errors in determining the percentage crystallinity, as much as $\pm 5\%$, there is a clear trend with time in that there is an initial rapid rise in crystallinity followed by a slow rise or plateauing of the value at long periods. There is a clear separation of the increase in crystallinity with temperature in that the higher crystallinities are achieved at higher temperatures. The change in melting point and crystallinity appear to follow one another.

Figure 6.14 and Figure 6.15 show the relationship between percentage crystallinity and change in mechanical properties; yield stress and modulus respectively. Both properties show a positive trend in that yield stress and modulus both increase with increased crystallinity, although this increase with ageing is not particularly large. These findings are consistent with the findings of El-Hadi et al [2] who also found both yield stress and modulus to increase with increased crystallinity. There is also a separation between ageing at low and high temperatures, although the greater scatter in the measurement of the modulus makes the trend less obvious for this property. However, it is apparent that ageing at higher temperatures makes the material stiffer with an increased modulus for the same degree of crystallinity. This could be due to the effect of lamellae thickness as the material aged at higher temperature has a higher melting point and accordingly the lamellae are thicker, and continue to thicken with time as the crystallinity increased. This is shown in Figure 6.16.

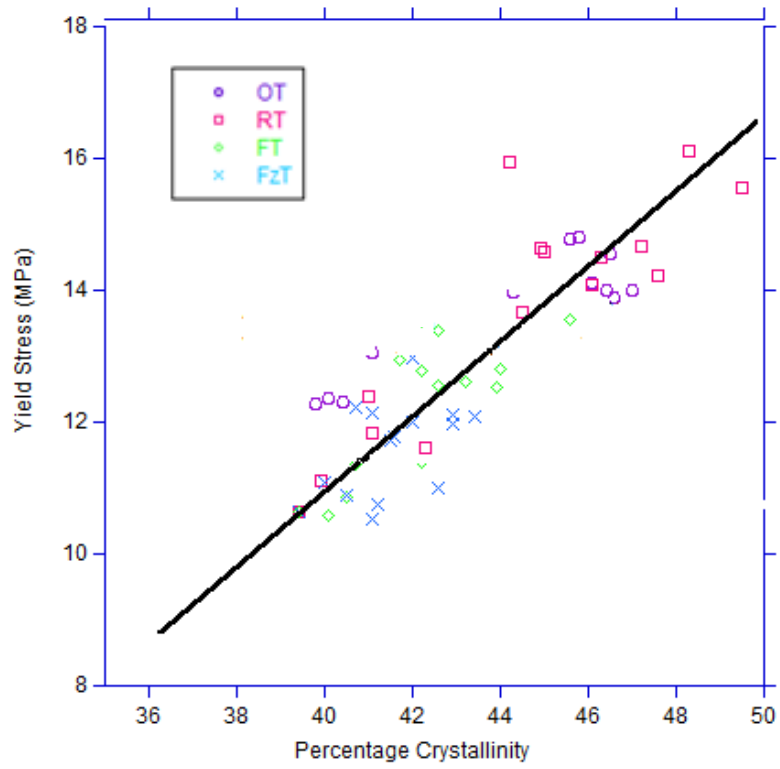


Figure 6.14 - Increase in yield stress as a function of % crystallinity at 50, 20, 5 and -18°C

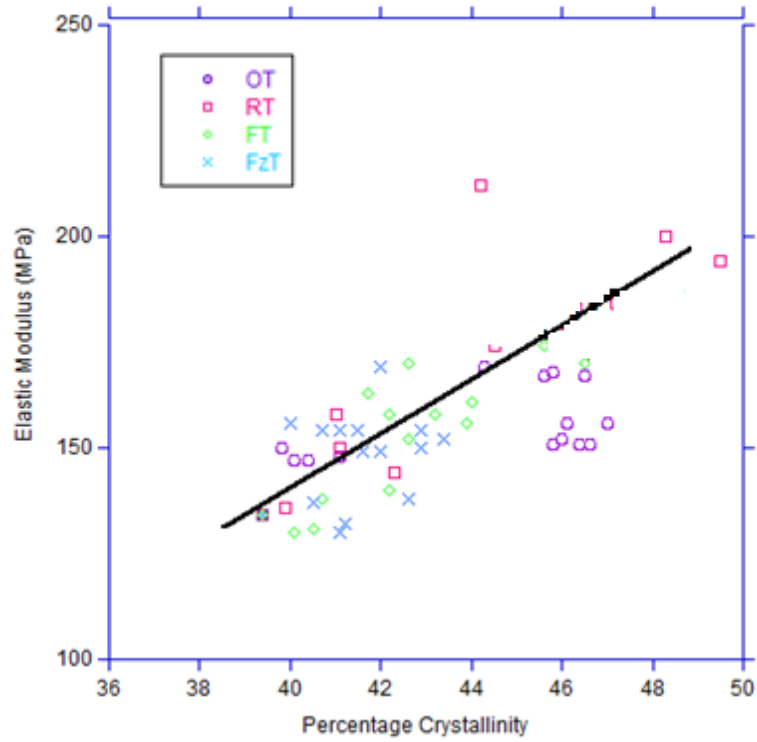


Figure 6.15 - Increase in modulus as a function of % crystallinity at 50, 20, 5 and -18°C

The large initial increase in the peak melting temperature and the change of the melting endotherm progressively to a higher temperature with the logarithm of time was attributed to secondary crystallisation by Chen et al in a study of PET [3]. They suggested that initially thin lamellae partially melted and were replaced with new lamellae with increased stem thickness since they had re-crystallising at a higher temperature. This is followed by secondary crystallisation in which the crystallinity increases with log time and at the same time the lamellae thicken progressively with increased melting points. In order to follow this train of thought the average stem length of the samples were calculated following the procedure adopted by Chen et al [3].

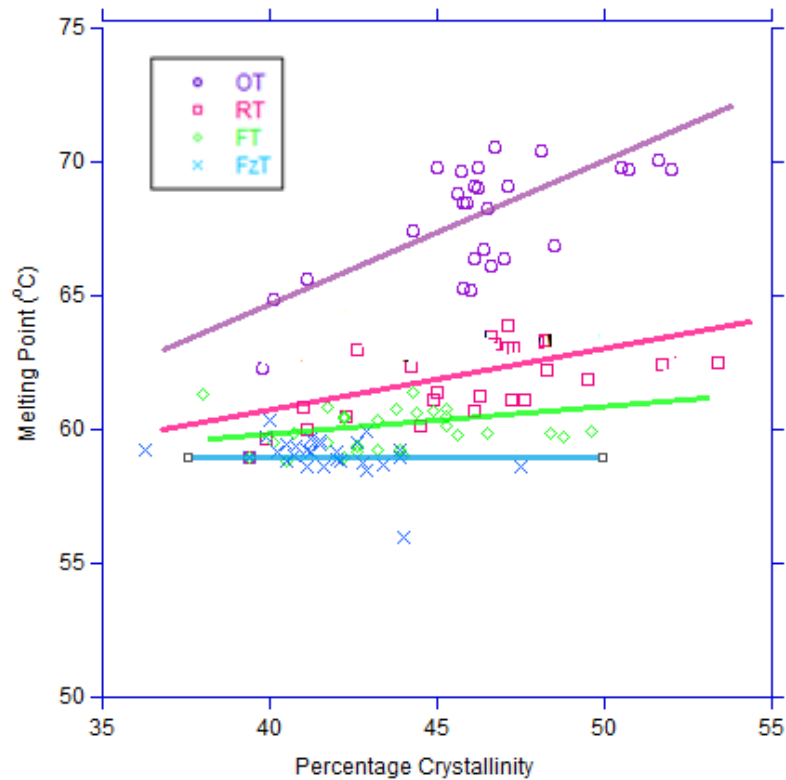


Figure 6.16 - The increase in melting point as a function of % crystallinity at 50, 20 , 5 and -18°C

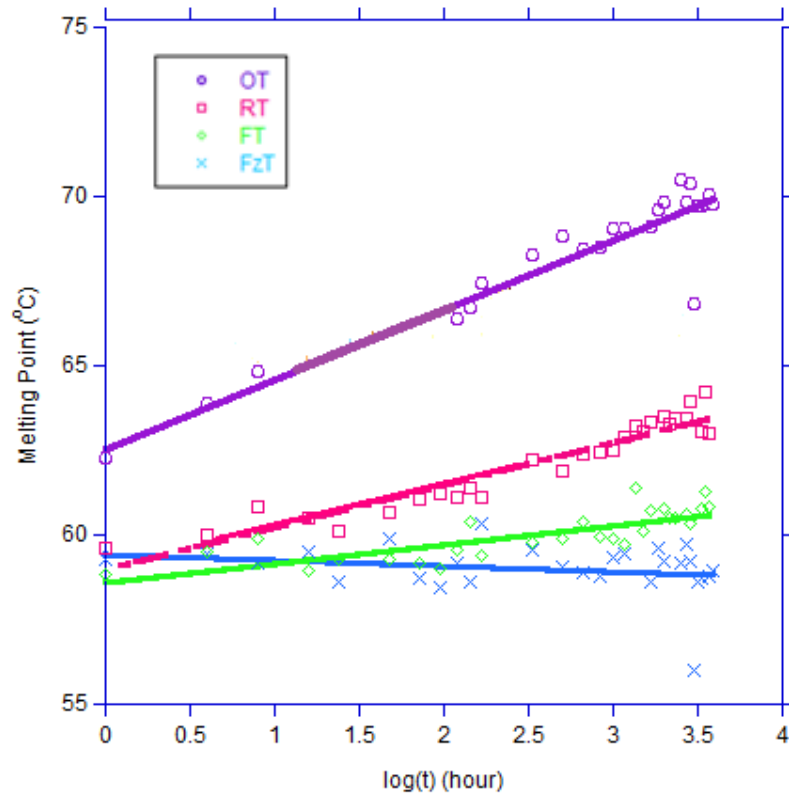


Figure 6.17 - Linear dependence of melting point on log(t)

6.1.4 Effect of Ageing on Lamellae Stem Length

Flory & Vrij [4] proposed a model for the dependence of the melting point of linear hydrocarbons on chain length, which was modified by Hay [5] for uniform oligomers in particular ethylene terephthalate oligomers, which gives the melting point of an oligomer with n repeat monomer units as

$$T_m \approx T_m^0 [1 - 2RT_m \ln(n)/n\Delta h - 2\sigma_e/n\Delta h + \Delta C_p \Delta T(n-1)/n\Delta h]$$

Equation 6.2

where Δh is the heat of fusion per repeat unit (for completely crystalline PCL this value is 139.3 J g^{-1} [1]) and ΔC_p is the difference in heat capacity between the crystalline and amorphous phases. Both of these terms were measured at the equilibrium melting point

T_m^0 taken to be 80°C. The term σ_e comes from the surface free energy of the crystal and $2RT_m \ln(n)$ from the entropy of mixing of the terminal segments. This term dominates all the others enabling the relationship between T_m and n to be simplified [6] to

$$T_m \approx T_m^0 [1 - 2RT_m \ln(n)/n\Delta h] \quad \text{Equation 6.3}$$

with all terms representing the variables as described above.

This is based on the work by Broadhurst [7] but adapted to include temperature dependence of the thermodynamic parameters and to include the entropy of mixing of the terminal units with the rest of the n groups on melting. The adaptation by Hay was from modifying the term $R \ln(n)$ introduced by Flory & Vrij to $2R \ln(n)$ to account for the two terminal units and two surface free energy terms. In using the equation it was assumed that n was large and ΔT is comparatively small.

In the melting range the DSC temperature recorded was used as T_m and the vertical height above the baseline provided a relative measure of the mass of material melting at T_m . T_m was converted to $\ln(n)/n$ by rearranging Equation 6.3 to give

$$n/\ln(n) \approx 2RT_m \Delta h / (T_m^0 - T_m) = A \quad \text{Equation 6.4}$$

and then the value of n determined from a polynomial fit of n against $\ln(n)/n$. This process is described in more detail by Chen et al [3].

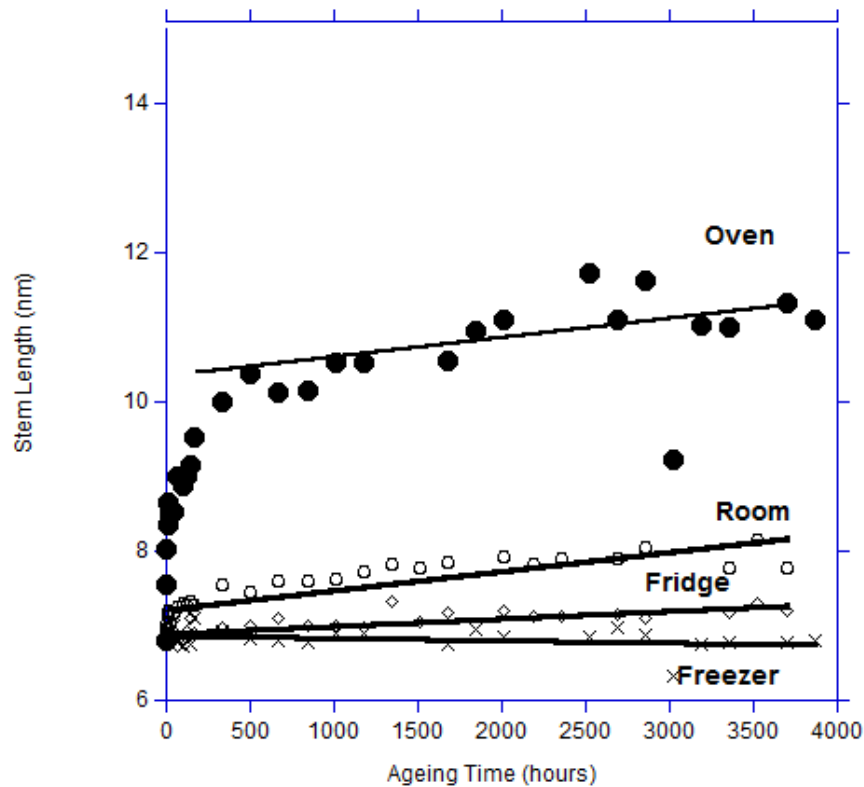


Figure 6.18 – Change in average stem length with time

Figure 6.18 shows the change in average stem length with time, calculated as defined above. There is a general trend of increased stem length with storage time and the rate of increase was greater at higher temperatures, implying that the thickening can't be nucleation controlled as this mechanism would be expected to show the opposite dependence on temperature. The non-linear portion of the curve depicting change in average stem length over time at the oven storage temperature was attributed to partial melting and recrystallization of the samples. The relationship seen when plotting average stem length as a function of the square root of time, given in Figure 6.19, exhibits a progressive increase in the rate of growth. There is a drop in the growth rate as the temperature decreases, implying that the process is not nucleation controlled but is a thermally activated process obeying an Arrhenius relationship.

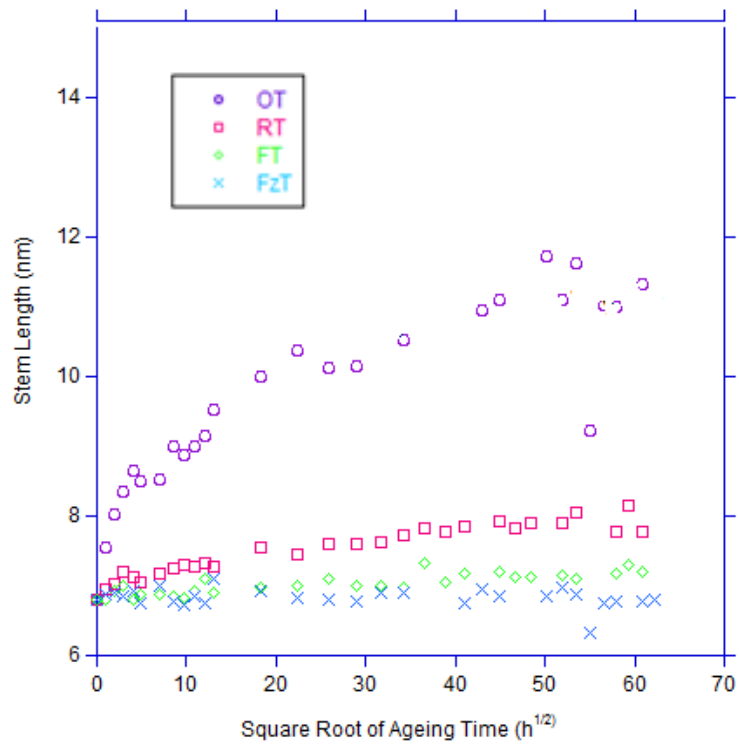


Figure 6.19 – Dependence of the average stem length on the square root of time

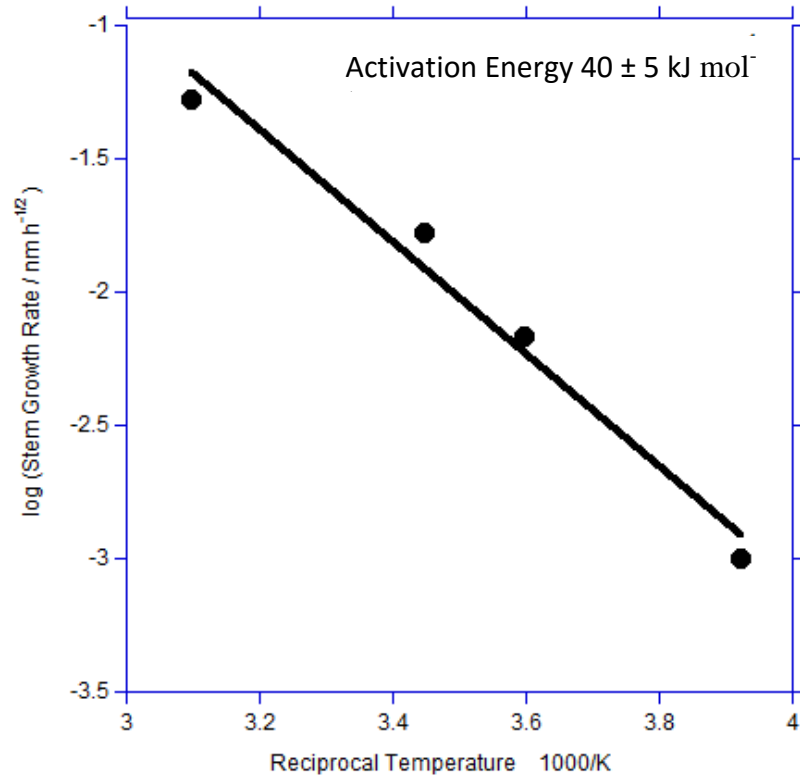


Figure 6.20 – Arrhenius plot of the logarithm of stem growth rate against reciprocal temperature

The dependence of the stem length on the square root of time suggests that growth is diffusion controlled and since diffusion is a thermally activated process it should follow an Arrhenius relationship of

$$g = A \exp(-\Delta E_d/RT) \quad \text{Equation 6.5}$$

where g is the crystal growth rate, A is a pre-exponential factor, R is the gas constant and ΔE_d is the activation energy for diffusion. The rate data presented in Figure 6.20 is given as an Arrhenius plot of $\log(g)$ against reciprocal temperature and implies an increase in growth rate with increasing temperature which is the opposite to that seen in primary crystallisation, where growth rate slows with increasing temperature. The relationship exhibited in secondary crystallisation may suggest that the diffusion process is governed by reptation, where an increase in thermal energy increases mobility of the polymer chains and therefore increases the rate of crystal growth [8-9].

6.2 Conclusions

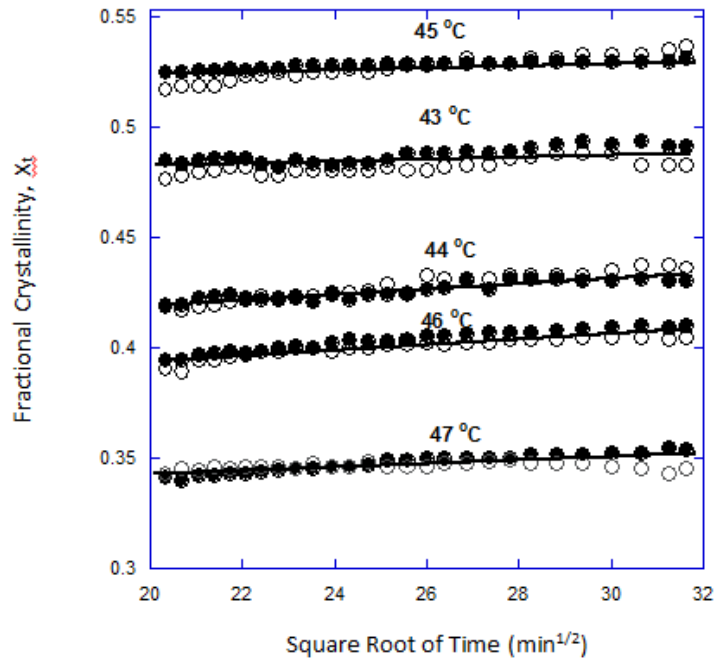
The storage of PCL samples at different temperatures ranging from -18 to 50°C results in an increase in crystallinity with time and increasing the temperature of storage increases the rate at which the crystallinity developed. This increase in crystallinity alone accounts for the change in mechanical properties by the stiffening effect of increasing the hard crystalline phase within the soft rubber-like amorphous phase. The change in the melting endotherms to higher temperatures is due to a progressive thickening of the lamellae with storage which causes an increase in melting point. The increase in rate of thickening with temperature along with the increase in stem length as a function of the square root of time suggests that ageing is controlled by diffusion and that the crystallinity develops with all the characteristics of secondary crystallisation. This will be considered further in Chapter 7.

6.3 References

1. Koeng, M. F. & Huang, S. J. (1995), Biodegradable blends and composites of polycaprolactone and starch derivatives, *Polymer*, **36**, 1877-1882
2. El-Hadi, A., Schnabel, R., Straube, E., Müller, G. & Hennings, S. (2002), Correlation between degree of crystallinity, morphology, glass temperature, mechanical properties and biodegradation of poly(3-hydroxyalkanoate) PHAs and their blends, *Polymer Testing*, **21**, 665-674
3. Chen, Z., Hay, J. N. & Jenkins, M. J. (2013), The effect of secondary crystallisation on melting, *European Polymer Journal*, **49**, 2697-2703
4. Flory, P. J. & Vrij, A. (1963), Melting points of linear-chain homologs. The normal paraffin hydrocarbons, *Journal of the American Chemical Society*, **85**, 3548-3553
5. Hay, J. N. (1976), Use of model compounds to determine equilibrium melting points of polymers, *Journal of Polymer Science: Polymer Chemistry Edition*, **14**, 2845-2852
6. Mills, P. J. & Hay, J. N. (1984), The lamella size distribution in non-isothermally crystallised low density polyethylene, *Polymer*, **25**, 1277-1280
7. Broadhurst, M. G. (1962), Extrapolation of the orthorhombic n-paraffin melting properties to very long chain lengths, *The Journal of Chemical Physics*, **36**, 2578-2581
8. Kim, K. D., Sperling, L. H. & Klein, A. (1994), Reptation time, temperature, and cosurfactant effects on the molecular interdiffusion rate during polystyrene latex film formation, *Macromolecules*, **27**, 6841-6850

9. Kelly, C. A., Murphy, S. H., Leeke, G. A., Howdle, S. M., Shakesheff, K. M. & Jenkins, M. J. (2013), Rheological studies of polycaprolactone in supercritical CO₂, *European Polymer Journal*, **49**, 464-470

Chapter 7. Secondary Crystallisation of PCL



- X_c ○ $1-X_a$

Figure 7.1 – The increase in fractional crystallinity due to secondary crystallisation with the square root of the crystallisation time.

In Chapter 5, secondary crystallisation was attributed to the linear thickening of lamella with time following an Avrami equation with n value of 1.0 ± 0.2 . It was previously mentioned that Chen [1] had recently associated it with a diffusion controlled crystallisation, since he found that the stem length increased with the square root of time and the rate of growth increased with temperature. This was also observed in this thesis during the ageing of PCL, as shown in Figure 6.19 of the previous chapter. As a result of this, the development of crystallinity with time has been revisited but only in the region of secondary crystallisation. The fractional crystallinity is plotted as a

function of the square root of time and shown in Figure 7.1 which exhibits an excellent linear dependence, as supported by the strength of the R^2 values presented in Table 7.1.

Table 7.1 – R^2 values to show the strength of linear relationship between fractional crystallinity and the square root of time

Temperature (°C)	R^2 value
43	0.937
44	0.989
45	0.934
46	0.961
47	0.989

The rate constant determined from the slope of the line increased with temperature; although there is scatter in the results there is a general trend for the rate constant to increase with increasing temperature. Values of the rate constant for each crystallisation temperature are given in Table 7.2. This relationship is inconsistent with a nucleation controlled process, but rather suggests a diffusion controlled process.

Table 7.2 – Diffusion coefficient for secondary crystallisation

Crystallisation Temperature (°C)	Fractional Crystallinity $X_{p,\infty}$	Diffusion Rate $k_s \times 10^3$ (min ^{-1/2})
43	0.49 ± 0.01	1.92 ± 0.5
44	0.40 ± 0.01	4.25 ± 2.0
45	0.52 ± 0.01	1.00 ± 0.5
46	0.40 ± 0.01	3.39 ± 1.0
47	0.34 ± 0.01	3.72 ± 1.0

Several kinetic equations have been derived to follow the development of secondary crystallisation with time. Most authors consider that it obeys an Avrami equation with $n = 1.0$ due to a 1-dimensional increase in thickness of the lamellae with impingement on adjacent lamellae. However, this suggests a dependence of $\log(X_t)$ on time and does not account for the observed dependence of X_t on \log time. It also gives a poor fit of the crystallisation - time data [2,3]. Recently it was observed that secondary crystallisation of PET [4,5] is associated with an increase in lamellae thickness and local diffusion of the chain segments on to the growth face for which the secondary crystallinity, $X_{s,t}$, increases with the square root of the crystallisation time. If it is assumed that secondary crystallisation occurs within the boundaries of the spherulites, developing with the extent of primary crystallisation, $X_{p,t}$ then

$$X_t = X_{p,t} + X_{s,t} = X_{p,t} + X_{p,t} k_s t^{1/2} = X_{p,\infty} (1 - \exp(-Zt^n)) (1 + k_s t^{1/2})$$

Equation 7.1

At values of $X_t > X_{p,\infty}$, the function $\exp(-Zt^n) = 0$ and the increase in fractional crystallinity with time becomes, crystallization equation becomes

$$X_{s,t} = X_{p,\infty} (1 + k_s t^{1/2})$$

Equation 7.2

$X_{s,t}$ is the measured fractional crystallinity, above $X_{p,\infty}$, determined from the crystalline carbonyl absorption but it can also be independently determined from the amorphous content, $X_{s,t}$ since $X_{c,t} = 1 - X_{a,t}$. Both $X_{c,t}$ and $1 - X_{a,t}$ after the primary process are plotted against $t^{1/2}$ in Figure 7.1 and the linear plot observed were used to determine the rate constant, k_s . The large uncertainty in k_s , listed in Table 7.2, is a result of the error in determining X_c and the very small increment in it over the whole secondary process. Nevertheless there was an increase in diffusion rate with temperature consistent with it being a thermally activated process obeying Arrhenius dependence, i.e.

$$k_s = A \exp(-\Delta E/RT)$$

Equation 7.3

where A is pre-exponential factor, ΔE the activation energy for diffusion, R gas constant and T temperature. The activation energy over this limited temperature range was determined to be $100 \pm 50 \text{ K J mol}^{-1}$.

Two different crystallisation mechanisms have been observed in the crystallisation of PCL which are associated with primary and secondary crystallisation. From this and previous work [1,4-6] these are considered to be universally applicable to the melt crystallisation of most polymers.

The primary and secondary stages are readily distinguished by their different time dependences. The primary stage develops by nucleation and growth of branching lamellae which develop into spheres and grow linearly with time. An Avrami equation with $n= 3.0$ readily accounts for the exponential increase in fractional crystallinity with time and with the observed linear growth of spherulites. The temperature dependence of growth and the thickness of the lamellae are nucleation control and can be accounted for by the theory of Hoffman et al [7] The lamellae grow by secondary nucleation on the lateral face in Regime I and the nucleation of the growth face is rate determining. Since this is followed by rapid coverage of the nucleated surface, the growth face is molecularly smooth and the lamellae thickness is constant at a critical value determined by the degree of super-cooling.

A different mechanism is required to explain the very low time dependence of the secondary process, the change in melting point and lamellar thickening with the extent of secondary crystallisation, the linear dependence of the increase in crystallinity with the square root of time, and the increase in rate with temperature. These observations are inconsistent with nucleation but consistent with diffusion control.

7.1 Reptation Theory and Segmental Diffusion

De Gennes [8-9] and later Doi & Edwards [10] have pointed out that the long ranged mobility of polymer chains in a polymer melt are highly restricted by entanglements between adjacent chains. These are so restricting that long range mobility can only occur by reptation of the chain segments. They envisaged that each chain exist in a virtual tube created by the presence of adjacent chains which were excluded from it. An individual chain could only move by segments rotating backwards and forwards within the tube - a process of reptation. The tube is not created by van der Waals forces creating an excluded volume but by the presence of the entanglements between adjacent chains such that the diameter of the tube is of the order of the distance between adjacent entanglements along a chain. The diameter of the tube is of the order of several microns. It is considered that as the tube disappears immediately an entanglement disappears and reforms around the remaining entanglements; it also follows the contour of the chain as it diffuses through the melt. This theory has been successful in accounting for the melt viscosity of polymer melt and partly its dependence on the molecular weight of a polymer above the onset of entanglements, i.e. $M^{3.4}$.

Two diffusion mechanisms and the time dependence of segmental mobility are important in the Reptation Theory [11] and have been observed in self diffusion studies using deuterated polymers [12,13] and computer modelling of polymer chains diffusing [14]; these are a dependence of diffusion distance on time, i.e. t and on the square root of time, i.e. $t^{1/2}$. In diffusion over distances greater than the tube diameter the

displacement of the segments is constrained by entanglements and the process is that of large segments reptating. For this, the displacement increases linearly over time, t , i.e.

$$\langle \mathbf{R}_n(t) - \mathbf{R}_n(0) \rangle = k' t \quad \text{Equation 7.4}$$

Incorporating the reptation theory of the melt mobility into Hoffman and Weeks model of nucleation of lamellar crystals primary crystallization occurs by the lateral extension in the ab direction of the unit cell and involves the sufficient segments of the chain to cover the full stem length. This is many times greater than the number of segments between entanglements in the melt and the reeling in of the chain segments on to the growth face will be inhibited by entanglements. Diffusion of this length of chain will follow Equation 7.4 and a linear dependence of the growth rate on time will be observed. The average lamellae stem length is many times the radius of the virtual tube, about 5 to 20 nm cf. 3-5 nm. Diffusion of the segments on to the critical size nuclei and subsequent growth will be constrained by chain entanglements and growth will be linear with time. The growth, however, is nucleation controlled as the rate determining step.

If the segmental displacement is less than the distance between adjacent entanglements then the segments involve is not constrained by the entanglements and the displacement of chain segments is

$$\langle \mathbf{R}_n(t) - \mathbf{R}_n(0) \rangle = kt^{1/2} \quad \text{Equation 7.5}$$

where k' and k are the corresponding diffusion coefficients. If as suggested lamellae thickening occurs at edge and step dislocations [15] the reduced surface energy contribution will decrease the critical thickness of the tertiary nuclei to below the entanglement distance and growth will increase along the thickness of the lamellae with the square root of time and nucleation ceases to be the rate determining step.

7.2 Conclusions

The secondary crystallisation occurs by extension of the ‘fold surface’ and the thickening of the lamellae. The time dependence of growth can only be explained by small segments of the chain being incorporated on to the crystal on the time scale of the local segmental mobility and independent of entanglements. This does not have the characteristics of a nucleation controlled process but increases in rate with increasing temperature.

7.3 References

1. Chen, Z., Hay, J. N. & Jenkins, M. J. (2013), The kinetics of crystallisation of poly(ethylene terephthalate) measured by FTIR spectroscopy, *European Polymer Journal*, **49**, 1722-1730
2. Hillier, I. H. (1965), Modified avrami equation for the bulk crystallisation kinetics of spherulitic polymers, *Journal of Polymer Science Part A*, **3**, 3067-3078
3. Hay, J. N. & Booth, A. (1972), The effect of a secondary process on the course of polymer crystallisation, *British Polymer Journal*, **4**, 19-26
4. Chen, Z. Hay, J. N. & Jenkibs, M. J. (2013), The effect of secondary crystallisation on melting, *European Polymer Journal*, **49**, 2697
5. Chen, Z., Hay, J. N. & Jenkins, M. (2014), Annealing of poly(ethylene terephthalate), *European Polymer Journal*, **50**, 235
6. Wurm, A., Zhuravlev, E., Eckstein, K., Jehnichen, D., Androsch, R., Wunderlich, B. & Schick, C. (2012), Crystallisation and homogeneous nucleation kinetics of poly(ϵ -caprolactone) (PCL) with different molar masses, *Macromolecules*, **45**, 3816

7. Hoffman, J. D. & Weeks, J. J. (1962), Rate of spherulitic crystallisation with chain folds in polychlorotrifluoroethylene, *Journal of Chemical Physics*, **37**, 1723
8. De Gennes, P. G. (1971), Reptation of a polymer chain in the presence of fixed obstacles, *The Journal of Chemical Physics*, **55**, 572-579
9. De Gennes, P. G. (1983), Diffusion controlled reactions in polymer melts, *Radiation Physics Chemistry*, **22**, 193-196
10. Doi, M. & Edwards, S. F. (1978), Dynamics of concentrated polymer systems Part 1: Brownian motion in the equilibrium state, *Journal of the Chemical Society, Faraday Transactions 2: Molecular and Chemical Physics*, **74**, 1789-1801
11. Edwards, S. F. & Doi, M. (1988), *The Theory of Polymer Dynamics*, Oxford University Press, Oxford: UK
12. Kim, K., Sperling, L. H. Klein, A &, Hammouda, B (1994), Reptation time, temperature, and cosurfactant effects on the molecular interdiffusion rate during polystyrene latex Film formation, *Macromolecules*, **27**, 6841
13. Klein, J. & Briscoe, B. J. (1979), The diffusion of long-chain molecules through bulk polyethelene, *Proceedings of the Royal Society of London. Series A, Mathematical and Physical Sciences*, **365**, 53
14. Baumgartner, A., Ebert, U. & Schafer, L. (1998), Segment motion in the reptation model of polymer dynamics II. Simulations, *Journal of Statistical Physics*, **90**, 1375

15. Abo el Maaty, M. I. & Bassett, D. C. (2005), Evidence for isothermal lamellar thickening at and behind the growth front as polyethylene crystallises from the melt, *Polymer*, **46**, 8682

Chapter 8. Conclusions & Further Work

8.1 Conclusions

Partially crystalline PCL stored at different temperatures well above the glass transition temperature ages with the development of further crystallinity and an increase in melting point, yield stress and elastic modulus with time. The change in mechanical properties can readily be accounted for by the increased crystallinity and the melting point to an increase in lamellae thickness. Over the temperature range studied, the rate of ageing increase with temperature and the dependence of stem length on the square root of storage time observed are both consistent with diffusion control and inconsistent with nucleation control.

It is clear that partially crystalline PCL ages by a continuation of the crystallisation at a rate determined by the storage temperature and by the mechanism occurring prior to ageing. In this thesis, the crystalline samples were produced on slow cooling, had a high degree of crystallinity which had developed into the secondary crystallisation prior to ageing; subsequent ageing occurred by a continuation of the secondary crystallisation. Only on ageing at 50°C was there a different mechanism due primarily to the initial partial melting of the sample, followed by re-crystallisation from seeds left by the residual lamellae. Secondary crystallisation only became apparent at a later stage when the resulting spherulites or lamellae clusters had stopped growing by impinging with adjacent ones.

Secondary crystallisation occurs by extension of the “fold surface” and the thickening of the lamellae. This does not have the characteristics of a nucleation

controlled process but appears to increase in rate with increasing temperature. The time dependence of growth can only be explained if small segments of the chain are incorporated on to the crystal face and the local mobility is independent of entanglements. The growth face must be small and much less than the number of segments between entanglements. The reeling-in of the chain segments on to the growth face can be determined by local mobility within the virtual tube. Diffusion of this length of chain will follow Equation 7.5 and a dependence of the growth rate on the square root of time will be observed.

During isothermal crystallisation, the rate of heat evolution is a measure of the crystallisation rate and the extent to which this is measured is limited by the sensitivity of the thermal sensors. In measuring the isothermal kinetics of crystallisation by DSC only the primary stage of the crystallisation could be studied with sufficient accuracy to determine the rate parameters and their temperature dependence. The subsequent secondary process made little or no contribution to the overall development of crystallinity with time and the derived rate parameters had little significance. However, DSC was used to investigate the primary crystallisation, as this is a common practice and well documented in the literature [1-4] and the rate parameters were consistent with a mechanism of growth of predetermined spherulites for which the Avrami n value was around 3.0 and the half-life decreased with decreasing crystallisation temperature, consistent with nucleation control of growth.

FTIR spectroscopy was found potentially capable of studying the overall crystallisation kinetics of PCL since the ester carbonyl band at $1720\text{-}30\text{ cm}^{-1}$ changed progressively with crystallinity. This was confirmed by 2D correlation spectroscopy on spectra measured during melting and crystallising. The *angel* pattern obtained for the

symmetrical correlation map confirmed the presence of two overlapping bands attributed to amorphous and crystalline phases, with a simultaneous change in intensity and a shift in position. The carbonyl peak at 1725 cm^{-1} was due to absorption of crystalline and 1735 cm^{-1} to the amorphous regions and the linear correlation of the absorbances of each at constant temperature was consistent with this interpretation. Accordingly the absorbance of the separated components was used as a measure of the fractional crystallinity and amorphous content and each was measured directly from absorbance and not limited by the sensitivity of the spectrometers response but only by the length of time one was prepared to wait for the change in absorbance.

Versions of the Avrami equation, modified so that they could be applied to each process, gave exponent values, n , of 3.0 ± 0.4 and 1.0 ± 0.2 respectively. This was consistent with a primary crystallisation mechanism of the growth of spherulites up to impingement during primary crystallisation and one-dimensional growth of the thickening of lamellae during secondary crystallisation. A modified version of the Hoffman & Lauritzen equation was applied to the temperature dependence of the rate parameters and the result suggested that primary crystallisation was initiated by secondary nucleation in Regime I and secondary crystallisation was initiated in Regime II with multiple nucleation of the growth face.

8.2 Future Work

The ageing of a sample of PCL has been studied in some detail and the changes observed in material properties correlated with the increase in overall crystallinity with square root of the dwell time. The ageing mechanism has been attributed to secondary crystallisation with an increase in thickness of the lamellae originally present in the sample. The increase in crystallinity and in stem length stiffens the crystalline polymer

by the lamellae reinforcing the mobile melt. It would be very interesting to extend this study to a range of PCL samples with very different molecular weight; to samples with molecular weights above and below the entanglement molecular weight and to samples with different degrees of crystallinity and different lamellae stem lengths. It would also be interesting to change the polymer systems particularly to those partially crystalline polymers with glass transitions well above conventional working temperatures to see how universal the ageing process is. This would increase the knowledge on the effect of ageing on material properties and the understanding of the mechanism of secondary crystallisation.

FTIR thermal analysis has been extremely useful in following the overall crystallisation behaviour of PCL; both primary and secondary crystallisations have been studied equally well. The analysis relies on the deconvolution of the carbonyl band into amorphous and crystalline bands; it would be useful to extend this technique to other polymer systems, to see how universally applicable the technique is and to establish other IR absorption bands which are sensitive to structural rather than any differences in the configuration.

Finally the kinetics of secondary crystallisation of other polymer systems should be measured to confirm or otherwise the propose mechanism of growth controlled by local segment migration.

8.3 References

1. Hay, J. N. & Mills, P. J. (1982), The use of differential scanning calorimetry to study polymer crystallisation kinetics, *Polymer*, 23, 1380-1384
2. Lui, M., Zhao, Q., Wang, Y., Zhang, C., Mo, Z. & Cao, S. (2003), Melting behaviours, isothermal and non-isothermal crystallisation kinetics of nylon 1212, *Polymer*, 44, 2537-2545
3. Mucha, M. & Krolikowsko, Z. (2003), Application of DSC to study crystallisation kinetics and polypropylene containing fillers, *Journal of Thermal Analysis and Calorimetry*, 74, 549-557
4. Saadi, S., Ariffin, A. A., Ghazali, H. M., Miskandar, M. S., Boo, H. C. & Abdulkarim. S. M. (2012), Application of differential scanning calorimetry (DSC), HPLC and pNMR for interpretation of primary crystallisation caused by combined low and high melting TAGs, *Food Chemistry*, 132, 603-612